

الجمهورية الجزائرية الديمقراطية الشعبية  
Democratic and Popular Republic of Algeria  
وزارة التعليم العالي والبحث العلمي  
Ministry of Higher Education and Scientific Research

Mohamed Khider University – BISKRA  
Faculty of Exact Sciences and Science  
of Nature and Life  
**Department:** Material sciences  
Ref: .....



جامعة محمد خيضر بسكرة  
كلية العلوم الدقيقة وعلوم الطبيعة والحياة  
قسم: علوم المادة  
المرجع: .....

Thesis submitted for the award  
of the diploma of  
**Doctor of Science in: Physics**  
**Option : Semi-Conductors**

Elaboration and characterization of chalcogenide thin films by  
chemical bath deposition technique

Presented by :

**Mr. Azzeddine BEGGAS**

Publicly defended on: 25/06/2018

**In front of the jury composed of:**

<b>M : Nadir ATTAF</b>	<b>Prof.</b>	<b>Constantine University</b>	<b>President</b>
<b>M : Saad RAHMANE</b>	<b>Prof.</b>	<b>Biskra University</b>	<b>Examiner</b>
<b>M : Abdallah ATTAF</b>	<b>Prof.</b>	<b>Biskra University</b>	<b>Supervisor</b>
<b>M : Boubaker BEN HAOUA</b>	<b>Prof.</b>	<b>El oued University</b>	<b>Co-Supervisor</b>

# Contents

<b>DEDICACE</b> . . . . .	<b>x</b>
<b>ACKNOWLEDGMENTS</b> . . . . .	<b>xi</b>
<b>INTRODUCTION</b> . . . . .	<b>1</b>
<b>CHAPTER 1: LITTERATURE REVIEW</b> . . . . .	<b>6</b>
1.1 Semiconductors . . . . .	6
1.2 Survey on cadmium sulphide thin films: . . . . .	7
1.2.1 Structural properties . . . . .	7
1.2.2 Optical Properties . . . . .	16
1.2.3 Compositional Analysis . . . . .	20
1.3 Survey on lead sulphide thin films: . . . . .	21
1.3.1 Structural properties . . . . .	21
1.3.2 Optical properties . . . . .	25
<b>CHAPTER 2: FILMS DEPOSITION AND CHARACTERIZATION</b>	<b>38</b>
2.1 Thin film materials . . . . .	38
2.2 Thin deposition . . . . .	39
2.3 Chemical bath deposition technique . . . . .	40
2.4 Principle of ( <i>CBD</i> ) technique . . . . .	41
2.5 Mechanism of the ( <i>CBD</i> ) process . . . . .	42
2.5.1 The simple ion-by-ion mechanism . . . . .	43
2.5.2 The simple cluster by cluster ( <i>Hydroxide cluster</i> ) mechanism	44

2.5.3	The complex decomposition ion-by-ion mechanism . . . . .	46
2.5.4	The complex decomposition cluster mechanism . . . . .	47
2.6	Deposition kinetics . . . . .	47
2.7	Thin films preparation . . . . .	49
2.7.1	Elaboration of <i>PbS</i> and <i>CdS</i> thin films . . . . .	49
2.7.2	Growth of <i>CdS</i> thin films . . . . .	49
2.7.3	Growth of <i>PbS</i> thin films . . . . .	51
2.8	Films Characterization . . . . .	53
2.8.1	Structural properties . . . . .	53
2.8.2	Optical Properties . . . . .	58
2.8.3	Fourier transform infrared spectroscopy (FTIR) . . . . .	61
<b>CHAPTER 3: CHARACTERIZATION OF <i>CDS</i> THIN FILMS</b> . . . . .		<b>65</b>
3.1	Evolution of properties of <i>CdS</i> thin films . . . . .	65
3.1.1	Film Thickness and Growth Kinetics . . . . .	66
3.1.2	Results of the XRD measurements . . . . .	69
3.1.3	Optical properties of the <i>CdS</i> thin films . . . . .	76
3.2	Chemical reactions and solution preparation . . . . .	79
3.2.1	FTIR spectrum of cadmium carbonates ( <i>CdCO<sub>3</sub></i> ) . . . . .	80
3.2.2	FTIR spectrum of calcined products from A and B . . . . .	80
3.2.3	Effect of ammonia on B solution . . . . .	82
3.3	The total elimination effect of <i>CdCO<sub>3</sub></i> on the properties of the <i>CBD</i> <i>CdS</i> thin films . . . . .	85
3.3.1	Film Thickness and Growth Kinetics . . . . .	85
3.3.2	Results of the XRD measurements . . . . .	86
3.3.3	Optical properties of the <i>CdS</i> thin films . . . . .	91
<b>CHAPTER 4: CHARACTERIZATION OF <i>PBS</i> THIN FILMS</b> . . . . .		<b>98</b>
4.1	Effect of deposition time . . . . .	98
4.1.1	Evolution of crystal structure . . . . .	98

4.1.2	Optical properties of the PbS thin films . . . . .	105
4.2	Effect of lead nitrate concentration . . . . .	111
4.2.1	Evolution of crystal structure . . . . .	111
4.2.2	Optical properties of the <i>PbS</i> thin films . . . . .	117
4.2.3	FT-IR measurements . . . . .	122
<b>CONCLUSIONS AND OUTLOOK . . . . .</b>		<b>126</b>
<b>ABSTRACT . . . . .</b>		<b>129</b>

# List of Tables

1.I	Unambiguous crystallographic planes and their diffraction angles in the cubic and hexagonal structures of <i>CdS</i> [32] . . . . .	10
1.II	Some properties of thin films and ions sources. . . . .	19
2.I	Deposition parameters of the first series of <i>CdS</i> samples . . . . .	50
2.II	Deposition parameters of the second series of <i>CdS</i> samples . . . . .	51
2.III	The component of the solutions <i>A</i> , <i>B</i> and <i>C</i> (volume of each solution was 50 ml) . . . . .	51
2.IV	: Deposition parameters of the first series of <i>PbS</i> samples . . . . .	52
2.V	: Deposition parameters of the second series of <i>PbS</i> samples . . . . .	53
3.I	Various structural parameters calculated for <i>CdS</i> thin films with different deposition times. . . . .	75
3.II	Various structural parameters calculated for <i>CdS</i> thin films with different deposition times . . . . .	90
4.I	Various structural parameters calculated for <i>PbS</i> thin films with different disposition times. . . . .	103
4.II	Various structural parameters calculated for <i>PbS</i> thin films with different disposition times. . . . .	105
4.III	Estimated values of the Urbach and band gap energies for different deposition times. . . . .	110
4.IV	Variation of <i>PbS</i> peak orientation degree as a function of the lead nitrate concentration. . . . .	113

4.V	Various structural parameters calculated for PbS thin films with different lead nitrate concentrations. . . . .	117
4.VI	Various structural parameters calculated for PbS thin films with different lead nitrate concentrations. . . . .	118
4.VII	Estimated values of the Urbach and band gap energies for different lead nitrate concentrations. . . . .	121

# List of Figures

1.1	cubic (a) and hexagonal (b) structure of CdS . . . . .	9
1.2	Typical transmittance spectra of CdS thin films deposited with different techniques: (A) thermal evaporation, (B) chemical bath, (C) sputtering and (D) electron beam evaporation [66, 24, 67, 68]) . . . . .	18
1.3	Typical cubic structure of PbS . . . . .	21
2.1	Schematic diagram showing the probable steps involved in the ion-by-ion mechanism for the case of <i>CdS</i> . . . . .	44
2.2	Representation of the influence of increased impinging ion concentration of $Cd^{2+}$ and $S^{2-}$ . . . . .	45
2.3	Cluster (hydroxide, colloidal) mechanism of CdS film formation on substrate. . . . .	46
2.4	Variation of film thickness as a function of deposition time using CBD technique. . . . .	48
2.5	Bragg diffraction . . . . .	55
2.6	Full width at half maximum (FWHM)of an arbitrary peak . . . . .	56
2.7	Presents the transmission curve of an arbitrary transparent thin film semiconductor . . . . .	59
2.8	Absorption Coefficient Plot an arbitrary transparent thin film semiconductor . . . . .	61
2.9	Determination of the disorder by extrapolation from the variation of $\ln(\alpha)$ According to $(hv)$ for a thin film. . . . .	62

3.1	Variation of film thicknesses and growth rate as a function of deposition times. . . . .	68
3.2	XRD spectra of CdS thin films deposited with different times	70
3.3	Evolution of the grain size and the growth rate of CdS films with deposition time. . . . .	72
3.4	Variation of microstrain and thickness with deposition times. .	73
3.5	Optical transmission spectra of CdS thin films deposited with different times. . . . .	76
3.6	Tauc's plot used for determination of optical band gap of CdS thin films. . . . .	77
3.7	Variations of the Urbach energy and the microstrain as function of the deposition time. . . . .	79
3.8	FTIR spectrum of carbonate cadmium salt. . . . .	81
3.9	FTIR spectrum of carbonate cadmium and calcined powder samples obtained from A and B solutions. . . . .	82
3.10	FTIR spectrum of residual solution obtained from A. . . . .	83
3.11	FTIR spectrum of residual solution obtained from B. . . . .	84
3.12	FTIR of the products obtained from the reaction between ammonia and thiourea (solution C). . . . .	85
3.13	Schematic illustration of the formation process of CdS. . . . .	86
3.14	Variation of film thicknesses and growth rate as a function of deposition times. . . . .	87
3.15	XRD spectrum of CdS thin films under different deposition times. . . . .	88
3.16	Variation of crystallite size and growth rate as a function of deposition times. . . . .	89
3.17	Optical transmission spectra of CdS thin films deposited with different times. . . . .	91

3.18	Tauc's plot used for determination of optical band gap of CdS thin films. . . . .	93
3.19	Variation of the optical gap and the band tail width as a function of the deposition times. . . . .	94
4.1	XRD spectra of PbS thin films deposited with different deposition times. . . . .	99
4.2	Variation of film thicknesses as a function of deposition times.	101
4.3	Variation of film thicknesses and dislocation density as a function of deposition times. . . . .	104
4.4	Wavelength dependence of transmittance of <i>PbS</i> thin films deposited for different durations. . . . .	106
4.5	Absorbance versus wavelength of <i>PbS</i> thin films deposited for different durations. . . . .	107
4.6	Reflectance versus wavelength of <i>PbS</i> thin films deposited for different durations. . . . .	108
4.7	Plot of $(\alpha hv)^2$ vs the photon energy ( $hv$ ) of the <i>PbS</i> thin films deposited at 55 °C for different time durations. . . . .	109
4.8	Variation of the films disorder and optical band gaps as function of deposition times. . . . .	110
4.9	XRD pattern of the <i>PbS</i> thin films deposited for various molar concentrations. . . . .	112
4.10	Variation of film thicknesses and growth rate as a function of lead nitrate concentrations. . . . .	115
4.11	Transmittance and Reflectance versus wavelength of <i>PbS</i> thin films deposited for different molar concentrations. . . . .	119
4.12	Tauc's plot used for determination optical band gap of PbS thin films deposited for different molar concentrations. . . . .	120
4.13	Variation of the films disorder and optical band gaps as function of lead nitrate molar concentration. . . . .	121

4.14	FTIR spectra of all <i>PbS</i> thin films obtained of different lead nitrate concentrations. . . . .	123
------	--	-----

# Dedicace

To the soul of my father, whose serious memories are source of inspiration for me.

To my lovely daughter, Lina.

To anyone have taught me one letter in this world.

# Acknowledgments

First and foremost, thank you God! The challenge was too much during the course of this work but you gave me the strength, courage and patience. I will forever be thankful. I am deeply grateful to Pr. A. Attaf, for his kind help, support, patience, and guidance throughout this work. I am really thankful to Pr.B. Benhaoua, for his help and support. I express my sincere gratitude and appreciation to my reading committee members, Professor Nadir Attaf of Constantine university and Professor Saad Rahmane of Biskra university for their time to read my thesis and for accepting to judge this dissertation. I would like to thank Professor Mohamed Salah Aida, and to express to him my deepest gratitude for advising me on the subject of this thesis and for helping me constantly, his advice, encouragement and kindness have been of great importance to me in carrying out this work. May he find here all my respect and gratitude for his help.

I am also grateful to Ms M. Aiadi, for her help with the DRX and Uv analysis measurements, Mr. A. Tliba and S. Nani for their help with the FTIR measurements.

Finally, I am thankful for unconditional support from my family, especially my Mother, wife, sons and daughters whose constant support and encouragement made me to undertake this study.

# Introduction

It is well known that the world's energy requirements have been steadily increasing for the last several decades with increasing levels of development and increasing population. World energy use nearly doubled between 1975 and 2005 [1]. Nearly 80% of this energy requirement is currently sourced from crude oil, natural gas, and coal [1], which are fundamentally limited in nature. In addition to the knowledge of this limited supply and the increasing demand for energy, it is well-known that energy production by burning fossil fuels may contribute to global warming and produces hazardous pollutants, such as oxides of sulfur, hydrocarbons and most significantly, carbon monoxide. Given the continued dominance of fossil fuels, world  $CO_2$  emissions are expected to increase more rapidly than the energy consumption (2.1% per year on average) [2]. Thus, traditional fossil energy resources are not only rapidly depleting, but also contribute to unpredictable and possibly irreversible climate changes in the near future [3]. These and other factors have prompted scientists and researchers all over the world to look for alternative sources of energy. Renewable energy sources seem to provide an optional solution to the global energy problem. Due to their sustainable nature, renewable energy technologies are capable of preserving resources, ensuring the security and diversity of the energy supply and providing energy services virtually without any environmental impact. A more sustainable pattern of energy supply for the future will inevitably lead to the need for greater utilization of renewable energy sources, such as solar and other kinds of energy, which many people consider to be sustainable, at least for the foreseeable future [3].

As cited above among renewable energy sources, solar energy is an exciting

alternative to fossil fuels, which is the most abundant, inexhaustible and clean of all the renewable energy resources till date [4]. Solar cell is consider a major candidate for obtaining energy from the sun, since it can provide nearly permanent power at low operating cost and is virtually free of pollution. The physical phenomenon responsible for converting light to electricity is the photovoltaic effect. Photovoltaic cells are known to convert solar light directly into electricity. The main scientific goal of photovoltaics is to produce solar cells and solar systems with high stability, high efficiency and which are economically acceptable. Thin films can be used for this propose and for various uses. This can be achieved if their structure, inter-band transitions and other optical properties are maximized to harvest enough solar radiation to provide energy. They consist of a p-type layer which has a majority hole carriers and an n-type layer that has a majority electron carriers. These layers form a diode in the form of a p-n junction that enables current to flow when electron-hole pairs are created at the junction [5]. When a photon with energy greater than the band gap of the semiconductor passes through such a cell, it may be absorbed by the material and this takes the form of a band-to-band electronic transition producing an electron-hole pair. Several types of thin films have been fabricated and used to manufacture photovoltaic cells. A number of binary sulphides are being examined as a possible absorber layers in thin film solar cells grown through chemical bath deposition technique. More recently, p-type *PbS* and n-type CdS thin films have drawn significant interest for their properties suitable for PV applications [5, 6]. These two materials which are chalcogenides will be the subject of our work.

A variety of methods has traditionally been used to prepare high quality transition metal chalcogenides. Each technique has its limitations. For example, solid state reactions require the use of high temperature to ensure the transition of solid reactants into the molten state. Spray pyrolysis, chemical vapor deposition and vacuum evaporation reactions also require high temperature to enable successful formation of the required chalcogenide. The heat is applied either directly by heat-

ing the reactants or indirectly through heating of the substrate. Chemical bath deposition (CBD) is one of the noble methods, generally requires lower temperatures for successful generation of quality films. Many researchers have devoted their efforts to this method because it is a non-expensive method for thin film preparation. Through this method many noble materials have been developed. Among these noble materials that are of great interest include metal chalcogenides especially binary (2) elements such as  $CdS$  and  $PbS$  from group II, IV and group VI elements [5]. A survey in the literature shows that during the last years, different cadmium sources have been used in this process to obtain  $Cd^{2+}$  from cadmium salt, such as cadmium acetate, cadmium sulphate, cadmium chloride, cadmium nitrate and cadmium iodide. While, thiourea is the most commonly used sulphur precursor. Ammonia is used as complexing agent. The main compounds used as source of  $Pb^{2+}$  are lead acetate  $Pb(CH_3COO)_2$  and lead nitrate  $Pb(NO_3)_2$ . It has been proposed that the mechanism by which a film grows can determine both quality and the properties of the resulting film.

Despite the advances that have been made using CBD, the full development of the technology has been hampered by poor understanding of the relationships between process chemistry and film structure, factors that are dependent on the properties of the bath and deposition precursors. The optimal deposition parameters are generally different for each compound deposited [7].

Although there have been numerous papers published reporting the preparation of chalcogenides thin films using CBD process, Kaur et al point out that the process has remained recipe oriented with little understanding of the kinetics of the process [8]. There is, therefore, a need for careful investigation of the CBD process and identification of the conditions that favor high quality coherent deposits.

## Problem statement for the study

It is generally agreed that thin films deposited by CBD have good qualities and they can be deposited on large scales areas. Chemical bath deposition will be used to deposit *CdS* and *PbS* thin films. The optical properties of *CdS* and *PbS* are appropriate for solar cell applications as window and absorber layers respectively. Therefore there is need to optimize the elaboration of these two materials for photovoltaic cell applications. Films of these materials (*CdS* and *PbS*) have high and low optical transmittance respectively which need to improve their properties. In addition, very little information is available on transmittance, reflectance and absorbance of *PbS* thin films. Such investigation needs to be subject of study.

## Aims and objectives

The aim of this work is firstly, to study the use of another salt source of  $Cd^{2+}$  such as cadmium carbonate, which, to our best knowledge, was not used until now. Secondly, to monitor all reactions steps leading to *CdS* thin films formation, which is necessary for understanding well the kinetics and the mechanism of the CBD process. In order to achieve the aim of this research project, *PbS* thin films will be deposited aiming to investigate the effect of different bath parameters (time deposition and lead nitrate concentration) on the resulting deposited product.

In this study, structural, optical and reaction mechanisms of *CdS* and *PbS* will be investigated to identify the chemical reactions leading to the formation of *CdS* and *PbS* thin films prepared using CBD.

The thesis is structured in four chapters. Properties and applications of *CdS* and *PbS* thin films are explained in the first chapter. The later treats the relevant literature review that covers related work reported by other researchers by emphasises literature optical and structural properties of both *CdS* and *PbS* films deposited by Chemical Bath deposition method (CBD).

In the second chapter, we present the experimental details of the carried exper-

iment during the preparation of this thesis. In the beginning, historical development and basic principles of the chemical bath deposition technique will be given in some details. The growth mechanisms of the used technique will be outlined. The deposition condition of *CdS* and *PbS* films used in the present study and their characterization will be presented in the same chapter.

The third and fourth chapter explain the details of *CdS* and *PbS* thin films characterizations respectively. Data obtained from analytical techniques such as XRD, FTIR and UV/VIS spectrophotometer are presented in graphical format and discussed will finish this thesis by giving general conclusion and outlines.

## References

- [1]J, Randolph, G. M Masters, Energy for Sustainability: Technology, Planning, Policy, Island Press, United States of America, (2008)
- [2]E. Commission, World energy, technology and climate policy outlook 2030 - WETO, Luxembourg, Belgium (2003)
- [3]R. Trykozko, Principles of photovoltaic conversion of solar energy, Opto-Electr.Rev, 5(4) (1997) 271-277
- [4]J. P. Colinge, C. A. Colinge, Physics of Semiconductor Devices, Kluwer Academic Publishers, Dordrech (2002)
- [5]C. O. Mosiori, Inorganic Ternary Thin films, Anaysis of Optical Properties, Anchor Academic Publishing, Hamburg, (2015)
- [6]A. P. Alivisatos, J. Phys. Chem, 100 (1996) 13226-13239
- [7]G. Hodes, Chemical Solution Deposition of Semiconductor Films, Marcel Dekker, New York, (2002)
- [8]I. Kaur, D. K. Pandya, K. L. Chopra, J. Elect-Chem. Soc, 127 (1980) 943-948

# Chapter 1

## Litterature review

In this chapter a review of some related work on the deposition of cadmium sulphide and lead sulphide thin films has been done. *CdS* and *PbS* thin films are II-VI and IV-VI semiconductor compounds respectively that have developed great interests for many practical purposes such as photovoltaic cells, photoconductive materials, optical detectors, thin film transistors and other optoelectronic devices [1, 2]. Several studies have revealed much about their general nature, features of their chemical stability and their optical properties as semiconductors.

### 1.1 Semiconductors

Two general classifications of semiconductors are elemental and compound semiconductors. The elemental semiconductor materials are found in group IV of the periodic table and the compound semiconductor materials of the simple type AB consists of elements from columns symmetrically placed with respect to column 14 of the periodic table. The column IV semiconductors, silicon and germanium are called elemental semiconductors because they are composed of single species of atoms. The II-VI compounds semiconductor are formed from group II metals and group VI chalcogens of the periodic table. These compounds are referred to as  $A^{II}B^{VI}$ , where A denotes group II metal and B denotes group VI chalcogens such as ZnO, ZnS, ZnSe, CdTe, CdO and *CdS*. These compound semiconductors have

been the subject of extensive research in both fundamental studies and device applications; they have attracted a lot of attention in solar cells, light emitting diodes (LEDs), semiconductor lasers, and other optoelectronic applications [1, 2]. II-VI semiconductors have direct band gap with the exception of mercury compounds.

They generally exhibit large band gaps, making them popular for short wavelength applications in optoelectronics. The band gaps of these compounds cover the whole band gap ( $E_g$ ) range from  $E_g = 3.94\text{eV}$  for hexagonal ZnS down to semimetals (i.e.  $E_g = 0\text{eV}$ ) for most of the mercury compounds [3].

The IV-VI compounds semiconductor are formed from group IV metals and group VI chalcogens of the periodic table, such as PbTe, SnTe, GeTe, PbSe and *PbS*, are denoted  $A^{IV}B^{VI}$ . Such compounds have an average of five valence electrons per atom and form one of the most important groups of semiconductors, some of which is known for infrared detectors such as *PbS*.

## 1.2 Survey on cadmium sulphide thin films:

### 1.2.1 Structural properties

Although, during 1960s and 1970s II-VI materials did not receive much attention. Only in the 1980s and 1990s, a great interest has been given to  $A^{II}B^{VI}$  group of semiconductors. Actually, with advance of thin films deposition techniques, II-VI materials gain much interest because of their several applications in different fields. Among these materials, cadmium sulphide (*CdS*) is considered as one of the most important n-type II-IV semiconductors with a wide and direct energy band gap (2.4 eV) [2]. Therefore, we will focus our attention on *CdS* properties, hence it used for photovoltaic cells as an idea of Reynolds in 1954 [4] under its thin films form. The efforts of workers in many laboratories throughout the world lead to the development of the *CdS* thin film solar cell and it is still until today, the most important application of *CdS* thin films in photovoltaic cells [5]. *CdS* thin films are prepared by several methods such as: Spray pyrolysis [6], sputtering [7], electro

deposition [8], vacuum evaporation [9] and chemical bath deposition (CBD) [10]. By the way CBD is simple, operating at low temperature which considered as low cost method. It has been used in the deposition of  $CdS$  thin films since the 1960 [11].

Cadium sulfide can crystallize in four different crystalline structures:

- The hexagonal (Wutrzite  $\alpha$  phase)
- The cubic structure (zinc blende  $\beta$  phase)
- The cubic rock salt structure
- The distorted rock salt structure

Only the two first phases have been reported in literature of  $CdS$  thin films which formed by several deposition techniques [14]. Among these structures, the hexagonal wurtzite structure is the most common form and thus the most thermodynamically stable in the temperature range 200-900 °C [15]. The cubic phase is less common and experiments in both powders or layers form are metastables and converted to hexagonal  $CdS$  phase [16]. The two most important crystalline structures are the wutrzite and the zinc blende structures, the later are shown in Fig. 1.1. It is well known that  $CdS$  thin films may be exist in either cubic or hexagonal phase or as a mixture of them depending on many factors including deposition technique [18]. Both cubic and hexagonal phase of  $CdS$  thin films were observed using Close Spaced Sublimation (CSS) technique [19]. Ziabari et al [20] obtained a mixed (cubic/hexagonal) crystal structure of  $CdS$  thin films by sol-gel method, whereas Ghosh et al. [21] have found a mixed phase of both cubic and hexagonal structure in  $CdS$  films produced by CBD.

Deposition of CdS using CBD is based on the slow release of  $Cd^{2+}$  ions and  $S^{2-}$  ions in an aqueous alkaline bath and the subsequent condensation of these ions on substrates suitably mounted in the bath. The slow release of  $Cd^{2+}$  ions is achieved by adding a complexing agent (ligand) to the Cd salt to form some

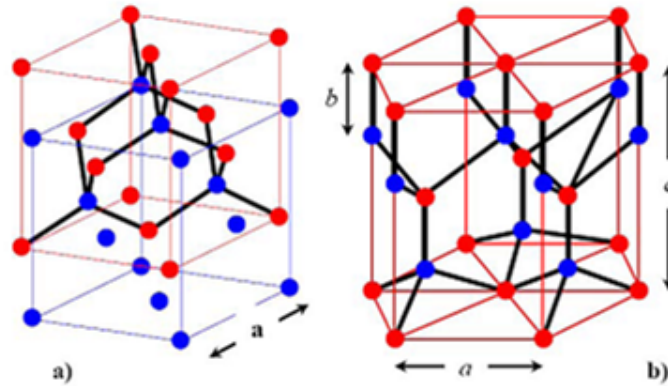


Figure 1.1: cubic (a) and hexagonal (b) structure of CdS

cadmium complex species which, upon dissociation, results in the release of small concentrations of  $Cd^{2+}$  ions. The  $S^{2-}$  ions are supplied by the decomposition of thiourea or sodium thiosulfate [5].

CdS films, which were deposited on glass substrates by the chemical bath deposition in an aqueous alkaline bath, can have either a hexagonal structure [22, 23] or a cubic structure [24] or as a mixed structure of them, depending on the condition in which the film is prepared [25, 26]. The amount of cubic phase in a mixed film was always smaller than that of hexagonal one [14, 27, 28], hence hexagonal structure is more stable than the cubic one. Relative to the cubic phase, the hexagonal CdS thin film is more suitable to be n type window layer for CdTe solar cells [29].

Generally it is hard to distinguish between the two structures cubic and hexagonal if their peaks appear at the angles ( $26.6$  ,  $43.7$  and  $53.8^\circ$ ) [30, 31]. The diffraction pattern indicates indistinguishable difference in  $2\theta$  value of hexagonal phase (002) versus cubic (111), hexagonal structure (110) versus cubic (220) and hexagonal structure (004) versus cubic (222) plane at the previously indicated angles, often it makes unambiguous phase assignment between hexagonal versus cubic phase challenging [32]. Unambiguous crystallographic planes and their diffraction angles in the cubic and hexagonal structures of CdS are summarized below:

Diffraction angle	Hexagonal structure	Cubic structure
26.6	002	111
43.8	110	220
53.7	004	222

Table 1.I: Unambiguous crystallographic planes and their diffraction angles in the cubic and hexagonal structures of *CdS* [32]

For CBD technique, it is known that there are two possible growth mechanisms: (i) ion by ion process (heterogeneous process) and (ii) cluster by cluster process (homogeneous process), the first process leads to a pure hexagonal structure or mixed cubic and hexagonal however, the later process leads to a pure cubic structure [33, 34]. Thereafter, the presence of the pure hexagonal phase in the deposited CdS films suggests that the growth process is achieved through the ion by ion mechanism growth rate of films emphasized that the low deposition rate is achieved through ion by ion growth process [25].

Thiourea,  $SC(NH_2)_2$ , is the best known source of sulfide ions  $S^{2-}$  which is widely used for the synthesis of metal sulfide films, its chemical properties and decomposition mechanisms are well documented [35].

Ammonia commonly used as complex agent. The role of complexing agent is to ensure the slow release of  $Cd^{2+}$  and  $S^{2-}$  in the aqueous alkaline solution and the subsequent condensation on a dropped substrate in the bath and to reduce or minimize the powder formation and precipitation by homogeneous reaction which do not lead to deposited product. The effect of ammonia on chemical bath deposited cadmium sulfide thin films is well described in literature [36, 37], while Munikrishna Reddy et al [38] reported the influence of ammonia concentration varying from 0.1 to 3.0 M. When 0.1 M of ammonia is added to the solution no film is formed on the substrate even after a deposition time of over 3 hrs. However, when the ammonia concentration is equal to or exceeds 2.5 M, nothing was deposited on the substrates except much yellow powder was produced in the bath after CBD deposition.

Some researchers have noted that low ammonia concentration in solution leads to CdS wurtzite phase formation because the  $Cd(OH)_2$  will be clearly visible suspension (not completely dissolve) [25]. Ximello-Quebras et al [37] studied the influence of thiourea concentration and found that the growth rate is faster when the quantity of thiourea is much greater than cadmium chloride concentration in the solution, and when the S/Cd ratio in the CBD bath is higher, the band gap value also increases. Raniero et al [39] reported that during CBD deposition, the growth rate increases with increase in temperature and cadmium salt concentration, and with decrease in thiourea concentration.

Effect of cadmium sources on chemical bath deposited CdS thin films is reported in literature where different cadmium sources such as; cadmium sulfate, chloride, iodide, acetate and nitrate have been used [5, 37, 39].

Extensive studies have been performed on CBD of CdS, most of these studies were generally concentrated on deposition of CdS thin films by varying the concentration of cadmium salt, thiourea or ammonia in a narrow range, as well as substrate quality and bath temperature too, their influences on the properties of these films were reported [5, 39].

CdS thin films have been deposited on glass substrates by CBD method using an aqueous solution of cadmium salt, ammonia and thiourea. The CdS thin film grown from the solution consisting of iodides former has wurtzite structure, while that of chlorides has zinc blend structure [40]. H. zhan et al [41] have indicated that the structure of CdS film, obtained from chloride, transforms from cubic structure to mixed cubic and hexagonal structure, by increasing the pH of the reaction solution. The reason of this may be that when pH increases, large particles such as CdS and  $Cd(OH)_2$  may be generated, which reduce CdS deposited on the substrate.

Ammonium salt is used to control  $OH^-$  concentration and stabilize the tetra ammine complex ions. Consequently, CdS colloid formation is minimized, which is the aim of all studies.

The stability of the complex also depends on temperature and pH of the reaction

bath. Increasing the solution temperature will make the tetra ammine complex ions less stable, thus increasing the free cadmium concentration may be achieved. One effect of this is that the reaction rate is increased, cluster by cluster is believed to occur, leading to difficulties in obtaining high quality CdS thin films [42]. Whereas an increase in the PH value of the reaction bath generally makes the tetra ammine complex ions more stable, which reduces the availability of free metal ions. This will decrease the reaction rate resulting in higher terminal thickness.

A comprehensive study of the effect of cadmium sources on CBD of CdS thin films is reported [24], four different cadmium sources; cadmium sulfate, chloride, iodide, and acetate have been used while thiourea was used as sulfur precursor. Ammonia was used as a complexing agent. Ammonium salt as  $NH_3$  buffer was employed in each preparation to ensure a stable complex: when  $CdSO_4$  was used as Cd source,  $(NH_4)_2SO_4$  was used as a buffer and when  $CdCl_2$  was used as Cd source,  $NH_4Cl$  was used as a buffer and so forth. All films were found to be cubic, regardless of the Cd salt used.

The effect of annealing on the optical properties of CBD grown CdS thin films has been studied by Narayanan et al [43], thermal annealing was found to remove the present strain in the CdS thin films. A reduction in the optical band gap of the films was showed, which was attributed to the cubic-hexagonal phase transition caused by thermal annealing, since the later may cause a phase transition from the cubic phase to the hexagonal phase [44]. The annealing process can improve the crystallinity of the CdS films [42]. Further, several authors report that the transition from this metastable cubic phase to the stable hexagonal phase occurs approximately at 300 °C [45, 46]. For mixed structure annealing at 480 °C in air preserves the hexagonal structure and transforms CdS cubic phase to CdO cubic phase [18], while Chun et al [47] found that the hexagonal structure of CdS thin films changes into cubic CdO after  $CdCl_2$  heat treatment. Growth of the films will be discussed below.

The  $CdCl_2$  treatment of the films contain a mixture of cubic and hexagonal CdS

structures is obviously strengthened the hexagonal phase [41]. This may because  $CdCl_2$  treatment prevents the volatilization of Cd ion and ensure stoichiometric ratio between Cd and S. Annealing thin films led to increasing in grain size and reducing the crystal defects [14]. Also, thermal annealing affects the interplanar distance of the CdS thin films, the change in the interplanar distance is similar to that of the crystallite size with increasing annealing temperature [48]. It can be concluded that annealing process changes the structural, optical and electrical properties of the CdS films.

Ammonia  $NH_3$  which is the most commonly used as complexing agent [11, 49]. The volatilization of ammonia in the solution (accelerated when the water bath temperature was improved) during film preparation [50] which led to reduce the complexing ability of the complex agent and the pH solution will be altered during film formation. Furthermore, and beside the cadmium toxicity, it is well known the toxicity of ammonia (Ammonia in aqueous solution is irritating to the eyes, skin and the respiratory and digestive systems, highly toxic to aquatic animals) and therefore is classified as dangerous to the environment.

In order to avoid the toxicity effects and volatility during the deposition films of CdS use of ethanolamine, as complexing agent instead of commonly used ammonia with thiourea and  $CdCl_2$  as source of  $S^{2-}$  and  $Cd^{2+}$  respectively, was preferred [23]. The obtained film exhibits a pure hexagonal structure with (101) as preferential orientation. However, in CBD deposited CdS using ammonia as complexing agent the preferential orientation is generally along (002) plane for the hexagonal structure or (111) plane for the cubic structure [51, 52]. While in the aim to overcome the ammonia evaporation from the bath, reaction vessel was sealed with mercury liquid seal [53].

Isaiah et al [36] reported the influence of ammonia concentration (0.2-0.9 M) on CdS film thickness. The thickness peaks at about 0.6 M of ammonia, it means that the ammonia concentration of 0.6 M was sufficient to bind  $Cd^{2+}$  into cadmium tetra amine complex ions  $Cd(NH_3)_4^{2+}$  needed for ion-by-ion mechanism leading to

slow growth and maximizes film thickness. Their work also showed the relatively feeble thickness at low ammonia concentration and decreases rapidly at higher concentrations, by varying the ammonia concentration from 0.1 to 3.0 M the author found that when 0.1 M of ammonia was added to the solution no film was formed on the substrate even after a deposition time of over 3 hrs [54]. However, when the ammonia concentration was equal to or exceeds 2.5 M, nothing was deposited on the substrates except much yellow powder was produced in the bath after CBD deposition.

Unlike other deposition methods, the growth rate in the CBD technique cannot be kept constant during film deposition. The growth rate decays with time as the concentrations of reactants in solution decrease. Q. Q liu et al [55] reported that, after a steep, initial increase of the film growth rate, the growth reaches a maximum and then decreases slowly, they also studied the influence of ammonia concentration on the growth rate. Ortega-Borges and Lincot [56] studied the *CdS* growth rate dependence on Cd salt and found that the initial growth rate decreases in the order  $CdCl_2$ ,  $Cd(CH_3COO)_2$ ,  $Cd(NO_3)_2$ ,  $CdSO_4$ ,  $CdI_2$ .

The growth process appears to be strongly temperature dependent. An increase of 10 °C, between 45 °C and 55 °C multiplies the growth rate by 2.5. At room temperature, 20 °C, no deposition occurs within a few hours [57]. These results corroborate the fact that atom-by-atom growth is favored by slow growth rate and colloid formation by fast growth rate [36]. In general, the growth of good quality semiconductor thin films proceeds at a slow rate.

The pH of the chemical solution determines the extent to which the metal complex is formed and also is important in determining to what extent the undesirable precipitation of cadmium hydroxide occurs. A higher pH (more alkaline) the rate of deposition will generally increases (as the thiourea decomposition rate will be increased), however increasing the reaction rate too far will increase the likelihood of homogeneous deposition which will reduce the final film thickness [63]. When the pH value of the reaction bath increases, the metal complex usually becomes

more stable, reducing the availability of free metal ions. This will decrease the reaction rate resulting in higher terminal thickness.

Often it is found that by moving too far away from an optimum pH a film is no longer produced, either no reaction occurs, the reaction is homogenous or cadmium hydroxide  $Cd(OH)_2$  is precipitated rather than  $CdS$ . Paul O' Brien et al [58] reported that they succeeded in depositing  $CdS$  thin films from an acidic bath for the first time. The structure of the  $CdS$  thin film obtained from acidic bath was hexagonal [58]. Later et al [59] have deposited CdS hexagonal thin films from different cadmium salts ( $CdSO_4 - CdCl_2 - Cd(CH_3COO)_2$ ) by using acidic chemical bath deposition process; in their work, thioacetamide( $CH_3CSNH_2$ ) was used as complexing agent and thiourea as source of  $S^{2-}$ , the pH values of the solutions were adjusted to 4.9-5.1 by a diluted HCl solution. The film thickness initially increases with an increase in the ionic concentration of the reactants. However, at high concentration the precipitation becomes very fast, leading to decrease in film thickness.

It was found that when  $CdSO_4$  is used as a Cd source, the CdS film thickness was higher than ones when  $Cd(CH_3COO)_2$  or  $CdCl_2$  were used, they also reported the least thickness when  $CdCl_2$  was used [60]. Effect of cadmium sources on chemical bath deposited was studied leading to the same results [24]. The latter, ranked the Cd salts based on the least film thickness, obtained from the lowest to the highest, in the following order:  $CdSO_4$ ,  $Cd(CH_3COO)_2$ ,  $CdCl_2$ ,  $CdI_2$ . Using  $CdSO_4$  resulted in a much faster growth rate, this may indicate that the cluster by cluster deposition dominated the deposition process and consequently resulted in a much larger grain size. However, in the case of the other films, ion by ion deposition dominated the deposition process and as a result a much smaller grain size and thinner films were obtained [24]. Also Kitaev et al [61] reported that the least thickness when  $CdI_2$  was used. Similar results were obtained in studying the CdS growth rate by Ortega-Borges and Lincot [56] in which growth dependences on the Cd salt. The grain size decreases in the order  $CdSO_4$ ,  $CdCl_2$ ,  $Cd(CH_3COO)_2$ ,

$CdI_2$  as reported [24].

The variation of the CdS film thickness according to the deposition time where reported [61, 62] the authors have found that the film thickness is increased with increasing time deposition, while other authors reported that the thickness reaches a maximum at certain deposition time and then decreases as the deposition time increases [63]. This trend in the CdS thickness may be explained by the desorption and/or the dissolution process predominates over the heterogeneous and homogeneous precipitation, resulting in a decrease in the film thickness as reported.

The grain size of the CdS thin films with the film thickness, the temperature solution and cadmium sources were undergone by several researchers. It initially increases as the film thickness increases, and become nearly constant into its final size [63]. Grain size increases with increasing the temperature solution [62] and decreases in the order  $CdSO_4$ ,  $CdCl_2$ ,  $Cd(CH_3COO)_2$ . In general, as a result of dominated deposition ion by ion the deposition process leads to much smaller grain size and thinner films [24, 60].

### 1.2.2 Optical Properties

There are many optical properties, including the most well known: reflection, refraction, transmission and absorption. CdS has been proved to be an ideal material for use as the window layer in solar cells [65]. Mainly high transparency is one of the requirements to be fulfilled by CdS thin films dedicated for this propose.

The optical properties are sensitive to the deposition parameters including the used deposition technique. fig. 1.2. Shows the typical transmittance spectra of CdS thin films deposited by: (A) thermal evaporation [66], (B) chemical bath deposition [24], (C) sputtering technique [67] and (D) electron beam evaporation [68]. A part films deposited by chemical bath deposition are characterized by the presence of interference fringe in their transmission spectra in the long wavelength range, this fringes are rarely observed in transmission spectra of CBD films [69]. The interference fringes is a signature of the surface smoothness. The absence of

these fringes in films deposited by CBD is due to the roughness of these films. This indicates that films deposited by CBD have a rough surface by comparison to films deposited by other techniques. On contrary to other II.VI semiconductors, CdS thin films exhibit a specific feature which is characterized by the presence of a shoulder in the optical transmittance spectra. This shoulder is present especially in films prepared with CBD technique, fig. 1.2 (B). This singularity behavior in CdS thin films has been interpreted as an indication of disorder effects (disorder in structure) [70] it has been also explained due to the phase duality of cubic and hexagonal phase [28].

The optical transmittance decreases with increasing bath temperature. This decrement can be explained by the increase of the film thickness, this trend is climbed by many authors [71, 24]. The effect of cadmium and sulfur ion concentrations on the optical spectra of CdS films were studied. Sasikala et al [53] observed that the transmittance of the film decreases with the increase in cadmium ion concentration up to 0.8 M after which it starts increasing with further increase in cadmium ion concentration.

The study of optical properties such as transmission is important in understanding the semiconductor thin films behavior. A fundamental property of semiconductors is band-gap energy. The later of the crystalline CdS material is phase dependant which is reported equal to 2.4 eV in the cubic structure and 2.5 eV in the hexagonal one [72]. Based on the literature, there are a lot of factors that affect the band gap, such as bath temperature, particle size, concentrations of the cadmium salt and thiourea. CdS band gap energy, as reported in literature [73], is inverted to the temperature bath chemical. Other studies have found variations in the band gap energy as a function of temperature, and they found that the lowest  $E_g$  value was found to be at 60 °C [71] and 65 °C [62] while it increased beyond and below that temperature [62, 71].

In their studies [60, 74], they found that when the concentrations of thiourea or cadmium salt increases the grain size increases and the energy gap value was

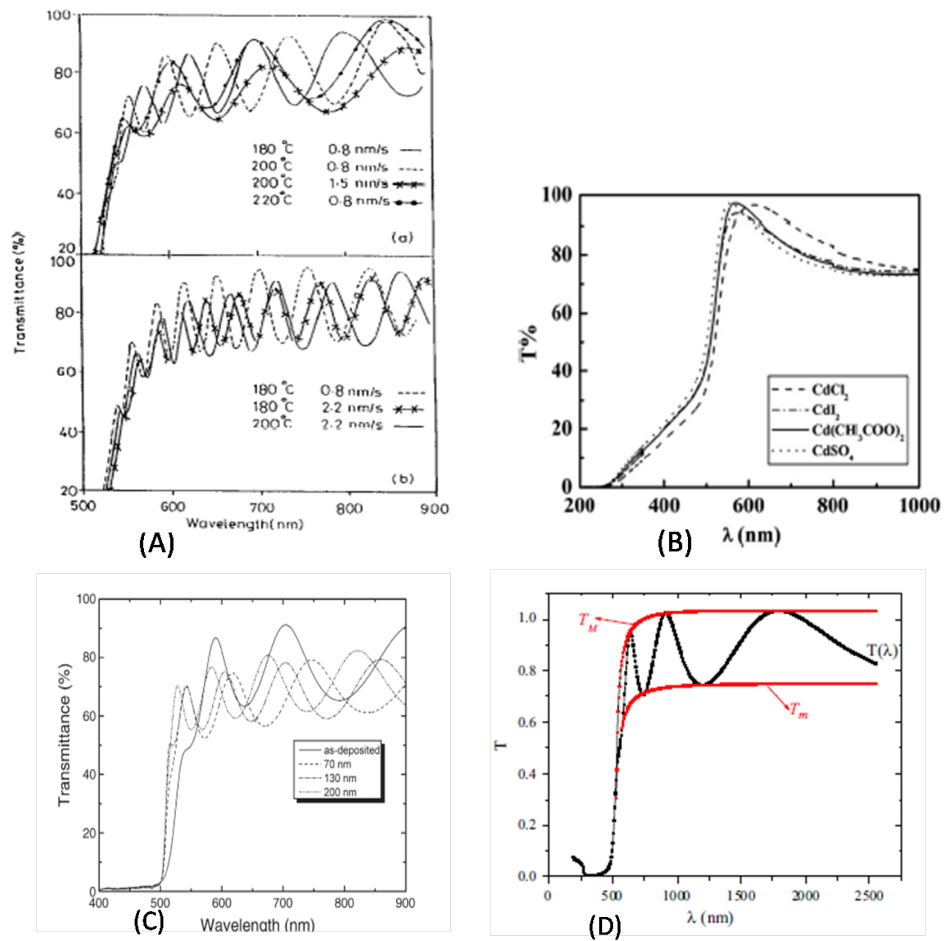


Figure 1.2: Typical transmittance spectra of CdS thin films deposited with different techniques: (A) thermal evaporation, (B) chemical bath, (C) sputtering and (D) electron beam evaporation [66, 24, 67, 68])

found to be decreases. Other studies have found variations in the energy gap as a function of cadmium source [24, 74]. The dependence of band gap on particle size in semiconductor nanocrystals has been extensively studied by L. E. Brus [75], the author found that the decreasing particle size causes an increase in the band gap. The decrease of the band gap may be produced by an increase in the structural disorder induced by the change from cubic to hexagonal phase of *CdS* [76], but with annealing treatment the band gap of the *CdS* film becomes narrower [77]. Table 1.II: summarizes some properties of *CdS* thin films and Cd and S ions sources.

Cadmium sources	Complexing agent	Complexing agent	Structure Phase	Thickness	Bandgap	Grain size(nm)	Ref
$CdSO_4$	Ammonium	$(NH_4)_2SO_4$	Cubic(111)	95	2.36	145	[24]
$Cd(CH_3COO)_2$	Ammonium	$NH_4CH_3COO$	Cubic(111)	90	2.31	14	[24]
$CdCl_2$	Ammonium	$NH_4Cl$	Cubic(111)	82.5	2.25	16	[24]
$CdI_2$	Ammonium	$NH_4I$	Cubic(111)	65	2.31	13	[24]
$Cd(NO_3)_2$	Ammonium	TEA	Cubic(111)	200-300	255-260	-	[78]
$CdCl_2$	Ethanolamine	-	Hex(101)	-	2.22-2.32*	26-40*	[23]
$Cd(CH_3COO)_2$	Ammonium	$NH_4CH_3COO$	Mixed	-	2.41-2.45**	42.2-32.4	[79]
$CdCl_2$	Glycine	KOH	Hex(002)	-	2.43-2.45	54.9-49.3	[79]
$CdCl_2$	Alanine	KOH	Hex(002)	-	2.5-2.52***	45.0-35.6	[79]
$CdSO_4$	Ammonium	-	Cubic(111)	-	2.2-2.34"	43-26.4"	[62]
$CdCl_2$	Ammonium	$NH_4Cl$	Mixed	-	2.15	10-20	[18]
$CdCl_2$	Ammonium	-	Cubic(111)	950	2.43-2.42-2.41	21-22-23	[80]
$Cd(CH_3COO)_2$	thioacetamide	HCl	Hex(002)	106	2.37	147	[59]
$CdSO_4$	thioacetamide	HCl	Hex(002)	89	2.43	103	[59]
$CdCl_2$	thioacetamide	HCl	Hex(002)	107	2.41	126	[59]

Table 1.II: Some properties of thin films and ions sources.

\* t=(40-120)mints, \*\* PH=(8-10), \*\*\* PH=(10.5-11), " T=(55, 60, 65, 70)°C, [18] PH=(10.5, 11, 11.5), [59] (Ph values were adjusted to 4.9-5.1)

### 1.2.3 Compositional Analysis

Several techniques were used to estimate the composition of the CdS thin films, such as electron dispersion X-Ray (EDX) was generally used to estimate the rate S / Cd of the thin films, whereas some composition studies are performed with Rutherford backscattering spectrometry (RBS) [24] or X-ray photoelectron spectroscopy (XPS) [34]. Using EDX analysis [90] found that the [S]/[Cd] atomic ratio is 0.94 excess of cadmium in the deposited film is observed. The RBS data [24] showed that when  $CdCl_2$  is being used as Cd source results in highly stoichiometric films (S:Cd ratio=1:1) as well as  $CdI_2$  whereas more Cd was detected when  $CdSO_4$  and  $Cd(CH_3COO)_2$  salts were used. The S:Cd ratio were found to increase in the order  $CdSO_4$ ,  $Cd(CH_3COO)_2$ ,  $CdI_2$  and  $CdCl_2$ . The excess of cadmium found by many authors [24, 90], suggesting the presence of either sulphur vacancies or interstitial Cd ions in the films acting as donors and resulting in carrier concentration increase leading in a decrease in the resistivity. In contrary to the other deposition techniques, films deposited with CBD are more stoichiometric, the ratio in these films is close to the unity. Even though the sulfur concentration was maintained higher in the solution with a ratio S/Cd equal to 5. The S/Cd ratio in the films do not exceed the unity [52, 91, 92]. In CBD technique the film grow, in a solution, through the chemical reaction of Cd and S species.

The XPS composition analysis of CdS films showed that the films are mainly composed of CdS with some cadmium oxide CdO, cadmium hydroxide  $Cd(OH)_2$  and water inclusion [34]. The S deficiency of the films corroborates the presence of the cadmium oxide species absorption. The S profile is quite abrupt showing that there is no sulfur diffusion in the under layer, while the Cd diffuses into the (substrate)  $SiO_2$  during the CBD process.

## 1.3 Survey on lead sulphide thin films:

### 1.3.1 Structural properties

Lead sulfide ( $PbS$ ) belongs to IV-VI group and is an important semiconductor, which has attracted much considerable attention owing to its special small direct band gap (0.41 eV at room temperature) [93] and a relatively large exciton Bohr radius 18 nm, with over  $10^5$  atoms [94], these two properties make these films very suitable for infrared detection and solar cell applications [95]. The structure of  $PbS$  thin films was indicated to be cubic face centered [95, 96].  $PbS$  thin films usually exhibit a p-type conduction, and their direct band gap can be varied in a wide range. It can be widened to the visible region by forming nanocrystals [97]. This material has been intensely researched since the 1950s due to its unique detection properties in the IR domain [98], it's also used in many fields such as solar cells, solar absorbers, photoresistance, laser diodes and LED devices [99, 100].

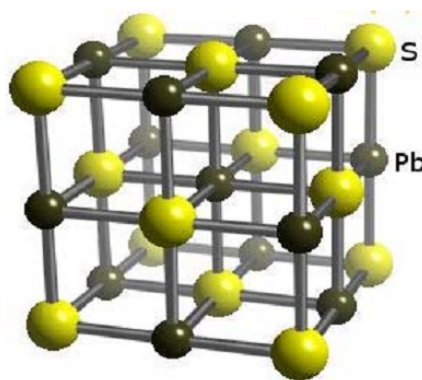


Figure 1.3: Typical cubic structure of PbS

Historically, lead sulfide was the first compound to be deposited chemically. In 1869, Puscher described a deposition process of  $PbS$  from a thiosulfate solution [101]. Emerson-Reynolds [102] reported deposition of  $PbS$  films in 1884, while in 1933 Bruckman [103] deposited  $PbS$  thin films by CBD technique. Presently,  $PbS$  thin films can be prepared by different methods, such as vacuum deposition

[104], electrochemical deposition [105], pulsed laser deposition [106], spray pyrolysis [107], sol-gel [2] chemical bath deposition [108], Among the different PbS thin film fabrication methods, chemical bath deposition CBD techniques is a more promising method than the others due to its low cost and high quality films [109]. In addition, toxic gases are not needed in the CBD method. The deposition of *PbS* is based on the slow release of  $Pb^{2+}$  and  $S^{2-}$  ions in a solution, when the ionic product of  $[Pb^{2+}]$  and  $[S^{2-}]$  ions exceed the solubility product of *PbS* ( $10^{-28}$ ) [110], the insoluble solid *PbS* will be produced either in solution or on the surface of the substrate:  $Pb^{2+} + S^{2-} \rightarrow PbS$ .

The CBD of *PbS* thin films is based on the decomposition of thiourea ( $NH_2CSNH_2$ ) in an alkaline solution containing a lead salt. Thiourea is the most commonly used as source of sulfide ions, which is widely used for the synthesis of metal sulfide films. The main compounds used as source of  $Pb^{2+}$  are lead acetate  $Pb(CH_3COO)_2$  [97, 111] and lead nitrate  $[Pb(NO_3)_2]$  [99, 112].

According to solubility considerations, a precipitate will be formed when the product of the concentrations of anions and cations exceeds the solubility product. In addition, fast precipitation rate will result into no deposition on the substrates [113]. Hence, in alkaline solution a complexing agent is needed to keep the metal ion in solution and to prevent rapid bulk precipitation of the desired product. Using a suitable complexing agent ensure the slow releases of  $Pb^{2+}$  ions. Jana et al [114] have used NaOH as complexing agent, while Chattarki et al have employed TEA instead NaOH [111]. Polyethylenimine (PEI) have been used as complexing agent too [115]. The sodium hydroxide (NaOH) with tri-sodium citrate (TSC), ( $C_6H_5Na_3O_7$ ) were used as complexing reagents [116].

The effect of various process parameters, such as deposition time, temperature, concentration of species, pH etc., on the growth and quality of the films is studied experimentally. The optimization of these parameters leads to nanoparticles with different size and shapes exhibiting different structural, optical and electrical properties [117]. There have been many attempts to understand structural,

morphological, optical and electrical PbS thin films properties.

PbS thin films prepared by CBD are reported to have a cubic centred structure with a preferential orientation along (200) perpendicular in direction to the plane of the substrate [95] and its intensity depends on deposition time [100]. While Altioikka et al [118] have reported that the preferred crystallographic orientations of the films obtained in absence of  $Na_2SO_3$  are (200). Conversely, the preferred crystallographic orientations of the films are (111) when the  $Na_2SO_3$  is used as an inhibitor. The films grow preferentially along (111) or (200) directions depending on the molar concentration as reported [119, 120]. In the case of varying the pH solution, the preferred orientation changed from (200) plane to (111) plane at pH value 9 and the intensity of the peaks increased when the pH increased [121]. Preetha et al [121] reported that the intensity of the diffraction peaks increases considerably with increasing molar concentration.

With different deposition time PbS thin films prepared by CBD technique, at room temperature, reveal that the colors of the product changed from light grey to dark grey with increasing deposition time. For all the obtained films generally exhibit poor crystalline structure [116] because of broad peak; the films have a poor crystalline structure, and they are formed by the adsorption of PbS particles and not ion- by-ion deposition [122]. It is also observed that the peaks became sharper and having higher intensity with increasing deposition time or deposition temperature, this effect can be related to the increase of both, thickness and grain size of the PbS films, also it is reported that, the crystal size was increased as the film thickness increased [123].

The thickness of the films was found to vary with the increase in deposition time from 20 to 90 min, it was observed that the thickness increases with deposition time up to (70) min related to what found in literature [124] and (60) min for others [99]. Subsequently, a quasi saturation stage starts, the saturation can be related to insufficient quantity of reactive species after that times and the deposition rate decreases, resulting in a terminal thickness [99, 124]. From the studies carried out

by García-Valenzuela et al [125] where a large increase in immersion time from 4 to 20 h was realized, it can be noted that an increase in immersion time leads to an increase in both, thickness and particle size of PbS thin films, which increases the film roughness [126], and, therefore, this would result in a greater effective surface area susceptible to oxidation by exposure to an alkaline aqueous medium and air. Pentia et al [98] have reported that polycrystalline PbS films are usually p-type.

*PbS* thin films were deposited by traditional chemical bath deposition CBD and CBD under UV radiation using a commercial UV-lamp (Photo CBD, or PCBD). The influence of the UV light was determined, and it was found that PCBD gives a significantly accelerated growth rate with decreasing the deposition time to attain specific film thickness [127].

The key in CBD deposition is to control the reaction rate, so that they occur slowly enough to allow progressive deposition on the substrate (ion-by-ion process) [128]. Because the fast precipitation of PbS lowers the quality of the film layer [128]. Hence, the rate of sulphide ion generation, and therefore reaction rate, can be controlled through the pH variation. The addition of  $OH^-$  ions makes the complex more stable. The metal ions are well arrested by the complex agent, which controls the releasing rate of metal ions causing decrease in the reaction rate and layer thickness. Therefore, the effect of pH was studied by many authors [111, 121], where the variation of film thickness with pH is reported. It has been observed that, the terminal thickness decreased continuously with the increasing pH from 9 to 12.5, and that for low pH values (less than 10.5), the decrease in growth rate was faster whereas, at higher pH values (more than 10.5) the growth rate became less dependent on pH value [111].

By CBD method, the dimensions of the crystallites can be varied by controlling deposition parameters: reaction time, temperature, pH, and presence of impurities in the solution [129], Pentia et al [129] have used Hydroxylamine hydrochloride to accelerate the chemical deposition reaction so that acceleration causes a decrease in the size of the crystallites. The study carried out by Altiokka et al [118] showed

that, the use of a sodium sulfite ( $Na_2SO_3$ ) compound as an inhibitor decreases the crystal size. Without an inhibitor, the reaction rate between  $Pb^{2+}$  and  $S^{2-}$  ions is relatively fast, which lowers the quality of the films layer. Therefore, an inhibitor is required to slow down the precipitation rate. Other study indicates that there is an increase in the grain size of the nanocrystals with temperature [125], similar behavior has been noticed by Rath et al [130]. The results carried out by Raniero [131] show that the thickness of the films was increased and the average grain size increases almost linearly with the thickness.

In order to study the effect of the substrate, PbS layers have been deposited chemically on Si, Ge and GaAs substrates from alkaline solutions and it is found that the thickness of the layers strongly depends on the chemical nature of the substrate. it is worth noting that the layers of PbS deposited on Ge and GaAs are thicker than those deposited on Si but have a relatively small grain size [94].

### 1.3.2 Optical properties

The dependence of the band gap  $E_g$  on the  $PbS$  films was determined from the optical transmission spectra. The spectral region most informative for determining the band gap from the optical spectra is the region, where the transmittance exhibits a noticeable variation depending on the wavelength.

The transmittance spectra of  $PbS$  films with different thickness prepared at  $55^\circ C$  by Abbas et al [132] showed that for low wavelengths there is no transmission because all the light is absorbed whereas for high wavelengths there are no appropriate electronic transitions so the transmission is high in this range, but it is not 100%, because of reflection in the same work and at  $45^\circ C$  the authors showed a decrease in transmission wavelength with increasing the thickness, in other work it was carried out which leads to a decrease in light scattering losses, which in turn lowers the transmission [24, 133]. These results can be explained through the film morphology, as the film thickness increases the grain size increases too, as it is mentioned previously, the surface roughness increases with increasing grain

size which led to decrease in transmission [133] which may be due to reflection phenomenon.

The increased absorbance of the films with the thickness reveals the Beer-Lambert law which can be explained by the effect that thicker films have more atoms with more states which are available for the photon energy absorption [134].

The reflectance and transmittance are below 40% in the wavelength range of 300- 1800 nm [99]. This is due to diffuse reflections from the surface of the thin films. A non-linear relationship between CBD deposition time and absorbance on as-deposited PbS films for varied deposition times has been observed by Amusan et al [135]. while Abbas et al [132] have characterized nano-crystalline PbS thin films synthesized by CBD with different thicknesses and have reported that all the films have low transmittance in region below 400 nm. Thereafter, the transmission increases with increasing wavelength towards the NIR regions. It should be emphasized that as the deposition time increases the transparency window decreases, due to the increasing thickness with time.

It was reported by Obaid et al [120] that the presence of both Pb and S elements and that the Pb:S ratio increases from 0.894 for the lower molar concentration to reach a steady value around 1.057 for higher molarity, the absorption for thin films with high molar concentrations is much higher than that for lower molar concentration. The absorption decreases for all samples with increasing wavelength, whereas the energy band gap was found to vary in a very narrow range 0.40 - 0.47 eV due to the increase in the grain size with increasing molar concentration, while in other work Obaid et al [119] have found that Pb:S ratio varies from 0.71 to 0.85 and that the value of  $E_g$  decreases from 2.35 to 1.59 eV with increasing molar concentration. It is worth noting that an increase in the band gap of the semiconductor with a decrease in the particle size was observed by Wang et al [136].

It was observed from the study of Mousa et al [137] that the band gaps decrease with increasing in pH bath. This decrease in band gap causes a strong red shift in the optical spectra, due to agglomeration of the nanocrystallites into larger

crystallites, similar behavior was indicated by Preetha et al [121] and have obtained band gaps in the range of 0.99 - 1.84 eV, which decrease with increase in pH. Tohidi et al [138] synthesized high quality PbS thin films on glass substrate from two different baths compositions. One of them (bath-I) contained an aqueous solution of lead acetate, thiourea, sodium hydroxide, and the second (bath-II) had additional triethanolamine. The introduction of triethanolamine in second bath solution reduced the grain size and increased the optical band gap of the *PbS* nanoparticles

The dependence of the optical band gap with different deposition times was studied by Göde et al [116] where it was found that the optical band gap decreased from 2.65 eV to 2.50 eV with increasing deposition time. While Pawar et al [124] reported that the band gap energy of *PbS* films is varied from 2.06 to 0.99 eV, with deposition time. Garcia et al [125] have found  $E_g$  equal to 0.93 and 0.87 eV, for the *PbS* thin films deposited during 4 and 20 h of reaction, respectively.

Additional *PbS* was deposited by immersing the glass/PbS samples into fresh solution. This result suggests that one-step films are too thin to provide a good absorption of the incident radiation, while three-step films contain an excessive concentration of Pb clusters on the surface, that would lead to a high reflectance, decreasing the spectral response, but the one deposited with two CBD steps exhibits the best spectral response at the wavelength of 2646 nm [139].

Regarding annealing, researchers observed that thermal treating process has its effect on the rate of *PbS* thin films absorptivity and consequently influence the optical characterizations of chemically deposited PbS [140, 141]. Thangavel et al [142] have reported that annealing of PbS films leads to a trivial loss in sulfur, and a small shift (0.2%) in the position of all the peaks toward lower  $2\theta$  values was noticed. Abbas et al [123] have found that the highest absorbance values are obtained from the annealed films at 150 and 200°C for films prepared at 55°C with 980 and 1000 nm thickness respectively. In addition, the  $E_g$  values were increased with increasing annealing temperature. Similar behavior was indicated

by Ezema et al [143] who assumed that high absorbtivity obtained in annealed samples may be resulted from minimizing the defects in *PbS* crystalline structure through annealing.

## References

- [1] J. Schrier, D. Demchenko, L. Wang, A. Alivisatos, *Nano Lett*, 7 (8), (2007) 2377 - 2382
- [2] M. C. Tamargo, *II-VI Semiconductor Materials and their Applications*, New York (2002)
- [3] C. Klingshirn, *Zinc Oxide*, Springer Berlin Heidelberg, (2010)
- [4] F. Shirland, *Advanced Energy Conversion*, Volume 6, Issue 4, (1966)201-202
- [5] G. Hodes, *Chemical Solution Deposition of Semiconductor Films*, Marcel Dekker, New York, 2002
- [6] I. K. Battisha, H. H. Afify, G. Abd El-Fattah, Y. Badr, *Phizika A* 11 (2002) 31
- [7] M. A. Islam, M. S. Hossein, M. M. Aliyu, P. Chelvanathan, Q. Huda, M. R. Karim, K. Sopian, N. Amin, *Energy Procidia* 33 (2013) 203 - 213
- [8] R. P. Raffaele, H. Forsell, T. Potdevin, R. Fridefeld, J. G. mantovani, S. G. Bailey, S. M. Hubbard, E. M. Gordon, A. F. Hepp, *Sol. Energy Mater. Sol. Cells* 57 (1999) 167
- [9] K. Senthil, D. Mangalaraj, S. K. Narayandass, *Appl. Surf. Sci.* 169-170 (2001) 476 - 479
- [10] A. I. Oliva, O. Solis-Canto, R. Castro-Rodriguez, P. Quintana, *Thin Solid Films* 391 (2001) 28 - 35
- [11] G. Kitaev, A. Uritskaya, S. Mokrushin, *Russ. J. Phys. Chem.* 39 (1965) 1101
- [12] S. Adachi, *Properties of Group-IV, III-V, and II-VI Semiconductors*, John Wiley & Sons, Chichester (2005)

- [13] N. Kh. Abrikosov, V. F. Bankina, L. V. Poretskaya, L. E. Shelimova, E. V. Skudnova, *Semiconducting II-VI, IV-VI, and V-VI Compounds*, Published by Plenum Press, New York (1969)
- [14] M. A. Mahdi, S. J. Kasem, J. J. Hassen, A. A. Swadi, S. K. J. Al-Ani, *Int. J. Nanoelectronics and Materials* 2 (2009) 163 - 172
- [15] G. SHIMAOKA, *Thin Solid Films*, 7 (1971) 405414
- [16] C. Y. Yeh, Z. W. Lu, S. Froyen, A. Zunger, *PHYS. REV. B*, 46, 16, (1992)-II
- [17] Landolt-Börnstein, new series , II-VI and I-VII Compounds; Semi magnetic Compounds, Volume 41B, Rossler , U.Ed , Springer Berlin Heidelberg (1999)
- [18] R. DEMIR, F. GODE, *Chalcogenide Letters*, 12, No. 2, (2015) 43 - 50
- [19] A. Nazir, A. Toma, N. Abbas Shah, S. Panaro, S. Butt, R. ur Rehman Sagar, W. Raja, K. Rasool, A. Maqsood, *J. Alloys Compd.* 609, 40 (2014)
- [20] A. A. Ziabari, F. E. Ghodsi, *Sol. Energy Mater. Sol. Cells* 105, 249 (2012)
- [21] B. Ghosh, K. Kumar, B. K. Singh, P. Banerjee, S. Das, *Appl. Surf. Sci.* 320, 309 (2014)
- [22] S. Ninomiya, S. Adachi, *J. Appl. Phys.* 78 (1995) 1183
- [23] A.Y. Jaber, S. N. Alamri, M. S. Aida, *Thin Solid Films* 520 (2012) 3485-3489
- [24] H. Khallaf, I. O. Oladeji, G. Chai, L. Chow, *Thin Solid Films* 516 (2008) 7306 - 7312
- [25] I. Kaur, D. K. Panday, K. L. Chopra, *J. Electrochem. Soc.* 127 (1980) 943
- [26] B. Ghosh, K. Kumar, B. K. Singh, P. Banerjee, S. Das, *Appl. Surf. Sci.* 320, 309 (2014)
- [27] N. S. Kozhevnikova, A. A. Rempel, F. Hergert, A. Magerl, *Thin Solid Films* 517 (2009) 2586 - 2589
- [28] J. P. Enriquez, X. Mathew, *Solar Energy Mater Solar Cells*, 76, (2003)

313 - 322

- [29] C. Y. Yeh, Z. W. Lu, S. Froyen, Phys. Rev. B: Condens. Matter 46 (16) (1992) 10086 -10097
- [30] K. Senthil, D. Mangalaraj, S. K. Narayandass, Appl. Surf. Sci. 169 - 170 (2001) 476
- [31] O. Vigil, Y. Rodriguez, O. Zelaya-Angel, C. Vazquez-Lopez, A. Morales-Acevedo, J. G. Vazquez-Luna, Thin Solid Films 322 (1998) 329
- [32] J. H. Kwon, J. S. Ahn, H. Yang, Current Appl. Phys, 13 (2013) 84 - 89
- [33] K. Ravichandran, P. Philominathan, Appl. Surf. Sci. 255 (2009) 5736
- [34] H. E. Maliki, J. C. Bernede, S. Marsillac, J. Pinel, X. Castel, J. Pouzet, Appl. Surf. Sci. 205 (2003) 65
- [35] B. Ravi, A. Jegatheesan, B. Neelakandaprasad, C. Sadeeshkumar, G. Rajarajan, Rasayan, J. Chem, Vol. 7 No.3 ( 2014) 287 - 294
- [36] I. O. Oladeji, L. Chow, J. Electrochem. Soc., Vol. 144, No. 7, (1997)
- [37] J. N. Ximello-Quiebras, G. Contreras-Puente, G. Rueda-Morales, O. Vigil, G. Santana-Rodriguez, A. Morales-Acevedo, Sol. Energy Mater. Sol. Cells 90 (2006) 727
- [38] Y. Munikrishna Reddy, M. Nagendra Vara Prasad, J. Applied Phys, 4, 4 (2013) 01-07
- [39] M. A. Martinez, C. Guillen, J. Herrero, Appl. Surf. Sci, 136 (1998) 8
- [40] T. Nakanishi, K. Ito, Solar Energy Materials and Solar Cells 35 (1994) 171 - 178
- [41] H. Zhan, J. kang Li, Y. F. Cheng, Optik 126 (2015) 1411 - 1414
- [42] L. Zhou, X. Hu, S. Wu, Surface & Coatings Technology 228 (2013) S171-S174
- [43] K. L. Narayanan, K. P. Vijayakumar, K. G. M. Nair, N. S. Thampi, K. Krishnan, J. Mater. Sci. 32 (1997) 4837
- [44] M. Muthusamy, S. Muthukumaran, M. Ashokkumar, Ceramics Inter 40 (2014) 10657 - 10666

- [45] O. Zeleya-Angel, F. L. Castillo-Alvarado, J. Avendano-Lopez, A. Escamilla- Esquivel, G. Contreras-Puente, R. Lozada-Morales, G. Torres-Delgado, *Solid State Commun* 104 (1997) 161 - 166
- [46] I. O. Oladeji, L. Chow, J. R. Liu, W. K. Chu, A. N. P. Bustamante, C. Fredricksen, A. F. Schulte, *Thin Solid Films* 359 (2000) 154 - 159
- [47] S. Chun, Y. Jung, J. Kim, D. Kim, *J. Cryst. Growth* 326, 152 (2011)
- [48] W. Dong Park, *Journal of the Korean Physical Society*, Vol. 54, No. 5 (2009)
- [49] C. Voss, Y. Chang, S. Subramanian, S. Ryu, T. Lee, C. Chang, *J. Electrochem. Soc.* 151 (2004) 655
- [50] G. Sasikala, P. Thilakan, C. Subramanian, *Sol. Energy Mater. Sol. Cells* 62 (2000) 275
- [51] J. N. Ximello-Queibras, G. Contreras, J. Aguilar-Hernandez, G. Santana-Rodriguez, A. Arias-Carbajal Readigos, *Sol. Energy Mater. Sol. Cells* 82 (2004) 263
- [52] K. S. Ramaiah, R. D. Pilkington, A. E. Hill, R. D. Tomlinson, A. K. Bhatnagar, *Mater. Chem. Phys.* 68 (2001) 22 - 30
- [53] G. Sasikala, P. Thilakan, C. Subramanian, *Solar Energy Materials & Solar Cells* 62 (2000) 275 - 293
- [54] M. Reddy Y, N. Vara Prasad M, *J. App. Physics*, 4, 4 ( 2013) 01 - 07
- [55] Q. Q. Liu, J. H. Shi, Z. Q. Li, D. W. Zhang, X. D. Li, Z. Sun, L. Y. Zhang, S. M. Huang, *Physica B* 405 (2010) 4360 - 4365
- [56] R. Ortega-Borges, D. Lincot, *J. Electrochem. Soc.* 140 (1993) 3464
- [57] D. Lincot, R. Ortega-Borges, *Ibid*, 139, 1880, (1992)
- [58] D. S. Boyd, P. O'Brien, D. J. Otway, O. Robbe, *J. Mater. Chem*, 9 (1999) 725 - 729
- [59] M. Cao, Y. Sun, J. Wu, X. Chen, N. Dai, *J. Alloys and Compounds* 508 (2010) 297 - 300
- [60] G. Sivakumar, V. Hariharan, K. Abith, *Elix. Opt. Materials* 48 (2012)

9433 - 9436

- [61] G. Kitaev, S. Mokrushin, A. Uritskaya, *Kolloidn. Z.* 27 (1965) 51
- [62] H. Moualkia, S. Hariech, M.S. Aida, *Thin Solid Films* 518 (2009) 1259 - 1262
- [63] Wug-Dong Park, *Trans. Electr. Electron. Mater.* 11(4) (2010) 173 - 170
- [64] S. Kasap, P. Capper Springer Hand book of Electronic and Photonic Materials, Springer Science, NewYork (2006)
- [65] M. A. Contreras, B. Egaas, K. Ramanathan, J. Hiltner, A. Swartzlande, F. Hasoon, R. Noufi, *Prog. Photovolt. Res. Appl.* 7 (1999) 311
- [66] A. Ashour, N. El-Kadry, S. A. Mahmoud, *Thin Solid Films* 269 ( 1995) 117 - 120
- [67] B. S. Moon, J. H. Lee, H. Jung, *Thin Solid Films*, (2006), 511, 299
- [68] A. Abdel-Galil, M. R. Balboul, A. Atta, I. S. Yahia, A. Sharaf, *Physica B* 447 (2014) 35 - 41
- [69] H. Oumous, H. Hadiri, *Thin Solid Films* 386 (2001) 87 - 90
- [70] S. Y. Shu, W. Water Liaw, J. T. J. *Eur. Ceramic Soc*, 23 (2003) 1593
- [71] W. G. C. Kumarage, L. B. D. R. P. Wijesundara, V. A. Seneviratne, C. P. Jayalath, B. S. Dassanayake, *Procedia Engineering* 139 ( 2016 ) 64 - 68
- [72] O. Vigil, A. Arias-Carbajal, F. Cruz, G. Contreras-Puente, O. Zelaya-Angel, *Mater.Res. Bull.* 36 (2001) 521
- [73] A. Cortes, H. Gomez, R. E. Marotti, G. Riveros, E. A. Dalchiele, *Sol. Energy Mater. Sol. Cells* 82 (2004) 21 - 34
- [74] A. H. Ali, S. A. Jassem , *World Scientific News* 23 (2015) 73 - 89
- [75] L. E. Brus, *J. Chem. Phys.* 80 (1984) 4403 - 4409
- [76] N.A. Shah, A. Ali, S. Hussain, *J. Coat. Technol. Res.* 7 (1) (2010) 105 - 110
- [77] H. Metin, R. Esen, *J. Cryst. Growth* 258 (2003) 141 - 148
- [78] H. Hu, P. K. Nair, *J. Crystal. Growth*, 152 (1995) 150
- [79] I. Carreón-Moncada, L. A. González, J. L. Rodrí

- guez-Galicia, J. C. Rendón-Angeles, *Thin Solid Films* 599 (2016) 166 - 173
- [80] E. Yücel, O. Şahin, *Ceramics International* 42 (2016) 6399 - 6407
- [81] Y. Kanemitsu, T. Inagaki, M. Ando, K. Matsuda, T. Saiki, C. White, *Appl. Phys. Lett.* 81 (1) (2002) 141 - 144
- [82] A. Ishizumi, K. Matsuda, T. Saiki, C. W. White, Y. Kanemitsu, *Appl. Phys. Lett.* 87 (13) (2005) 133104 - 133107
- [83] W. Runyan, T. Shaffner, *Semiconductor Measurements and Instrum.*, 2nd edn. Mc Graw Hill, NewYork (1997)
- [84] K. Subba Ramaiah, *J. Mater. Sci. Mater. Electron.* 10 (1999) 291
- [85] I. Mártil, G. González-Díaz, F. Sánchez-Quesada, *J. Vac. Sci. Technol.* A 2 (1984) 1491
- [86] P. K. Nair, M. T. S. Nair, J. Campos and L. E. Sansores, *Sol. Cells* 22 (1987) 211
- [87] A. F. Mayadas, M. Shatzkes, *Phys. Rev. B* 1, 1382 (1970)
- [88] F. Liu, Y. Lai, J. Liu, B. Wang, S. Kuang, Z. Zhang, J. Li, Y. Liu, *J. of Alloys and Compounds* 493 (2010) 305 - 308
- [89] S. Eitssayeam, U. Intatha, K. Pengpat, T. Tunkasiri, *J. Mater. Science* 40 (2005) 3803 - 3807
- [90] F. Ouachtari, A. Rmili, S. Elidrissi, A. Bouaoud, H. Erguig, P. Elies, *Journal of Modern Physics*, 2011, 2, 1073 - 1082
- [91] S. Mahanty, D. Basak, F. Rueda and M. Leon1, *J. of Elect. Mat.* 28 (1999) 559
- [92] K. Subba Ramaiah, A. K. Bhatnagar, R. D. Pilkington, A. E. Hill, R.D. Tomlinson, *J. Mater. Sci. Mater. Electron.* 11 (2000) 269 - 277
- [93] H. Kenazawa, S. Adashi, *Journal of Applied Physics* 83 (1998) 5997
- [94] A. P. Gaiduk, P. I. Gaiduk, A. N. Larsen, *Thin Solid Films* 516 (2008) 3791 - 3795
- [95] C. Orori Mosiori, *Inorganic Ternary Thin Films: Analysis of Optical Properties*, Anchor Academic Publishing (aap-verlag). Amazon France (2015)

- [96] S. V. Bhatt, M. P. Deshpande, B. H. Soni, N. Garg, S. H. Chaki, *Solid State Phenomena*, 209 (2014) 111 - 115
- [97] D. Kumar, G. Agarwal, B. Tripathi, D. Vyas, V. Kulshrestha, *Journal of Alloys and Compounds* 484 (2009) 463 - 466
- [98] E. Pentia, L. Pintilie, T. Botila, I. Pintilie, A. Chaparro, C. Maffiotte, *Thin Solid Films* 434 (2003) 162 - 170
- [99] S. Seghaier, N. Kamoun, R. Brini, A. B. Amara, *Materials Chem. Phys* 97 (2006) 71 - 80
- [100] S. Seghaier, N. Kamoun, C. Guasch, K. Zellama, *Fundamental. Applied Spectrometry* 935 (2007) 143 - 148
- [101] Puscher C. *Dingl J*; 190 (1869) 421
- [102] J. Emerson-Reynolds, *J. Chem. Soc. Trans*, 45 (1884) 162 - 165
- [103] G. Bruckman, Preparation and properties of thin lead sulfide films with special reference to their detector action . *Kolloid-z* 65 : (1933) 1-11
- [104] N. I. Fainer, M. L. Kosinova, Yu. M. Rumyantsev, E. G. Salman, F. A. Kuznetsov, *Thin Solid Films* 280 (1996) 16 - 19
- [105] A. Mondal, N. Mukherjee, *Mater. Lett*, 60 (2006) 2672 - 2674
- [106] J. Vaitkus, V. Kazlauskienė, J. Miskinis, J. Sinius, *Mater. Res. Bull.* 33 (1998) 711 - 716
- [107] B. Thangaraju, P. Kaliannan, *Semicond. Sci. Technol*, 15 (2000) 849 - 853
- [108] S. Bandyopadhyay, *Part. Sci. Tech.* 30 (2012) 43 - 54
- [109] A. A. Rempela, N. S. Kozhevnikova, A. J. G. Leenaers, S. van den Berghe, *J. Cryst. Growth* 280 (2005) 300 - 308
- [110] D. R. Lide, *Hand book of Chemistry and Physics*, 84th Ed., CRC Press, United Kingdom, (2003)
- [111] A. N. Chattarki, S. S. Kamble, L. P. Deshmukh, *Materials Letters* 67 (2012) 39 - 41
- [112] L. Raniero, C. L. Ferreira, L. R. Cruz, A. L. Pinto, R. M. P. Alves,

Physica B 405 (2010) 1283 - 1286

[113] T. Schneller, R. Waser, M. Kosec, D. Payne, Chemical solution deposition of functional oxide thin films Vienna, Springer Vienna Springer, (2013)

[114] S. Jana, R. Thapa, R. Maity, K. K. Chattopadhyay, Physica E 40 (2008) 3121 - 3126

[115] H. A. Pineda-Leon, G. Gutierrez-Heredia, A. De Leon, R. Ochoa-Landin, R. Ramirez-Bon, M. Flores-Acosta, S. J. Castillo, Chalcogenide Letters, 13 (2016) 161 - 168

[116] F. Göde, E. Güneri, F.M. Emen, V. Emir Kafadar, S. Ünlü, J. Luminescence 147 (2014) 41 - 48

[117] Z. Zhao, K. Zhang, J. Zhang, K. Yang, C. He, F. Dong, B. Yang, Sens. Actuat. B 156 (2011) 450

[118] B. Altıokka, M. C. Baykul, M. R. Altıokka, Journal of Crystal Growth 384 (2013) 50 - 54

[119] A. S. Obaid, M. A. Mahdi, Y. Yusof, M. Bououdina, Z. Hassan, Mat. Sci. Sc. Proc, 16 (2013) 971 - 979

[120] A. S. Obaid, M. A. Mahdi, Z. Hassan, M. Bououdina, inter. J. of Hydr. energy 38 (2013) 807 - 815

[121] K. C. Preetha, K. V. Murali, A. J. Ragina, K. Deepa, T. L. Remadevi, Curr. App. Phys, 12 (2012) 53 - 59

[122] T. P. Niesen, M. R. De Guire, J. Electroceram, 6 (2001) 169

[123] M. M. Abbas, A. Ab-M. Shehab, N-A. Hassan, A-K. Al-Samuraee, Thin. Solid. Films 519 (2011) 4917 - 4922

[124] S. B. Pawar, J. S. Shaikh, R. S. Devan, Y. R. Ma, D. Haranath, P. N. Bhosale, P. S. Patil, Appl. Surf. Sci. 258 (2011) 1869 - 1875

[125] J. A. García-Valenzuela, M. R. Baez-Gaxiola, M. Sotelo-Lerma, Thin Solid Films 534 (2013) 126 - 131

[126] A. Carrillo-Castillo, A. Salas-Villasenor, I. Mejia, S. Aguirre-Tostado, B. E. Gnade, M. A. Quevedo-López, Thin Solid Films 520 (7) (2012) 3107.

- [127] C. E. Pérez-Garcia, R. Ramirez-Bon, Y. V. Vorobiev, *Chal. Lett*, 12, 11, (2015) 579 - 588
- [128] M. A. Mahdi, S. J. Kasem, J. J. Hassen, A. A. Swadi, S. K. J.A l-Ani, *Int. J. Nanoelectronics and Materials* 2 (2009) 163 - 172
- [129] E. Pentia, L. Pintilie, I. Matei, T. Botila, E. Ozbay, *J. of Opto. and Adv. Mater.* 3, 2, (2001) 525 - 530
- [130] M. C. Rath, J. A. Mondal, D. K. Palit, T. Mukherjee, H. N. Ghosh, *J. Nanomater.* 4 (2007) 1
- [131] L. Raniero, C. L. Ferreira, L. R. Cruz, A. L. Pinto, R. M. P. Alves, *Physica B* 405 (2010) 1283-1286
- [132] M. M. Abbas, A. Ab-M. Shehab, A-K. Al-Samuraee, N-A. Hassan, *Energy Procedia* 6 (2011) 241 - 250
- [133] S. H. Jeong, S. Kho, D. Jung, S. B. Lee, J. H. Boo, *Surf. coat. technol.* 174 (2003) 187 - 192
- [134] F. I. Ezema, A. B. C. Ekwealor, R. U. Osuji, *Superficies Vacio.* 21 (1) (2003) 6
- [135] J. Amusan, G. Fajinmi, Y. Sasusi, *Res. J. App. Sci.* 9 (2007) 931 - 937
- [136] Y. Wang, N. Herron, *J. Phys. Chem.* 95 (1991) 525 - 532
- [137] A. M. Mousa, S. M. Hassen, S. Mohmoed, *Inter. Lett. of Chem. Phys. Astr.* 15 (2014) 1-10
- [138] T. Tohidi, K. Jamshidi-Ghaleh, Namdhar, R. Abdi- Ghaleh, *Mater. Sci. Semiconductor. Processing*, 11, (2013) 100
- [139] L. Raniero, C. L. Ferreira, L. R. Cruz, A. L. Pinto, R. M. P. Alves, *Physica B* 405 (2010) 1283 - 1286
- [140] J. A. Amusan, *Res. J. App. Sci.* 3, 1 (2008) 1- 4
- [141] R. Das, R. Kumar, *Mater. Res. Bul.* 47 (2012) 239 - 246
- [142] S. Thangavel, S. Ganesan, K. Saravanan, *Thin Solid Films* 520 (2012) 5206 - 5210
- [143] F. I. Ezema, A. B. C. Ekwealor, R. U. Osuji, *Superficies Vacio.* 21 (1)

(2003) 6

# Chapter 2

## Films deposition and characterization

This chapter gives a detailed description of the techniques which will be used for the preparation and characterization of cadmium sulphide and lead sulphide thin films in this thesis. As stated earlier, the technique used for sample preparation was (*CBD*) for both *CdS* and *PbS*.

In the first part of this chapter, historical development and basic principles of the chemical bath deposition technique are explained in some details, after having given, in the beginning, an insight on the thin film materials. The second part deals with detailed description of different analytical techniques used.

### 2.1 Thin film materials

Thin film is defined as a material created by the random nucleation and growth processes of individually condensing/reacting atomic/ionic/molecular species on a solid support called substrate [1]. Thin films encompass a considerable thickness range, varying from few nanometers to micrometer. Thin films have very interesting properties that are quite different from those of the bulk materials from which they are made of. As the film becomes thinner, the surface properties become more important than the bulk. The other cause of interest is the miniaturization of el-

ements which is useful for electronic thin film devices. The structural, chemical, metallurgical and physical properties of such materials are strongly dependent on a number of deposition parameters, thickness, crystalline orientation and also the deposition technique [1]. The atomistic random nucleation and growth processes give new exotic properties to thin film materials [2]. These properties can be controlled and reproduced by precisely modulating a range of deposition parameters [1].

## 2.2 Thin deposition

Methods of preparing thin films may be divided into:

- Physical methods are classified into (1) thermal evaporation (2) electron beam evaporation (3) molecular beam epitaxy (4) activated reactive evaporation (5) ion plating and (6) Sputtering and so on . . . Such methods, where the films are formed by condensation of incoming species on the substrate, are called solid sources. The physical methods involve expensive tools and high vacuum to deposit the films.
- Chemical methods include (1) chemical bath deposition (2) chemical vapor deposition (3) spray pyrolysis (4) electro deposition (5) anodisation (6) solution growth and (7) screen printing and so on . . . Such methods, where the films are formed by chemical reaction between incoming species on the substrate, use gas and liquid sources and they are simple and inexpensive.

Indeed there no standard deposition technique that can be used in different situation. Any application requires some specific properties. Each of the above mentioned methods has its own advantages and disadvantages. We will restrict our discussion only to the method which we have used in this thesis. For the preparation of films chemical bath deposition technique (CBD) has been employed.

## 2.3 Chemical bath deposition technique

Chemical bath deposition (CBD) is a simple and low cost technique as no elaborate arrangement is required, with a beaker containing the reaction bath and glass slides dipped in it onto which the layer will be deposited. It is to be specifically noted that the deposition is usually carried out at atmospheric pressure and at relatively low temperature therefore, is known as earlier as 1835 [3]. Liebig reported the first deposition in 1835 of silver by chemical solution - the silver mirror deposition- [4]. Some decades later, the first use of this technique to produce compound semiconducting films (*PbS*, *CuS*, *SbS*) for decoration (lustrous colors) have been reported [3]. Deposition of *PbS* films by reaction between thiourea and lead tartrate has been reported [5]. For a long time, CBD was essentially limited to *PbS* and *PbSe*. It was not until the 1960s that deposition of the CBD chalcogenides in particular *CdS*, was explicitly reported [6]. Moreover, the formation of *CdSe* and *ZnSe* were reported in the early 1970s [7]. As early as; 1982 Chopra et al [8] indicated that approximately 20 different non-metallic materials had been synthesized by *CBD*. The number of known materials now exceeds 50, most of which are semiconductors, the number of possible materials to be produced through this technique is bound to be multiply in subsequent years [9]. CBD have received an important impetus after *CdS* films deposited by this technique on *CdTe* and latter on *CuInSe<sub>2</sub>* absorbers were shown to give superior photovoltaic cells performance compared with the previously evaporated *CdS* [3, 10]. Nowadays *CBD* is universally used to form the *CdS* layer on both *CdTe* and *CuInSe<sub>2</sub>* thin film photovoltaic cells [10]. So to conclude the history of CBD technique. The scope of this technique in the field of photovoltaic is immense. This can form the most ideal technique for the production of large area thin films required for solar energy applications.

A thin film deposition technique involves three steps [8]:

- First step: Production of appropriate atomic/molecular/ionic species.

- Second step: Transportation of the unit species through a medium, (e.g. Liquid) to a substrate.
- Third step: Condensation of the unit species up on a substrate.

In principle, CBD can be used to deposit any compound that satisfies the following four basic requirements [3]:

- It should be possible to create the compound by simple precipitation. This generally, although not exclusively, refers to the formation of a stoichiometric compound formed by ionic reaction.
- The compound should be relatively (and preferably highly) insoluble in the solution used.
- The compound should be chemically stable in the solution.
- If the reaction proceeds via the free anion, then this anion should be slowly generated (to prevent sudden precipitation). If the reaction is of the complex-decomposition type, then decomposition of the metal complex should similarly occur slowly.

The main disadvantage of the chemical bath deposition is the wastage of the material due to the deposition on the walls of the container and precipitation into the solution. Preparation of the films with a definite geometric pattern on the substrate is difficult because perfect masking is not possible. The quality of the film deposited depends on the bath parameters like temperature, time of deposition, concentration of the reactants and the pH of the chemical bath [11].

## 2.4 Principle of (*CBD*) technique

All precipitation reactions are based on relative solubility of the product in the reaction bath. At a given temperature the formation of solid particles inside a

solution occurs only if the ionic product (IP) of reactants in the solution exceeds the solubility product ( $K_{SP}$ ) of the solid (final solid product) [12]. Whereas if the ionic product is less than the solubility product, then the solid phase produced will dissolve back to the solution. From another viewpoint, phase transformation occurs when the free energy of the new phase is lower than that of the initial (metastable) phase [3].

The solid product may be formed by two ways:

- (i) Formation of a precipitate (powder) in the solution, this process is called homogeneous process.
- (ii) Formation of a deposit on solid surface (substrate or the vessel walls), this process is called heterogeneous process.

Usually both these processes are concurrent and are present in the same time but with different rates [13, 14]. The predominance of one mechanism over the other is governed by the extent of heterogeneous and homogeneous nucleation, by picking out the experimental conditions favoring one process rather than the other [14, 15]. The heterogeneous process forms the basic principle behind any chemical deposition process. Or in other words, the principle of CBD technique is to control the chemical reaction so as to effect the deposition of a thin film by precipitation (heterogeneous process). CBD mechanism can happen by four ways exemplified as follows [16].

## 2.5 Mechanism of the (CBD) process

There are four ways by which the growth of the films in the CBD technique can proceed and have been briefly described below.

1. The simple ion-by-ion mechanism.
2. The simple cluster-by-cluster (Hydroxide cluster) mechanism.

3. The complex decomposition ion-by-ion mechanism.
4. The complex decomposition cluster mechanism.

### 2.5.1 The simple ion-by-ion mechanism

The ion-by-ion mechanism is the simplest mechanism, and occurs by sequential ionic reactions. The principle of this mechanism is explained with the example of  $CdS$ , and is given by the ionic reaction:



It is well known that the deposition of  $CdS$  occurs when the ionic product of  $[Cd^{2+}]$  and  $[S^{2-}]$  exceeds the solubility product ( $K_{sp}$ ) of  $CdS$ . Even though the solubility product is very low about ( $8.10^{-27}$  at  $25^{\circ}C$ ) [17], the precipitation of  $CdS$  takes place easily.

In order to avoid massive precipitation, the preparation of  $CdS$  thin films is based on the slow release of  $Cd^{2+}$  and  $S^{2-}$  in the solution. The ionic product of  $Cd^{2+}$  and  $S^{2-}$  is desired to just barely exceed the solubility product of  $CdS$  and in this case, the nucleation and growth of  $CdS$  films will be ion-by-ion condensation [11]. Slow release of the  $Cd^{2+}$  ions can be achieved by the dissociation of a complex species of cadmium. The  $S^{2-}$  ions can be prepared by decomposition of thiourea in alkaline solution (the most common case).

Fig. 2.1 Shows the schematic diagram showing the probable steps involved in the ion-by-ion mechanism for the case of  $CdS$ .

- A: Diffusion of  $S$  and  $Cd$  ions onto the substrate.
- B: Formation of  $CdS$  nuclei facilitated by the substrate.
- C: Growth of the  $CdS$  nuclei by adsorption of  $Cd$  and  $S$  ions from the solution while new  $CdS$  are nucleated.

D: Continued growth of  $CdS$  crystals which adhere to each other through van der Waals forces or possibly by chemical interactions. Adapted from [3].

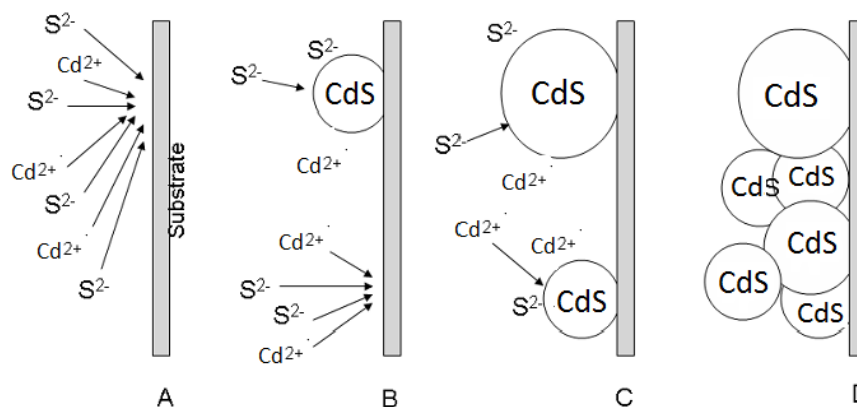


Figure 2.1: Schematic diagram showing the probable steps involved in the ion-by-ion mechanism for the case of  $CdS$ .

Since the  $S^{2-}$  is more electronegative than  $Cd^{2+}$  in the form of  $CdS$  it would theoretically form a temporary dipole of negative charge. This negatively charged cloud would be at the extremity of the interatomic bond length, attracting cadmium and sulfur ions as seen below in Fig 2.2. The adhesion of solid  $CdS$  to the substrate is generally, due to van der Waals forces. In Some Cases, chemical and electrostatic interactions between ions and substrate are possible.

### 2.5.2 The simple cluster by cluster (Hydroxide cluster) mechanism

Usually during the  $CBD$  process, complexation of the  $Cd$  was necessary to prevent  $Cd(OH)_2$  precipitation, which would impede the growth of  $CdS$  thin films. However, very often  $Cd(OH)_2$  (metal hydroxides in general) also play a role as reaction intermediates in the  $CBD$  process. The formation of metal hydroxide is hard to avoid under experimental conditions despite the presence of complex-forming agents [18]. These hydroxide colloidal particles adsorbed onto the substrate react with free  $S^{2-}$  ions slowly generated from the decomposition of thiourea in

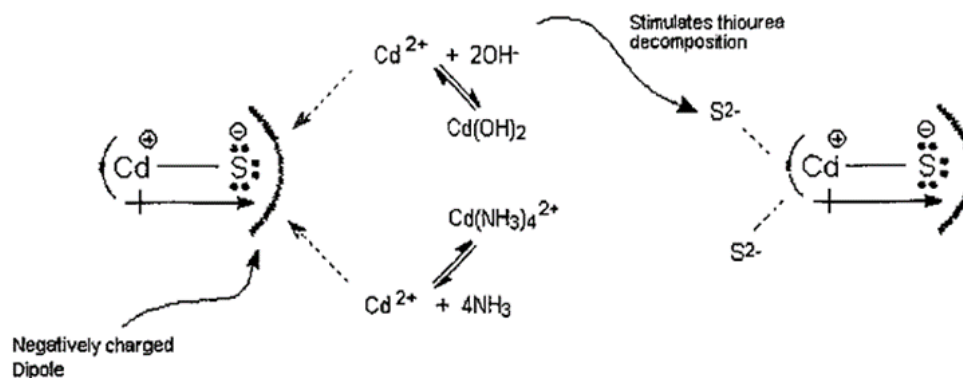
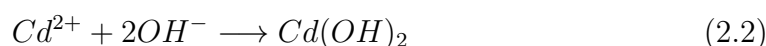


Figure 2.2: Representation of the influence of increased impinging ion concentration of  $Cd^{2+}$  and  $S^{2-}$ .

the solution resulting in displacement of hydroxide by these free  $S^{2-}$  ions. The  $CdS$  then is formed.



Followed by:



Such displacement reaction can occur both on the substrate and in the solution, and continues until most of the hydroxide converts into sulphide [19]. Studies on the kinetics of  $Cd(OH)_2$  transformation to  $CdS$  in aqueous thiourea solutions using  $NH_3$  as complex forming agent showed that the relative content of  $Cd(OH)_2$  in the precipitate decreases while that of  $CdS$  increases with deposition time [20]. In this case, sulphide formation will occur preferentially at the surface of the hydroxide rather than nucleate separately in the solution.

On the other hand, exchange reaction (2-2, 2-3) occurs and  $CdS$  is formed because the solubility product of  $CdS$  ( $K_{sp}$  is  $8.10^{-27}$ ) is much smaller than that for  $Cd(OH)_2$  ( $2.10^{-14}$ ).

Fig. 2.3 Shows the schematic diagram showing the probable steps involved in

cluster mechanism (hydroxide, colloidal) of film formation on substrate for the case of  $CdS$ .

- Diffusion of  $Cd(OH)_2$  colloidal particles towards the substrate; adsorption of particles.
- Interaction of particles with  $S^{2-}$  ions
- Exchange of hydroxide ions by sulfide ions proceeds on the substrate surface and in bulk solution
- Reaction continues until most of the hydroxide is converted to sulphide

$CdS$  particles adhere to each other and form an aggregated film. Non adsorbed particles will also aggregate and precipitate out of the solution.

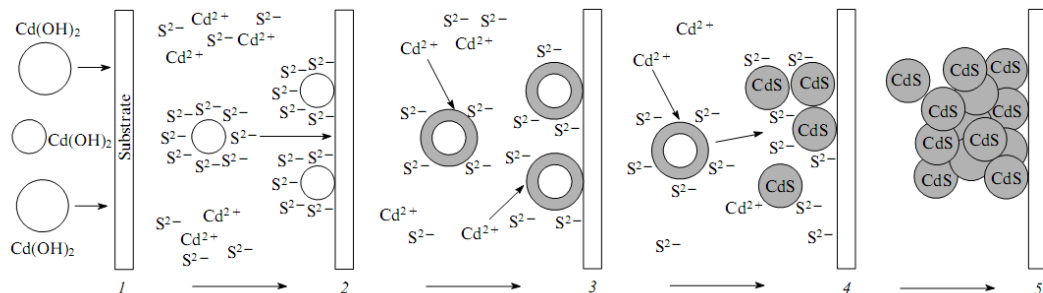
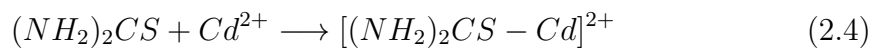


Figure 2.3: Cluster (hydroxide, colloidal) mechanism of  $CdS$  film formation on substrate.

### 2.5.3 The complex decomposition ion-by-ion mechanism

This mechanism has been suggested in the case of strong complexation between the chalcogen compound and the metal ion. Consider the complexation of a free  $Cd^{2+}$  ion by thiourea to give a  $Cd$ -thiourea complex-ion:

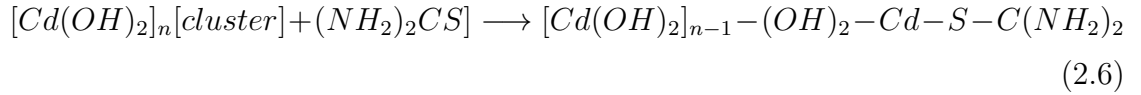


Then hydrolyze by breaking the  $S - C$  bond to form  $CdS$ :

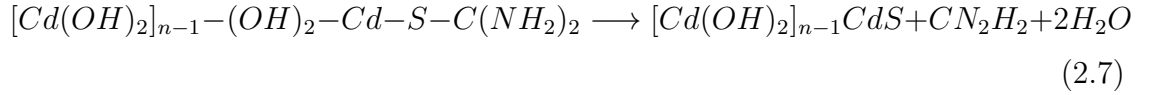


#### 2.5.4 The complex decomposition cluster mechanism

The basis of this mechanism is that a solid phase is formed but, instead of reacting directly with the free anion, it forms an intermediate complex with the “anion-forming” reagent for the example of  $CdS$ , this would be given as:



Where  $Cd(OH)_2$  is one molecule in the solid-phase cluster.



which continues until conversion of all the  $Cd(OH)_2$  to  $CdS$ .

## 2.6 Deposition kinetics

Regarding the time taken for a deposition, some depositions can be completed in a few minutes or less, while others can proceed for days and still be far from termination. In kinetic studies on the growth of CBD films, there are three definite regimes: induction, growth and termination. Fig. 2.4 presents the curve of an arbitrary thin film thickness as a function of deposition time using  $CBD$  technique.

- Induction (often called incubation) period: An induction regime at the beginning of the process indicates that no clearly observable growth occurs due to initial nuclei in solution.

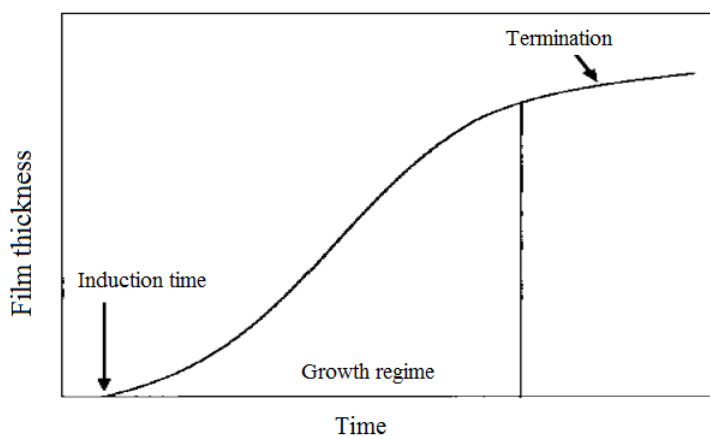


Figure 2.4: Variation of film thickness as a function of deposition time using CBD technique.

- Growth phase: The main phase of the reaction, in which ideal growth is achieved.
- Termination: Stage at which the reagent becomes depleted and the reaction begins to slow down and eventually stops. Films thicker than the terminal thickness may be obtained by repeated deposition.

*CdS* in solutions of  $SC(NH_2)_2$  forms much more slowly than in the solution of  $Na_2S$  containing. For instance, the formation of *CdS* using  $Na_2S$  at room temperature is observed a few seconds after the beginning of the reaction (cf. a few minutes for solutions of  $SC(NH_2)_2$ ) [18].

The terminal thickness depends largely on the deposition parameters. For a normal CBD reaction, if precipitation occurs homogeneously in solution, then that precipitate is lost for film deposition, with resulting reduction in terminal thickness. Therefore, the ion-by-ion process, with its lesser tendency for homogeneous precipitation, will usually result in a larger terminal thickness than the cluster process, for comparable initial reactant concentrations. Films thicker than the terminal thickness may be obtained by repeated deposition.

## 2.7 Thin films preparation

The goal of the present study is the deposition of *CdS* and *PbS* thin films by chemical bath deposition technique and characterization of the obtained thin films. Influence of different parameters related to CBD technique will be investigated. Brief description of thin films preparations will be given, and then various characterization techniques used in this thesis will be presented in the following sections.

### 2.7.1 Elaboration of *PbS* and *CdS* thin films

There have been a variety of methods reported in literature to prepare the binary sulphide thin films. Amongst all, the *CBD* process is the most attractive method to grow the films due to easy control of parameters, ability to prepare the films at relatively low temperatures. In this work, *CdS* and *PbS* thin films were prepared by the *CBD* process.

### 2.7.2 Growth of *CdS* thin films

#### 2.7.2.1 *CdS* thin films elaboration

In this study, cadmium carbonate ( $CdCO_3$ ) and thiourea  $SC(NH_2)_2$  were used as source of  $Cd^{2+}$  and  $S^{2-}$  respectively, ammonium hydroxide 27% ( $NH_3, H_2O$ ) was used as complexing agent. *CdS* thin films were grown on ordinary microscope glass slides (ref 217102) having dimension ( $75mm \times 25mm \times 1.1mm$ ), were used as the substrate as they are very cheap and easily available. Before deposition, glass substrates were cleaned in acetone and distilled water, respectively.

Two sets of samples were prepared. In each set only one parameter is varied while the rest of parameters were fixed. 50ml of solution was prepared at room temperature, which was composed of 0.0015M cadmium carbonate ( $CdCO_3$ ), 0.005M thiourea ( $CS(NH_2)_2$ ), 0.5ml ammonium hydroxide 27% ( $NH_3, H_2O$ ) and distilled water, for better dissolution of  $CdCO_3$ , a few drops of sulphuric acid were added for the first sets of the films. In Table. 2.I we have summarized the deposition

parameters of the first series deposited films where we have varied the deposition time. In Table. 2.III we have summarized the deposition parameters of the second set where, we have changed the quantity of sulphuric acid added and we have varied the deposition time. The mixture was stirred during 30 min to obtain a homogeneous solution. Just after immersing the substrate vertically in the bath, the solution temperature was fixed at  $55^{\circ}\text{C}$ . In typical conditions, only one substrate was used, that's what we have done. Experiments were carried out in a commercial electrical oven. The stirring was halted for the entire duration of deposition.  $\text{CdS}$  thin films were deposited with four deposition times for the first series of 30, 45, 60 and 90 min and are abbreviated as  $\text{CdS}_{30}$ ,  $\text{CdS}_{45}$ ,  $\text{CdS}_{60}$  and  $\text{CdS}_{90}$  respectively. While for the second series 15, 30, 60, 90 min and are abbreviated as  $\text{CdS}_1$ ,  $\text{CdS}_2$ ,  $\text{CdS}_3$  and  $\text{CdS}_4$  respectively. After the specified period of time, the deposited thin films were removed from the solution and were cleaned in distilled water to remove the loosely adhered  $\text{CdS}$  particles on the film followed by air drying. Very smooth and uniform coatings of  $\text{CdS}$  are formed.

Sample	$\text{CdCO}_3$ molarity (mol/l)	Thiourea molarity (mol/l)	ammonium hydroxide 27% (ml)	Deposition time (min)	Bath Temperature ( $^{\circ}\text{C}$ )
$\text{CdS}_{30}$	0.03	0.1	0.5	30	55
$\text{CdS}_{45}$	0.03	0.1	0.5	45	55
$\text{CdS}_{60}$	0.03	0.1	0.5	60	55
$\text{CdS}_{90}$	0.03	0.1	0.5	90	55

Table 2.I: Deposition parameters of the first series of  $\text{CdS}$  samples

### 2.7.2.2 Chemical reactions and solution preparation

In order to have an insight on the chemical reactions leading to  $\text{CdS}$  thin films formation, two solutions were prepared separately, (i) solution A (0.0015 M Cadmium carbonate ( $\text{CdCO}_3$ ), a few drops of sulphuric acid and distilled water) and (ii) solution B ( $A + 0.5$  ml ammonium hydroxide 27%). In conical flask the

Sample	$CdCO_3$ molarity (mol/l)	Thiourea molarity (mol/l)	ammonium hydroxide 27% (ml)	Deposition time (min)	Bath Temperature ( $^{\circ}C$ )	Sulphuric acid (ml)
$CdS_1$	0.03	0.1	0.5	15	55	3
$CdS_2$	0.03	0.1	0.5	30	55	3
$CdS_3$	0.03	0.1	0.5	60	55	3
$CdS_4$	0.03	0.1	0.5	90	55	3

Table 2.II: Deposition parameters of the second series of  $CdS$  samples

two solutions were constantly stirred for 30 min, and then the precipitates were filtered out and calcined under air condition. (iii)  $C$  solution is prepared by mixing ammonia with thiourea. In table 2.III we have summarized the component of the solutions  $A$ ,  $B$  and  $C$ . To investigate the calcined product, rest of both  $A$  and  $B$  solutions, and  $C$  solution, Fourier transform infrared ( $FTIR$ ) measurements were carried out using (Shimadzu, model IR AfñAnity-1) working in the range ( $400-4000\text{ cm}^{-1}$ ).

Solution	Cadmium carbonate (mol)	Sulphuric acid	hydroxide (ml) hydroxide (ml)	Thiourea (mol)
$A$	0.0015	few drops	-	-
$B$	0.0015	few drops	0.5	-
$C$	-	-	0.5	0.005

Table 2.III: The component of the solutions  $A$ ,  $B$  and  $C$  (volume of each solution was 50 ml)

### 2.7.3 Growth of $PbS$ thin films

Deposition parameters especially concentrations and period of deposition were varied to optimize them. The range of optimum concentration of the lead nitrate used is (0.01, 0.05, 0.075, and 0.10) mol/l. While the optimum period of deposition times were (30, 45, 60 and 90) min. Ordinary microscope glass slides (ref 217102) having dimension ( $75mm \times 25mm \times 1.1mm$ ), have been used as substrates. These

glass slides were cleaned in acetone and with distilled water before use.

### 2.7.3.1 Effect of deposition time

The previously cleaned substrates were vertically dipped into a 50 ml beaker, containing an aqueous solution of 0.025 M lead nitrate ( $Pb(NO_3)_2 \cdot 3H_2O$ ), 0.005 M thiourea ( $NH_2CSNH_2$ ) were used as precursors for  $Pb^{2+}$  and  $S^{2-}$  respectively, in addition 2,5 ml triethanolamine (TEA) served as complexing agent. In Table. 2.IV, we have summarized the deposition parameters of the first set, where we have varied the deposition time. The solutions were prepared in distilled water. The prepared solution was stirred with the help of homogenizer for around 20 min. The stirring was halted for the whole period of deposition. All the depositions process were made at constant temperature around  $55^\circ C$ . To optimize the deposition time, the  $PbS$  thin films were deposited for different deposition times (30, 45, 60, 75 and 90 min), at constant temperature of  $55^\circ C$  and are abbreviated as  $PbS_{30}$ ,  $PbS_{45}$ ,  $PbS_{60}$ , and  $PbS_{90}$  respectively. As in typical conditions, only one substrate was used. The beaker with the reactive solution was placed in a commercial electrical oven. After the deposition, the deposited films were rinsed with distilled water to remove the loosely adhered  $PbS$  particles on the film and finally dried in air. The as-deposited films were found to be uniform, specularly reflective (mirror-like) to the glass substrates.

Sample	Pb ( $NO_3$ ) <sub>2</sub> molarity (mol/l)	Thiourea molarity (mol/l)	Triethanolamine TEA (ml)	Deposition time (min)	Bath temp. ( $^\circ C$ )
$PbS_{30}$	0.025	0.1	2.5	30	55
$PbS_{45}$	0.025	0.1	2.5	45	55
$PbS_{60}$	0.025	0.1	2.5	60	55
$PbS_{90}$	0.025	0.1	2.5	90	55

Table 2.IV: : Deposition parameters of the first series of  $PbS$  samples

### 2.7.3.2 Effect of lead concentration:

The optimum concentrations of the lead nitrate [ $Pb(NO_3)_2$ ] used in this work were (0.01, 0.05, 0.075, and 0.10) mol/l. while the rest of parameters were fixed, the bath solution is fixed at  $55^\circ C$  and the deposition time was 60 min. In tables 2.V. We have summarized the deposition parameters of the second set where we have varied the lead salt molarity used as source of lead.

Sample	Pb ( $NO_3$ ) <sub>2</sub> molarity (mol/l)	Thiourea molarity (mol/l)	Triethanolamine TEA (ml)	Deposition time (min)	Bath temp. ( $^\circ C$ )
$PbS_1$	0.01	0.1	2.5	60	55
$PbS_2$	0.05	0.1	2.5	60	55
$PbS_3$	0.075	0.1	2.5	60	55
$PbS_4$	0.1	0.1	2.5	60	55

Table 2.V: : Deposition parameters of the second series of PbS samples

## 2.8 Films Characterization

Several techniques were used for the structural, morphological and optical characterization of the films, these techniques are described below:

### 2.8.1 Structural properties

#### 2.8.1.1 X-ray diffraction (XRD)

X-ray diffractometry (XRD) is one of the most useful characterization methods as it can provide a great deal of information about the film without requiring much sample preparation [21]. X-ray diffraction (XRD) can be used to:

- \* Study the crystallographic properties of the thin films prepared;
- \* Evaluate the orientation of the crystallites in a sample and the crystalline quality;
- \* Determine the crystallite sizes

Compared with ordinary chemical analysis the diffraction method has the advantage that it is much faster and is non-destructive [22]. A given substance always produces a characteristic X-ray diffraction pattern whether that substance is present in the pure state or as one constituent of a mixture of substances. The particular advantage of X-ray diffraction analysis is that it discloses the presence of a substance and not in terms of its constituent chemical elements. The basic law involved in the diffraction method of structural analysis is the Bragg's law. When monochromatic X-rays impinge upon the atoms in a crystal lattice, each atom acts as a source of scattering. The crystal lattice acts as series of parallel reflecting planes. Two beams with identical wavelength and phase approach a crystalline solid and are scattered off two different atoms within it. Path difference between two rays reflected from adjoining planes is:

$$2d \sin(\theta)$$

The intensity of the reflected beam at certain angles will be maximum (Constructive interference) when the path difference between two reflected waves from two different planes is an integral multiple of the wavelength of the radiation  $\lambda$ . This condition is called Bragg's law and is given by the relation [23]:

$$n\lambda = 2d_{hkl} \sin\theta \quad (2.8)$$

where  $d$  is the spacing between the atomic consecutive parallel planes in the crystal,  $hkl$  are the miller indices,  $\lambda$  is the wavelength of the X-rays,  $\theta$  the scattering angle and  $n$  an integer. Constructive interference will occur when the path difference for X-rays reflected in parallel atomic planes is a whole number of wavelengths, fig. 2.5 shows Bragg diffraction.

A diffraction pattern is obtained by measuring the intensity of scattered waves from a sample as a function of scattering angle. Very strong intensities known as Bragg peaks are obtained in the diffraction pattern at the points where the scattering angles satisfy Bragg condition. X-ray diffraction studies gives a whole

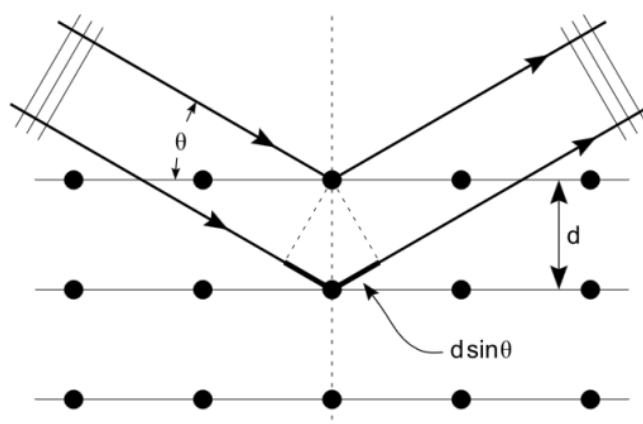


Figure 2.5: Bragg diffraction

range of information about the crystal structure, orientation and average crystalline size of the films. The diffraction patterns obtained experimentally of the sample are compared with the standard patterns of the likely elements and compounds present in the sample. Based on this comparison conclusions can be drawn about crystal structure and orientation of the sample.

### 2.8.1.2 Sample analysis conditions by DRX

In the present work, the measurements were carried out using X-ray diffractometer (XPERT-PRO X-ray diffractometer system), with  $Cu - K\alpha$  radiation  $\lambda = 1.54060 \text{ \AA}$  and energy incidence 40 kv, 40 mA). Angle scanning ( $2\theta$ ) value was between ( $20 - 70^\circ$ ). By comparing with the established JCBDS data (JCPDS No: 77 - 2306), the phases of the films were identified and the peaks in the patterns were indexed.

### 2.8.1.3 Determination of structural properties

Determination of grain size and lattice parameters:

From the X-ray diffraction pattern, the width generated in a peak which known as full width at half maximum ( $FWHM$ ) can be used to calculate the mean crystallites sizes of the film in a direction perpendicular to the respective ( $hkl$ ) planes

by using the Scherrers formula [24], which is given as:

$$D = \frac{0.9\lambda}{\beta \cos(\theta)} \quad (2.9)$$

Here,  $D$  is the average grain size,  $\lambda$  is the wavelength of the X-ray radiation,  $\beta$  is the full width at half-maximum intensity of the peak (*FMWH*) in radians and  $\theta$  is the angle of diffraction. (Or the complement of the angle of incidence) [25].

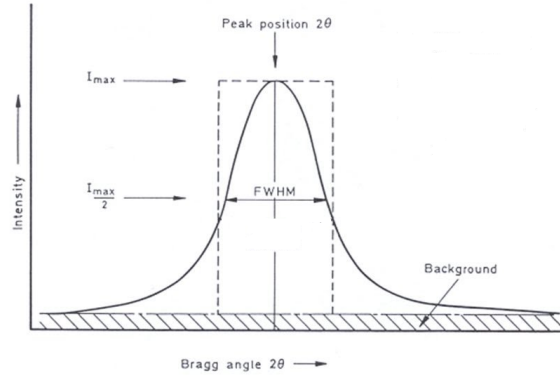


Figure 2.6: Full width at half maximum (FWHM) of an arbitrary peak

The possible interplanar spacing defined by the indices ( $hkl$ ) are determined by the shape of the unit cell. Rewriting Bragg's law we get :

$$\sin(\theta_{hkl}) = \frac{\lambda}{2d_{hkl}} \quad (2.10)$$

Therefore the possible ( $2\theta$ ) values where we can have reflections are determined by the unit cell dimensions. Experimentally, the Bragg law can be utilized by using X-rays of known wavelength ( $\lambda$ ) and measuring ( $\theta$ ), we can determine the spacing ( $d$ ) of various planes in a crystal.

The lattice parameter values for different crystallographic systems can be calculated from the following equations using the ( $hkl$ ) parameters and the interplanar spacing  $d$  [25].

Cubic system,

$$\frac{1}{d^2} = \frac{h^2 + k^2 + l^2}{a^2} \quad (2.11)$$

Hexagonal system,

$$\frac{1}{d^2} = \frac{4}{3} \left( \frac{h^2 + hk + k^2}{a^2} \right) + \frac{l^2}{c^2} \quad (2.12)$$

where  $a$  and  $c$  are the lattice constants,  $hkl$  are the miller indices.  $d_{hkl}$  is the interplanar spacing between the different lattice planes.

Determination of deformations:

A perfect crystal is an idealization; there is no such thing in nature. Atom arrangements in real materials do not follow perfect crystalline patterns. Nonetheless, most of the materials that are useful in engineering are crystalline to a very good approximation. The XRD method can be used to analyze structural defects such as microstrain and dislocation density. The knowledge of such parameters especially for new materials are important prior to their technical applications. The micro strain ( $\epsilon$ ), average stress ( $S$ ) and the dislocation density ( $\delta$ ) of thin films can be calculated by using the relations [26]:

$$S = \frac{(a - a_0)Y}{a_0 2\sigma} \quad (2.13)$$

$$\epsilon = \frac{\beta \cos \theta}{4} \quad (2.14)$$

$$\delta = \frac{1}{D^2} \quad (2.15)$$

Where  $a$  and  $a_0$  are the lattice parameters of the thin film samples and bulk samples respectively,  $Y$  and  $\sigma$  are the Young's modulus and Poisson's ratio of the bulk sample respectively. For  $PbS$ , the value of  $Y$  and  $\sigma$  are respectively 70.2 GPa and 0.28 [27].

Texture Coefficient:

Crystallographic texture in thin films, i.e. the preferred orientation of particular crystal planes relative to the film substrate, is a common and frequently useful phenomenon. The texture coefficient ( $TC$ ) represents the texture of the particular plane, deviation of which from unity implies the preferred growth [28]. The ( $TC$ ) of the samples can be calculated by using the relations [26]:

$$TC(hkl) = \frac{\frac{I(hkl)}{I_0(hkl)}}{\sum \frac{I(hkl)}{I_0(hkl)}} \times 100 \quad (2.16)$$

### 2.8.2 Optical Properties

Optical properties of the molecules provide perception into their band gap size and shape. The energy of photons from the visible to the near ultraviolet region can excite electrons from the valence band to the conduction band of a semiconductor material. The absorption of photon energy equal or more than the band gap of the semiconductor induces a photoexcitation, while transmittance can be defined as the fraction of light of a given wavelength incident to a material that passes through that material. Fig 2.7: presents the transmission curve of an arbitrary transparent thin film semiconductor. Incident photons with energies  $h\nu \geq E_g$  are absorbed, this absorption determined by the properties of the film (e.g. thickness & impurities), since there are numerous valence band electrons and the conduction band contains many empty states into which these electrons can be excited. A photon with energy  $h\nu < E_g$  is unable to excite a valence band electron to the conduction band, and as consequence they are transmitted, this explains why some semiconductors are transparent in certain wavelength ranges. Thus, for pure (intrinsic) semiconductors. There is negligible absorption of photons with  $h\nu < E_g$ , a photon will be absorbed only if there are available energy states in the forbidden band gap due to chemical impurities or physical defects, this process is called extrinsic transition. That is what we can see in fig 2.7, in the case where ( $\lambda \geq \theta$  nm). In fig 2.7 the region with the greatest rate of change of transmission (i.e.  $\alpha \rightarrow \beta$ ) is associated with photon absorption by the intrinsic band gap, this material is

transparent in certain wavelength ranges (i.e.  $\lambda \geq \beta$  nm) and opaque at the band edge (i.e.  $\lambda < \alpha$  nm).

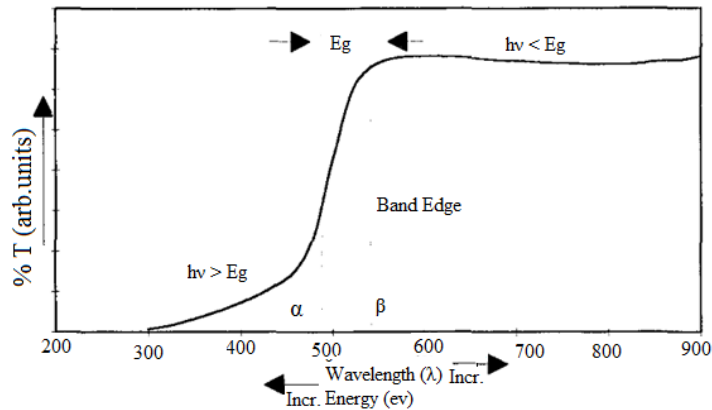


Figure 2.7: Presents the transmission curve of an arbitrary transparent thin film semiconductor

Much of the information about the properties of materials is obtained when they interact with electromagnetic radiation. When a beam of light (photons) is incident on a material, there is some predictable absorption, determined by the properties of the material. There is a dependence of the ratio of transmitted to incident photon intensity that depends on the thickness of the material and photon wavelength. The Lambert-Beer-Bouguer law [7-9] expresses this dependence:

$$I = I_0 \exp(-\alpha d) \quad (2.17)$$

where,  $I$  is the intensity of transmitted beam after passing through a thickness  $d$ ,  $I_0$  is the incident intensity of the light to the film and  $d$  is the thickness of the film.

If this condition for absorption is met, it appears that the optical intensity of the light wave, ( $I$ ), is exponentially reduced while traveling through the film. ( $\alpha$ ) is called “absorption coefficient”. From Eq. 2.17 it follows that:

$$\alpha = -\frac{1}{d} \ln\left(\frac{I}{I_0}\right) \quad (2.18)$$

For  $h\nu < E_g$  (direct), no electron hole pairs can be created, the material is transparent and  $(\alpha)$  is small. For  $h\nu \geq E_g$  (direct), absorption should be strong and it is clear that  $(\alpha)$  must be strong. The absorption coefficient  $(\alpha)$  is related to the incident photon energy  $h$  and the band gap  $E_g$  of the material as:

$$\alpha = \frac{A(h\nu - E_g)^{n/2}}{h\nu} \quad (2.19)$$

where  $A$  is a constant,  $E_g$  is the optical band gap, and  $n = 1$  for direct band gap material such as *CdS* and *PbS*.

### 2.8.2.1 Energy band gap calculation from the transmittance spectra

The energy band gap and transition type can be determine from mathematical treatment of data obtained from optical transmittance versus wavelength. According to Tauc's relation for direct bang gap semiconductor [29]:

$$(\alpha h\nu)^2 = A(\nu - E_g) \quad (2.20)$$

where  $A$  is a constant,  $E_g$  is the optical gap energy,  $\nu$  is the frequency of the incident photon and  $h$  is the Planck's constant.

Fig. 2.8 shows the plot of  $(\alpha \cdot E)^2$  versus  $(h\nu)$ , it reveals the linear nature of the plot near absorption edge indicates the existence of the direct transition between bands. Hence, this linear relationship is a clear indication that the material is direct band gap semiconductors [30]. Extrapolating the straight line portion of the absorption spectrum in fig. 2.8 intersects the zero absorption coefficients (energy axes). The value of energy at this interesting point indicates the energy of band gap  $E_g$ .

### 2.8.2.2 Determination of Urbach energy

It is well known that localised states near the band edge cause the appearance of band tails in the film band diagram. These band tail states are responsible of

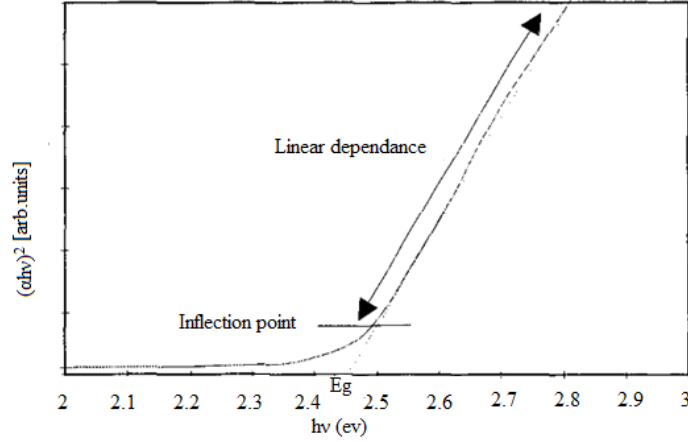


Figure 2.8: Absorption Coefficient Plot an arbitrary transparent thin film semiconductor

the sub-gap absorption in the low energy range, the spectral dependence of the absorption edge follows the Urbach formula [31].

$$\alpha = \alpha_0 \exp\left(\frac{hv}{E_u}\right) \quad (2.21)$$

where  $\alpha_0$  is the pre-exponential factor, ( $h$ ) the photon energy and ( $E_U$ ) is the band tail width commonly called Urbach energy. The band tail width is also related to the disorder in the film network. The Urbach energy, or the disorder, can be estimated from the inverse slope of the linear plot of  $\ln(\alpha)$  versus ( $hv$ ) as represented in Fig. 2.9.

### 2.8.3 Fourier transform infrared spectroscopy (FTIR)

*FTIR* spectroscopy is a technique for collecting spectra by the infrared radiation (*IR*) in the range of 400 to 4000  $cm^{-1}$  [32] *IR* radiation causes the excitation of the vibrations of covalent bonds within the molecule. These vibrations include the stretching and bending modes [33]. The stretching vibrations cause stronger absorptions of *IR* radiation compared to bending vibrations. The spectra can be interpreted by checking the peaks with the *IR* database to determine the chemical

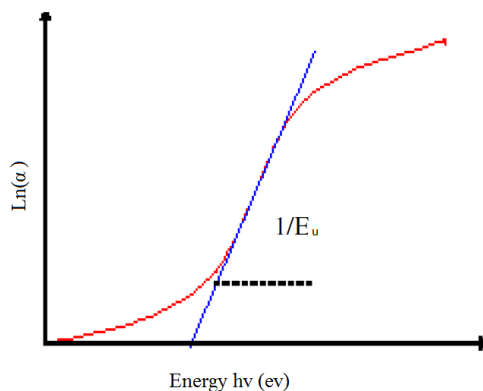


Figure 2.9: Determination of the disorder by extrapolation from the variation of  $\ln(\alpha)$  According to  $(hv)$  for a thin film.

structure of the sample. In the case of nanoparticles, this technique is very useful to know how the surfactant bonds to the surface of the nanoparticles by comparing FTIR spectra of the pure surfactant with the FTIR spectra of nanoparticles.

The deposition procedure was carried out at temperatures  $55^{\circ}\text{C}$  during deposition times (t): 30, 45, 60 and 90 min. Under physical methods we have vacuum evaporation and sputtering, where the deposition has been transferred to gaseous state either by evaporation or an impact process.

Chemical film fabrication method involves chemical reaction and the precursors are mostly components undergoing reaction at the substrate surface or in the vicinity of the substrate.

## References

- [1] K. L. Chopra, Thin-Film Phenomena, McGraw-Hill Book Company Inc, New York (1969)
- [2] P. D. Paulson, K. L. Chopra, V. Dutta, Thin-film solar cells: an overview. Progress in Photovoltaics: Research and Applications, 12, (2004) 69 - 92

- [3] G. Hodes, Chemical Solution Deposition of Semiconductor Films, New York, 2002
- [4] J. Liebig, A. Pharma, Ueber die Producte der Oxydation des Alkohols. Annalen der Chemie, 14 (2) (1835) 133
- [5] J. Emerson-Reynolds, J. Chem. Soc., Trans, 45 (1884) 162 - 165
- [6] G. Kitaev, A. Uritskaya, S. Mokrushin, Russ. J. Phys. Chem. 39 (1965) 1101
- [7] P.K. Nair, M. T. S. Nair, V. M. Garcia, O. L. Arenas, Y. Pen, A. Castillo, I. T. Ayala, O. Gomez-Daza, A. Sanchez, J. Campos, H. Hu, R. Suarez, M. E. Rincon, Solar Energy Materials and solar cells 52 (1998) 313 - 344
- [8] K. L. Chopra, S. R. Das, Thin Film Solar Cells, Springer publications, Plenum Press, New York, 1983
- [9] k.L. chopra, S.major ,D.K.Pandya, Thin solid films. 102 (1983)1
- [10] K. W. Boer, Handbook of the Physics of Thin-Film Solar Cells, Spinger-Verlag, Berlin, Heidelberg (2013)
- [11] M. A. Mahdi, S. J. Kasem, J. J. Hassen, A. A. Swadi, S. K. J. Al-Ani, Int. J. Nanoelectron. Mater. 2 (2009) 163 - 172
- [12] F. Amanullah, S. Al-Shammari, A. Al-Dhafiri, J. Phys. Stat. Sol. (Appl. Res), 202 (2005) 2474 - 2478
- [13] S. Gorer, G. Hodes, J. Phys. Chem. 98 (1994) 5338
- [14] I. Kaur, D.K. Pandya, K.L. Chopra, J. Electrochem. Soc. 127 (1980) 943
- [15] H. Khallaf, I.O. Oladeji, L. Chow, Thin Solid Films 516 (2008) 5967
- [16] H. M. Pathan, C. D. Lokhande, Mater. Sci, 27 (2004) 85
- [17] N. S. Kozhevnikova, A. A. Rempel, F. Hergert, ,A. Magerl, Thin Solid Films 517 (2009) 2586 - 2589
- [18] N. S. Kozhevnikova, A. S. Vorokh, A. A. Uritskaya, Russ. Chem. Rev. 84 (3) (2015) 225 - 250
- [19] P. J. Sebastian, H. Hu, Adv. Mater. Opt. Electr, 4 (1994) 407
- [20] A. S. Vorokh, N. S. Kozhevnikova, A. A. Uritskaya, A. Magerl. Russ. J.

Phys. Chem. 82 (2008) 1132

[21] M. Birkholz. Thin Film Analysis by X-ray Scattering. Wiley-VCH Verlag GmbH & Co. KGaA, Weinheim (2006)

[22] B. D. Cullity, S. R. Stock, Elements of X ray diffraction, Third edition, New Jersey, Prentice Hall, (2001)

[23] A. L. Patterson, The scherrer formula for X-ray particle size determination, Phys. Rev, 56 (1939) 978

[24] A. L. Patterson, The scherrer formula for X-ray particle size determination, Phys. Rev, 56, (1939) 978

[25] C. Kittel, Introduction to Solid State Physics, Seventh edn Wiley Eastern Limited (1996)

[26] K. L. Chopra, Thin Film phenomena , New York; Mc Grow Hill, (1969), p. 270

[27] M. J. Weber, Handbook of Optical Material, California, CRC Press, (2003) p.117

[28] C. S. Barret, T. B. Massalski, Structure of Metals, Pergamon Press, Oxford, (1980)

[29] J. J. Tauc, Amorphous and Liquid Semiconductor, Plenum Press, New York, 1976

[30] C. D. Lokhande, R. B. Kale, Semi. cond. Sci. Technol, 20 (2005) 1 - 9

[31] F. Urbach, Phys. Rev. 92 (1953) 1324

[32] P. R. Griffiths, J. A. D. Haseth, Fourier Transform Infrared Spectrometry, John Wiley and Sons Inc, Hoboken New Jersey (2011)

[33] H. Kuzmany, Solid State Spectroscopy: An introduction, Second Ed, Springer, New York (2009)

# Chapter 3

## Characterization of *CdS* thin films

This chapter deals with the detailed characterization of the *CdS* thin films grown by the *CBD* process as discussed in the previous chapter. In particular, this chapter presents the effects of deposition time on the evolution of crystal structural and optical properties of the *CBD CdS* thin films followed by the monitor of all reactions steps leading to *CdS* thin films formation. using Fourier transform infrared (FTIR). To achieve this chapter, the total elimination effect of cadmium carbonate from the bath solution on the structural and optical properties of the *CBD CdS* thin films was studied.

### 3.1 Evolution of properties of *CdS* thin films

In this work, *CdS* thin films were prepared for different deposition times at a low bath temperature of 55 °C. Since from the industry point of view, fabrication of devices at low temperatures is desirable for minimizing the thermal coast. The evolution of film properties with the deposition times was investigated by *XRD* and *UV* visible spectroscopy. However, controlling the evolution of the film in *CBD* process is very complicated since in the *CBD* process the ions get depleted with deposition time. Chain of chemical and mechanism reactions leading to *CdS* thin film formation were proposed based on Fourier transform infrared (FTIR) measurements for both calcined products and solutions.

### 3.1.1 Film Thickness and Growth Kinetics

One of the most important thin film parameters is thickness. Many properties of thin films depend on it: so these properties are used for its measurement. The measurements can be done when the film has been deposited. A number of techniques exist for film thickness measurement. However, the simplest is microbalance (weight gain method), which used in this study. This method is based on the direct determination of the mass of a film which was deposited onto the substrate. Using a microbalance method, a microscopic glass slide substrate was weighed before and after the film was deposited on it. With mass  $M_1$  for the substrate before deposition and  $M_2$  after deposition, the average thickness  $d$  was calculated by:

$$d = (M_2 - M_1)/SA \quad (3.1)$$

where  $S$  is the area of the film surface, and  $d$  is as thickness of the thin film and  $A$  is the density. Many errors are introduced in the measurement of film thickness. Nevertheless, the method gives an idea about the growth evolution and good estimate for film thickness for thicker films.

Due to the different pathways that can occur in the CBD process, the kinetics can vary widely from one deposition to another. Regarding the time taken for a deposition, some depositions can be completed in a few minutes or less, while others can proceed for days and still be far from termination. The deposition rate is estimated from the ratio of film thickness on the deposition time.

In Fig. 3.1 we report the variation of film thicknesses and growth rate as a function of deposition time from 30 to 90 min. It has been observed throughout this figure that the depositions investigated involve three distinct phases of growth:

1- Induction (or Incubation) period: At the early stages of the reaction, where the deposition time (around 11 min) indicates that no clearly observable growth occurs due to initial nuclei in solution (appearance of the yellow color of the solution). As a result, the induction period is similar to a countdown, where at the end of this period all the reactions have sufficient energies to interact with one another.

2- Growth period: The induction step is followed by a growth step (11 - 60 min), in which the solution became supersaturated and the product of the concentrations of  $Cd^{2+}$  and  $S^{2-}$  ions is desired to just barely exceeds the solubility product  $K_{sp}$  of  $CdS$ , nucleation of the  $Cd^{2+}$  and  $S^{2-}$  ions facilitated by the substrate to form  $CdS$  nuclei [1], the  $CdS$  nuclei grow by adsorption of  $Cd^{2+}$  and  $S^{2-}$  from solution and nucleation of new  $CdS$  crystals, in other word, the  $CdS$  crystals are formed by the adsorption of the  $Cd^{2+}$  and  $S^{2-}$  ions from the solution on the initial nuclei, along with new nucleation [2]. The growth of the crystals of  $CdS$  continues, which adhere to each other through van der Waals forces or possibly chemical interactions. The rate of nucleation of  $CdS$  on the substrate is governed primarily by the physical and chemical state of the surface, i.e. the number and orientation of dangling bonds, concentration of defects on the surface, contamination of the surface with dopants, etc [1]. The surface of all samples was treated in the same way and thus was similar with respect to defects or contaminations. Another important characteristic which strongly influences the nucleation process is the lattice mismatch between the substrate and deposited material. When the lattice parameters of  $CdS$  and the substrate match well, which facilitates nucleation. In this case, a huge number of nucleation sites is provided, which leads to a high density of small  $CdS$  crystallites deposited on the substrate. The formation of free ions in the solution is controlled because of the low deposition temperature ( $55^{\circ}C$ ). As result, an important increase of the thickness occurs. Several authors who have found that the deposition of the  $CdS$  during the primary steps of nucleation and growth is dominated by the ion-by-ion process, this model results in thin, hard and adherent films [3, 4].

3- Termination period: In the termination period (60 - 90 min) a modest increase in the thickness is observed maybe due to the lower concentration of the  $Cd^{2+}$  and  $S^{2-}$  ions in the reaction solution.

As seen the films thickness increases with deposition time from 30 to 90 min. The film deposition rate starts with 3.1 nm/min at the beginning and increases slightly with time to reach 3.2 nm/min then decreased to reach 1.9 nm/min. The

reduction of the growth rate and the thickness saturation is due to the rarefaction or consumption of the solution. The slow deposition rate can be due to the slow release of  $Cd^{2+}$  ions in the case of using cadmium carbonate as cadmium ions source. Indeed, it is hard to compare the deposition rate with other results in the literature. In fact, the deposition rate depends on the quantity of reactive species i.e.  $Cd^{2+}$  and  $S^{2-}$  which can be controlled by the variation of solution molarities, the chosen complexant agent, the bath temperature and the solution pH and so on

...

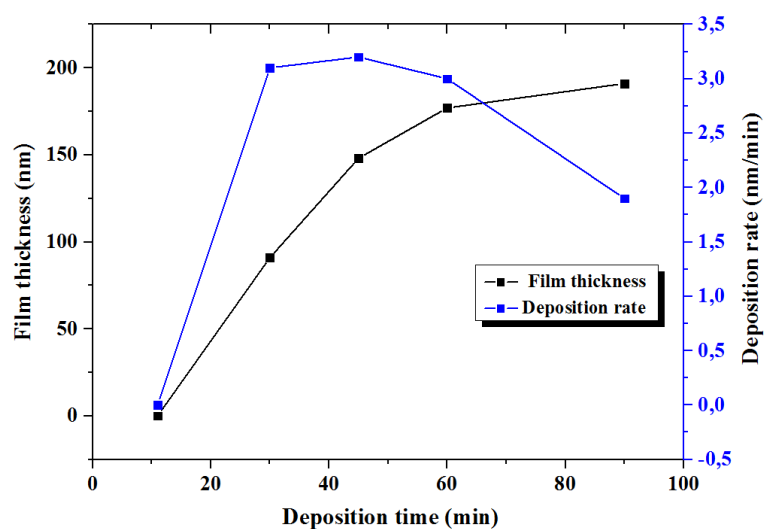


Figure 3.1: Variation of film thicknesses and growth rate as a function of deposition times.

### 3.1.2 Results of the XRD measurements

X-ray diffraction is an extremely important technique in the field of material characterization to obtain information on an atomic scale from both crystalline and non crystalline (amorphous) materials. It can be used to determine the phase content in many minerals and materials. It requires no elaborate sample preparation and is essentially non-destructive. In this study the X-ray diffraction traces of all samples were taken at room temperature. The horizontal axis of the graph is  $(2\theta)$ , twice the Bragg angle and the vertical axis is the intensity count rate.

Fig. 3.2 shows the typical XRD patterns of *CdS* thin films grown on the glass substrate at 55 °C for different deposition times ranging from 30 to 90 min. In the XRD patterns of the film deposited at low time 30 min, only a broad hump in the range of 20 – 36° was observed indicating that the film is poor crystallizing or is not thick enough for XRD analysis and the broad hump is due to the glass substrate on which the film is deposited. With increasing deposition time to 45 and 60 min, a peak located at 26,7° assigned to the (002) plane of the CdS hexagonal structure emerges. With further increasing deposition time to 90 min, the peak related to the plane (002) became finer and more intense, we notice also the emergence of two peaks located at 24,9° and 28,4° assigned to the planes (100) and (101) respectively of the hexagonal structure and much well with spatial group  $P_{63mc}(186)$  having Joint Committee Powder Diffraction System [JCPDS card No: 77 - 2306]. This asserts the pure hexagonal structure of the obtained films. It was observed that the peak intensity increases with increasing deposition time; this is a consequence of thickness increasing which leads to better crystallinity of *CdS* thin films. It is worth noting that *CdS* may crystallise in cubic or in hexagonal structure. However, for solar cell applications, hexagonal structured is preferred due to its thermodynamic stability [5]. The two main properties extracted from peak width analysis are the crystallite size and lattice strain, while the interplanar spacing and lattice constants can be estimated from the peak position  $(2\theta)$ .

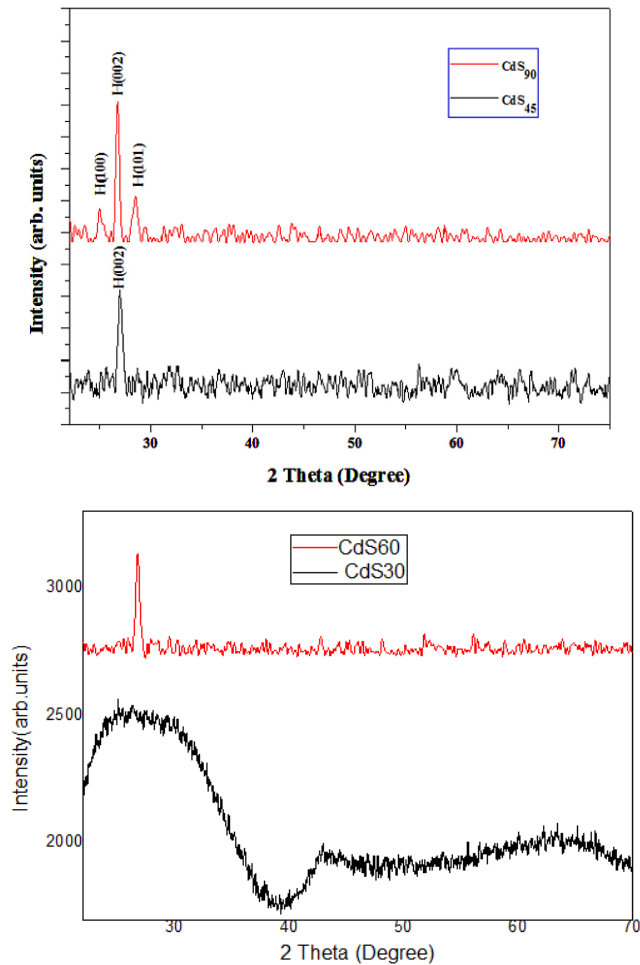


Figure 3.2: XRD spectra of CdS thin films deposited with different times

### 3.1.2.1 Interplanar Spacing and Lattice Constants

The interplanar spacing  $d_{hkl}$  between the different lattice planes is characterized by Miller indices ( $hkl$ ), it can be calculated from the X-ray diffraction profiles using the well known Bragg diffraction law (see eq. 2.8).

The calculated values of  $d_{hkl}$  spacing are recapitulated in Table. 3.I and are matched well with those of the [JCPDS card No: 77 - 2306] data for hexagonal *CdS*. Lattice constants can be determined using the relation for hexagonal systems (see eq. 2.12).

Miller indices and the  $d_{hkl}$  values can be obtained from X-ray diffraction spectrum; hence the lattice parameters  $a$  and  $c$  can be easily calculated from the above mentioned mathematical relations. The obtained values of  $a$  and  $c$  are comparable to standard ones of [JCPDS No: 77 - 2306], these values are illustrated in Table.3.I. From the later table, we can note that the values of both the interplanar spacing  $d_{hkl}$  and the lattice constants of the different peaks of  $CdS$  thin films compared to the reported values of the [JCDPS 77 - 2306] data for hexagonal  $CdS$  are slightly less suggests that the grains of the thin film are under stress and it may be due to the change in the nature and concentration of the native imperfections [6]. With increasing the deposition time from 30 to 90 min the lattice constants and interplanar spacing found to be increased, maybe due to the increase in thickness of the film which in turn reduces the strain in the film (as we will see later) [7, 8].

### 3.1.2.2 Crystallite Size

The crystallite size (D) can be found using the well known Scherer formula (see eq. 2.9).

The crystallite size is enhanced with deposition time; the estimated values are illustrated in Table. 3.I. In Fig. 3.3 we report the variation of crystallite size and growth rate as a function of deposition times.

As can be seen in Fig. 3.3, the grain size changes in the converse sens to the growth rate. This suggests that deposition time affects grain size through its influence on growth kinetics. At a low deposition time the rate of the spontaneous reaction  $Cd^{2+} + S^{2-} \rightarrow CdS$  is relatively high, this results in a rapid nucleation phase and consequently a high growth rate. In other words, when the growth rate is high, the concentration of the nucleation centers is high, so the increasing of the nuclei size is limited and blocked by the nuclei surrounding it, which explains the limited grow of the nuclei. This is in perfect agreement with the result of Gorrer et al. [9], they have reported that an increasing of nuclei number decreases the grain size. Prolonged time decreases the growth rate, which allows the grains to

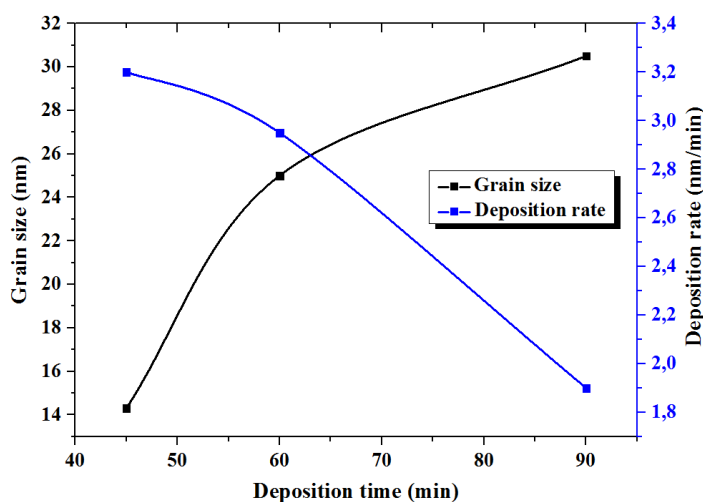


Figure 3.3: Evolution of the grain size and the growth rate of CdS films with deposition time.

increase slowly their size . Since the temperature of the solution is low, prolonged deposition time and slow growth rate allow the grains to reorganize, leading to an improvement in the crystal structure. The average grain size, in general, increases with increasing film thickness which in turn reduces the strain in the film (smaller the grain size more the stress in films) [7].

### 3.1.2.3 Strain and Dislocation

A perfect crystal is an idealization; there is no such thing in nature. Atom arrangements in real materials do not follow perfect crystalline patterns. Nonetheless, most of the materials that are useful in engineering are crystalline to a very good approximation. The XRD method is used to analyze structural parameters such as microstrain and dislocation density. The knowledge of such parameters are important prior to their technical applications. The micro strain ( $\epsilon$ ) and the dislocation density ( $\delta$ ) for an orientation of thin films deposited at different deposition times can be estimated using the formula given previously (eq. 2.14) and (eq. 2.15) respectively, theirs estimated values are represented in Table. 3.I. The micro

strain ( $\epsilon$ ) and the dislocation density ( $\delta$ ) are found to exhibit a decrease trend with deposition times which maybe due to the film thickness, decreases with the thickness maybe due to the reduction in the concentration of lattice imperfections originating from lattice misfit in the film. The decrease in ( $\epsilon$ ) and ( $\epsilon$ ) at higher thicknesses may be due to the movement of interstitial Cd atoms from inside the crystallites to the grain boundary, which in turn leads to a reduction in the concentration of lattice imperfections. With thickness, the strain stemmed from the lattice mismatch between film and substrate during epitaxial growth is relaxed. Typically, films of different materials grown on the previous film or substrate are chosen to match the lattice constant of the prior layer to minimize film stress. In fig. 3.4 we illustrate the variation of the microstrain and the thickness with different deposition times.

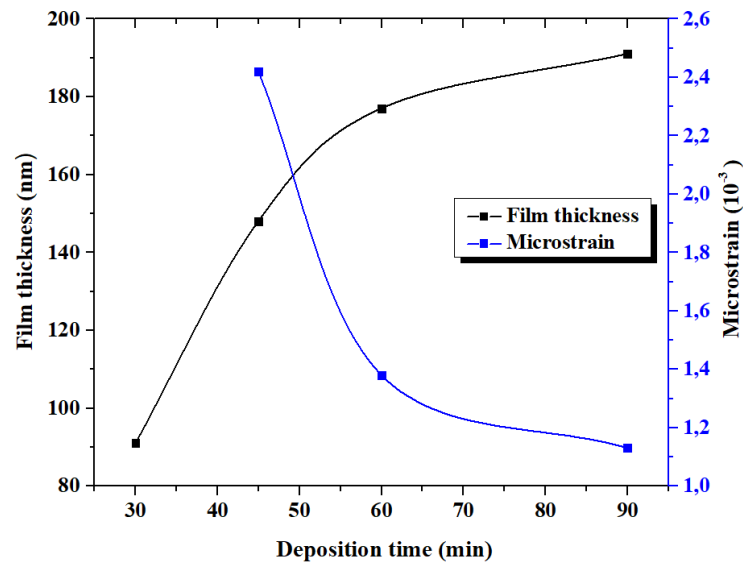


Figure 3.4: Variation of microstrain and thickness with deposition times.

For CBD deposition technique, it is known that there are two possible growth mechanisms: (i) ion by ion process (heterogeneous process) and (ii) cluster by cluster process (homogeneous process) the former process leads to a pure hexagonal structure or mixed cubic and hexagonal however, the later process leads to a pure cubic structure [10, 11]. Thereafter, the presence of the pure hexagonal phase in the deposited *CdS* films suggests that the growth process is achieved through the ion by ion mechanism. This is consistent with the low growth rate of films, several authors [9, 12, 13] have emphasized that the low deposition rate is achieved through ion by ion growth process. From all above observations we inferred that for the experimental conditions used in the present study, *CdS* film growth is exclusively achieved through ion by ion mechanism. This is consistent with our conclusion from XRD analysis. The cluster by cluster mechanism is absent since the later yields porous and highly defected material, which is contrarily to what suggest the structural study.

Material	(hkl)	Intensity		Interplanar spacing (Å)		Lattice constant (Å)		Average grain size (nm)	Dislocation density ( $10^{15}$ lines/ $m^2$ )	Strain ( $10^{-3}$ )
		observed	reported	observed	reported	observed	reported			
<i>CdS</i> <sub>30</sub>	002	100	100	3.312	3.357	$a = 4.081$	$a = 4.136$	14.3	4.89	2.42
		100	100	3.327	3.357	$c = 6.624$	$c = 6.713$			
<i>CdS</i> <sub>45</sub>	002	100	100	3.327	3.357	$a = 4.099$	$a = 4.136$	25.0	1.60	1.38
		100	100	3.573	3.583	$c = 6.654$	$c = 6.713$			
<i>CdS</i> <sub>60</sub>	100	45	100	3.336	3.357	$a = 4.126$	$a = 4.136$	30.5	1.07	1.13
	002	100	100	3.140	3.160	$c = 6.672$	$c = 6.713$			
	101	35								

Table 3.I: Various structural parameters calculated for CdS thin films with different deposition times.

### 3.1.3 Optical properties of the *CdS* thin films

#### 3.1.3.1 Transmittance

In Fig. 3.5, the variation of the optical transmittance in the UV-Visible range, of films deposited with different deposition times are presented. The vertical axis is transmittance of the materials and the horizontal axis is the wavelength of the incident photons. As can be seen, both films exhibit a high transmittance in the visible range; it is in order of 70% to 88% in the case of *CdS*<sub>60</sub> and *CdS*<sub>90</sub>, while, it's in order of 78% to 92% for *CdS*<sub>30</sub> and *CdS*<sub>45</sub> for wavelength greater than 500 nm. As can be observed from the later figure that for the *CdS*<sub>30</sub> and *CdS*<sub>45</sub> films showed relatively very high transmittance compared to the *CdS*<sub>60</sub> and *CdS*<sub>90</sub> films in entire wavelength range studied here, which may be due to its lower thickness. The reduction of the transparency in the long wavelength range more than 500 nm for thicker films may originate from the light scattering on the film surface in one hand and to the film thickness increases with the deposition time on the other hand.

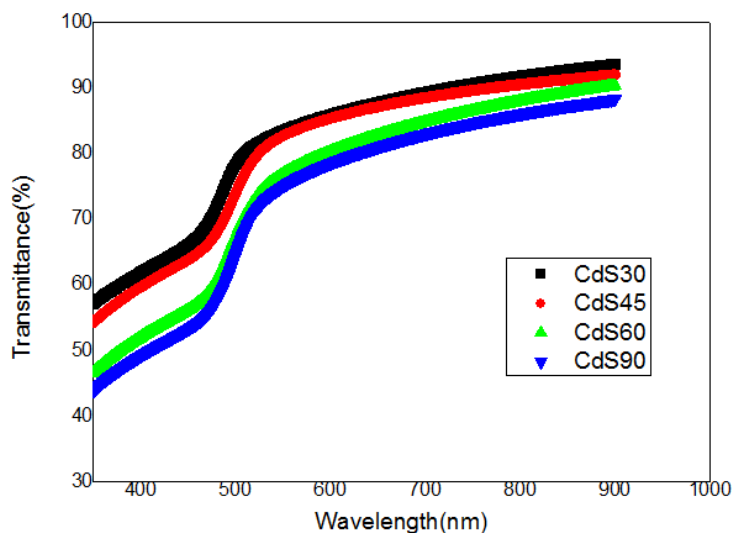


Figure 3.5: Optical transmission spectra of CdS thin films deposited with different times.

### 3.1.3.2 Band gap

The band gap energy of thin films is one of the most important parameters for optical window applications as we have seen in the previous chapter. The optical band gap of *CdS* films can be estimated from the plot of  $(\alpha hv)^2$  as a function of photon energy ( $hv$ ). According to Tauc's relation for direct bang gap semiconductor (see Eq. 2.20)

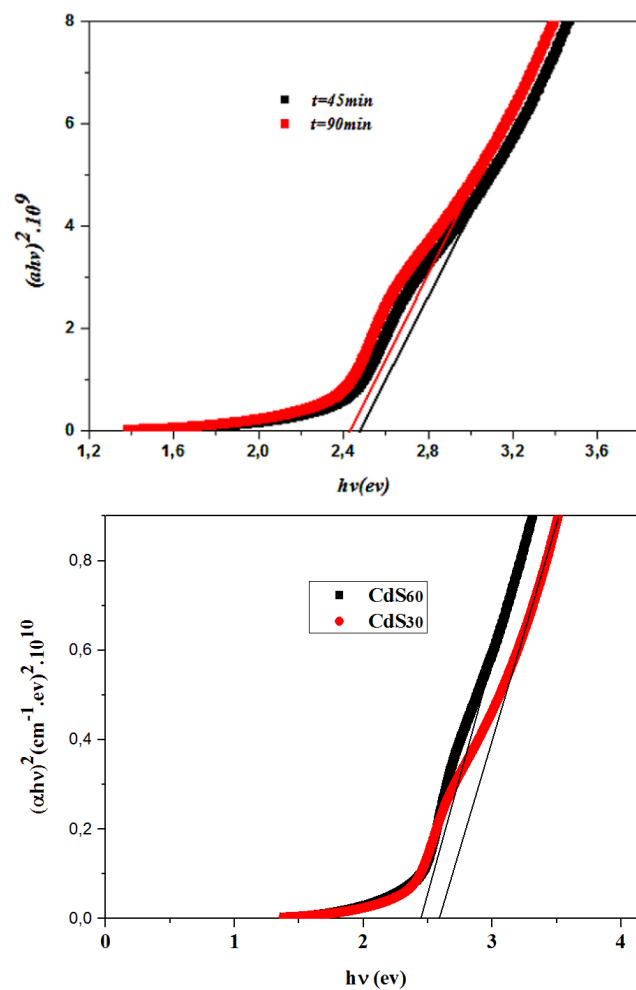


Figure 3.6: Tauc's plot used for determination of optical band gap of CdS thin films.

The optical band gap  $E_g$  values were obtained by extrapolating the straight line portion, of the plot  $(\alpha hv)^2$  versus  $hv$  to the energy axis  $(\alpha hv)^2 = 0$  (where  $\alpha$  is

the absorption coefficient and  $hv$  is the photon energy) as shown in Fig. 3.6. The linearity indicates the existence of the direct allowed transitions. The obtained band gap values for the films deposited with different deposition times are listed in Table. 3.1.3.2. Those values are agreed with ones reported in literature [5, 14, 15].

Deposition time (min)	films	Band gap (ev)
30	$CdS_{30}$	2.58
45	$CdS_{45}$	2.46
60	$CdS_{60}$	2.44
90	$CdS_{90}$	2.42

From Table. 3.1.3.2, we notice that the optical gap of the deposited film is decreased with increasing the deposition time, it varies from 2,58 to 2,42 eV with increasing the deposition time from 30 minutes to 90 minutes, which can be attributed to quantum confinement effect due to the increase in the particle size in CdS thin films [16, 17].

### 3.1.3.3 Urbach energy

Chemical bath deposition is a technique in which the film is grown by chemical reaction of  $S^{2-}$  and  $Cd^{2+}$  ions on the substrate surface or by adhesion of the  $CdS$  clusters from the solution according to the dominant growth mechanism. In such situation, the ions arrive on the substrate can be adsorbed at the point of their incidence. Consequently, the atoms in the film network are not generally in an ideal position, hence the appearance of deviations in the length or angle of the  $Cd - S$  bond. These discrepancies, which are considered as defects "disorder" of structure, are manifested by the appearance of continuous states near the edges of the band [18]. These states are called localized states formed at the tail of the band at the boundaries of the band gap in the valence band and in the conduction band. The Urbach energy  $E_u$ , or the disorder, can be estimated from the inverse slope of the linear plot of  $\log(\alpha)$  versus  $hv$  as we have seen in the previous chapter.

Since this energy is associated with the micro-structural lattice disorder, the variations of the Urbach energy and the microstrain as function of the deposition time are presented in Fig. 3.7. It can be suggested that the variation of deposition times causes an effect on both the disorder and defects in the thin films on one hand and the Urbach energy on the other hand in the same way. Indeed, as shown in Fig. 3.7, a good correlation between the microstrain and the Urbach energy is found. The presence of a band tail for these films indicates that the structural inhomogeneous and disorder are present. In addition, both Urbach energy and microstrain decrease with deposition times which maybe due to the film thickness.

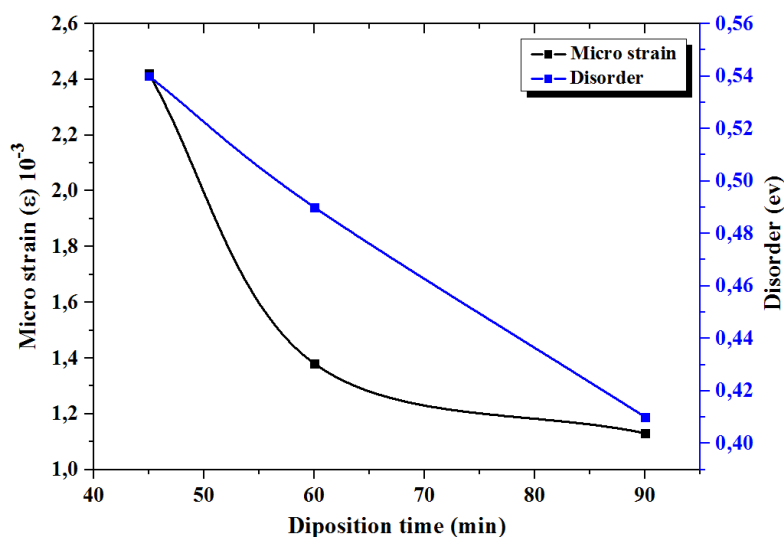


Figure 3.7: Variations of the Urbach energy and the microstrain as function of the deposition time.

## 3.2 Chemical reactions and solution preparation

In order to have an insight on the chemical reactions leading to *CdS* thin films formation, two solutions were prepared separately, (i) solution A (0.0015 M cadmium carbonate ( $CdCO_3$ ), a few drops of sulphuric acid and distilled water) and (ii) solution B (A+ 0.5 ml ammonium hydroxide 27%). In conical flask the

two solutions were constantly stirred for 30 min, and then the precipitates were filtered out and calcined under air condition. (iii) C solution is prepared by mixing ammonia with thiourea. To investigate the calcined product, rest of both A and B solutions, and C solution, Fourier transform infrared (FT-IR) measurements were carried out using (Shimadzu, model IR Affinity-1) working in the range ( $400\text{-}4000\text{ cm}^{-1}$ ).

### 3.2.1 FTIR spectrum of cadmium carbonates ( $CdCO_3$ )

Fig. 3.8 shows the FTIR spectrum in the wave number range ( $400\text{-}4000\text{ cm}^{-1}$ ) of cadmium carbonate ( $CdCO_3$ ) powder which was used as precursor in the present study. A broad absorption band centred at  $3440\text{ cm}^{-1}$  and a small band, around  $1620\text{ cm}^{-1}$ , are due to the  $-OH$  groups stretching vibration [19]. As mentioned in the figure, a strong broad absorption centred at about  $1448\text{ cm}^{-1}$  is connected with the asymmetric stretching vibration which is attributed to the vibrations in  $CO_3^{2-}$  anion. Two absorption bands, strong sharp band at  $852\text{ cm}^{-1}$  and at  $718\text{ cm}^{-1}$  are assigned to the bending out plane vibrations of this anion [20]. FTIR spectrum contains also peaks at  $1795\text{ cm}^{-1}$  and  $2472\text{ cm}^{-1}$  which are expected for  $CdCO_3$ [21].

### 3.2.2 FTIR spectrum of calcined products from A and B

The infrared spectrum for fine calcined powdered samples of A and B were obtained from FTIR in KBr as support in the range  $400\text{-}4000\text{ cm}^{-1}$  and compared with carbonate cadmium one which are represented in Fig. 3.9. It was noticed that all the three spectra are similar in shape. Nuance at around  $3400\text{ cm}^{-1}$  maybe is due to the presence of different amount of humidity in the products. From this similarity one can inferred that the precipitates in both A and B are only an amount of no dissociated carbonate cadmium.

FTIR spectrum of obtained solution after filtration from A ( $CdCO_3$  with water and  $H_2SO_4$ ) is represented in Fig. 3.10. Peaks at  $1054$ ,  $1080$  and  $1180\text{ cm}^{-1}$

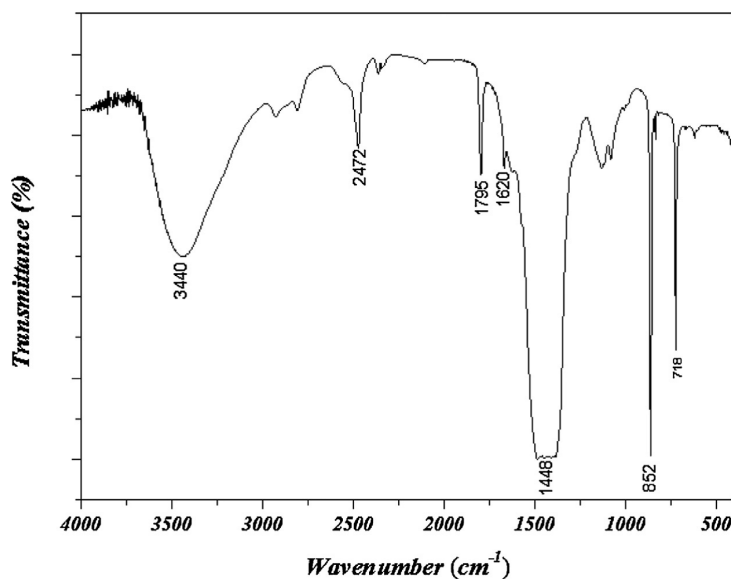


Figure 3.8: FTIR spectrum of carbonate cadmium salt.

indicate the presence of the coordinated  $SO_4^{2-}$  ion [22, 23], whereas peaks at 1633 and  $3443\text{ cm}^{-1}$  are due to OH groups stretching vibration [24, 25]. The spectra shows a peak around  $2360\text{ cm}^{-1}$  is assigned to the antisymmetric stretching mode of  $CO_2$  [26]. Peak at around  $2083\text{ cm}^{-1}$  indicated the presence of  $CO$  [27] which may be formed from  $CO_2$ . From such observations a possible chemical reaction, to describe what has happened in the solution A to lead to free  $Cd^{2+}$ , can be written as follows:



FTIR spectrum of the obtained solution after filtration from B ( $CdCO_3$  with water,  $H_2SO_4$  and  $NH_3$ ) is represented in Fig. 3.11. Peaks at 617, 670 and  $3267\text{ cm}^{-1}$  confirm the presence of  $NH_3$  [28], peak at  $462\text{ cm}^{-1}$  is correlated to the  $Cd - N$  bond [29], Peaks at 981 and  $1103\text{ cm}^{-1}$  are attributed to  $SO_4^{2-}$  [30]. The presence of  $NH_4^+$  is confirmed by the two peaks at 3046 and  $1400\text{ cm}^{-1}$  [31, 32], peaks at 3434 and  $1633\text{ cm}^{-1}$  are due to the  $-OH$  groups stretching vibration

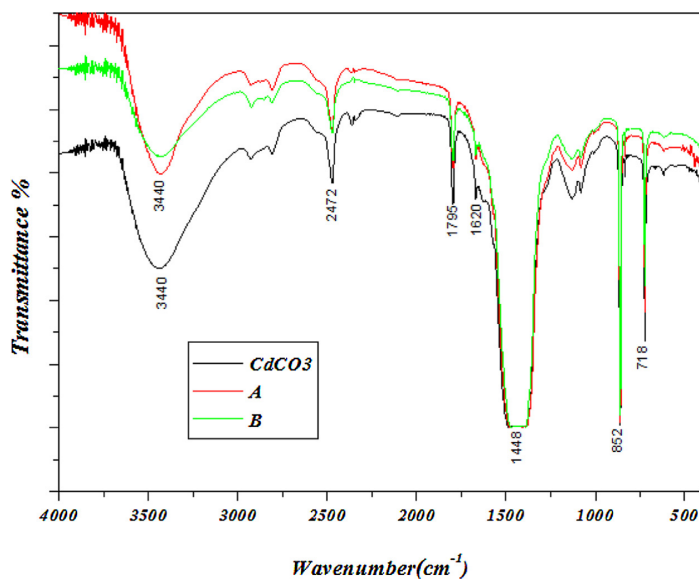
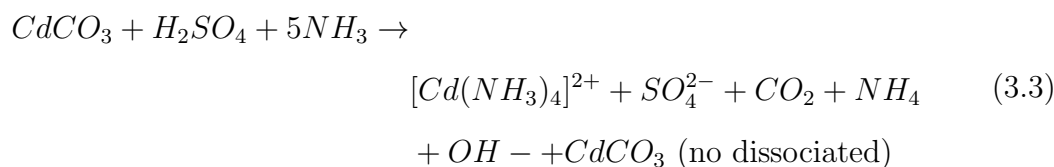


Figure 3.9: FTIR spectrum of carbonate cadmium and calcined powder samples obtained from A and B solutions.

[25, 26]. From all above resulting peaks evidence, the structure of the compound products are:  $SO_4^{2-}$ ,  $NH_4^+$  and cadmium tetramin  $[Cd(NH_3)_4]^{2+}$  complex ion, which reduces the overall speed of reaction. It is worth noting the absence of such peaks at 3531, 3588 and 3607  $cm^{-1}$  [22, 26], which are related to the presence of  $Cd(OH)_2$ , confirming its non-existence in the final state. From such observations a possible chemical reaction to describe what has happened in the solution B can be written as follows:



### 3.2.3 Effect of ammonia on B solution

In other hand, the FTIR of the products of the reaction between ammonia and thiourea  $CS(NH_2)_2$  is given in Fig. 3.12. The peaks obtained at 2065  $cm^{-1}$  and

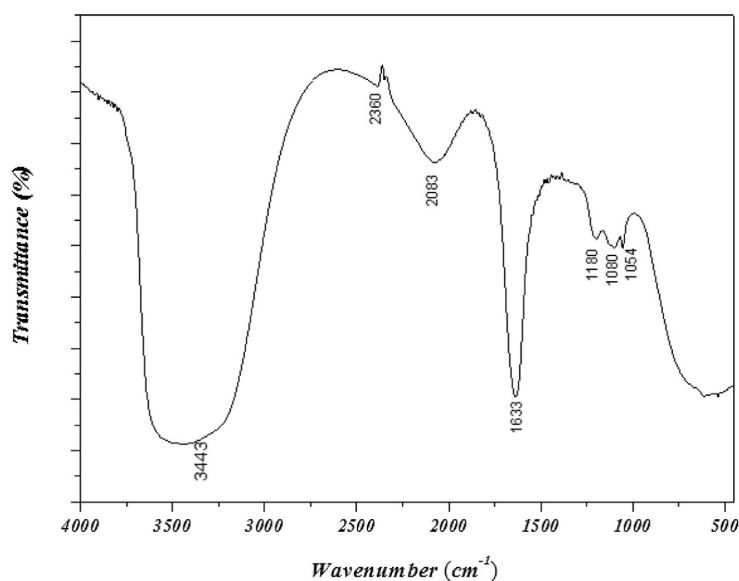


Figure 3.10: FTIR spectrum of residual solution obtained from A.

$1083\text{ cm}^{-1}$  are assigned to  $N \equiv C$  and  $N - C$  respectively [33, 34], while peaks at  $1627$  and  $3376\text{ cm}^{-1}$  are assigned to  $NH_2$  [35], which means the formation of  $(NCNH_2)$ . Peaks at  $1400$  and  $1476\text{ cm}^{-1}$  indicate the presence of  $NH_4^+$  [31, 32], peaks around  $1633$  and  $3434\text{ cm}^{-1}$  which overlap with  $NH_2$  peak completely. The two peaks are assigned to  $H_2O$  [25, 26].

Then, it may be concluded that the reaction of thiourea and ammonia can be written leading to free  $S^{2-}$  ions as follows:



The overall reaction can be written as follow:

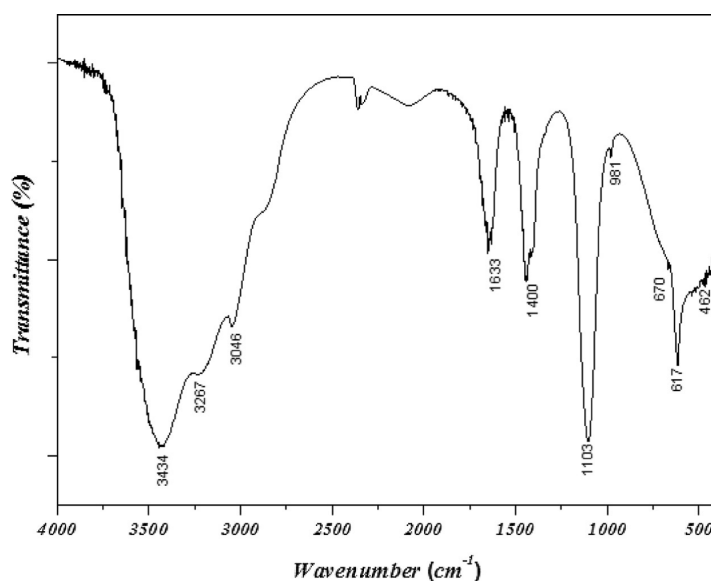
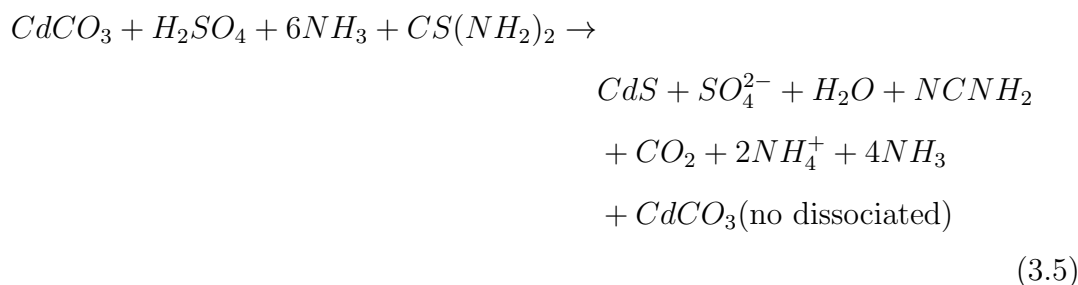


Figure 3.11: FTIR spectrum of residual solution obtained from B.



From the global equation, it's clear that the quantity of ammonia ( $\text{NH}_3$ ) should be more sufficiently to ensure the transformation of  $\text{Cd}^{2+}$  into cadmium tetramin  $[\text{Cd}(\text{NH}_3)_4]^{2+}$  (Eq. (5)) and showing up ( $\text{NH}_4^+$ ,  $\text{OH}^-$ ) as if they formed from equilibrium of ammonia in water:  $\text{NH}_3 + \text{H}_2\text{O} \rightleftharpoons \text{NH}_4^+ + \text{OH}^-$  to make basic solution which is necessary for occurring reaction (6). The later combined with reaction (5) lead to  $\text{CdS}$  thin film formation as shown in schematic illustration below where chain of chemical and mechanism reaction may be proposed as follow:

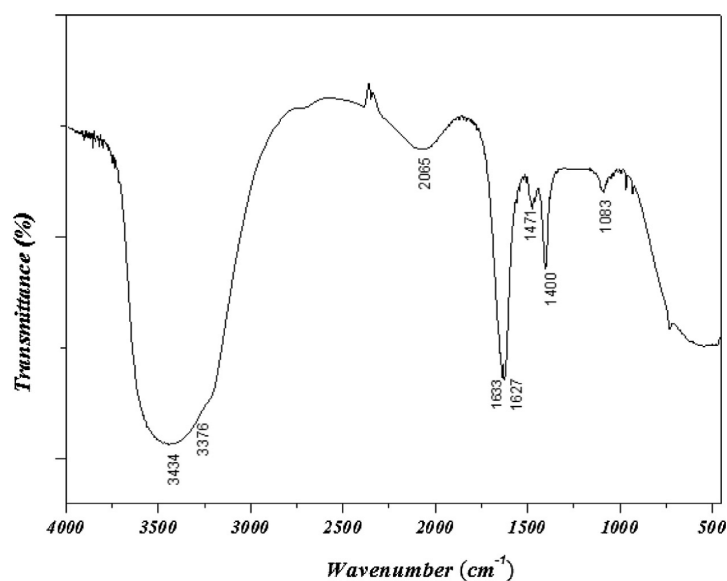


Figure 3.12: FTIR of the products obtained from the reaction between ammonia and thiourea (solution C).

### 3.3 The total elimination effect of $CdCO_3$ on the properties of the $CBD CdS$ thin films

In this part of work,  $CdS$  thin films were prepared in bath solution where all the carbonate cadmium was eliminated from the bath solution by adding enough amount of sulphuric acid.  $CdS$  thin films were prepared for different deposition times 15, 30, 60, 90 min at a low bath temperature of 55 °C. The structural and optical properties have been studied.

#### 3.3.1 Film Thickness and Growth Kinetics

In Fig. 3.14 we report the variation of film thicknesses and growth rate as a function of deposition time from 30 to 90 min. As seen the films thickness increase with deposition time. The growth rate starts with 8.3 nm/min at the beginning and decreases with time to reach 5 nm/min. The solution becomes depleted of ions, resulting in a lower rate of deposition and thickness saturation. The termination

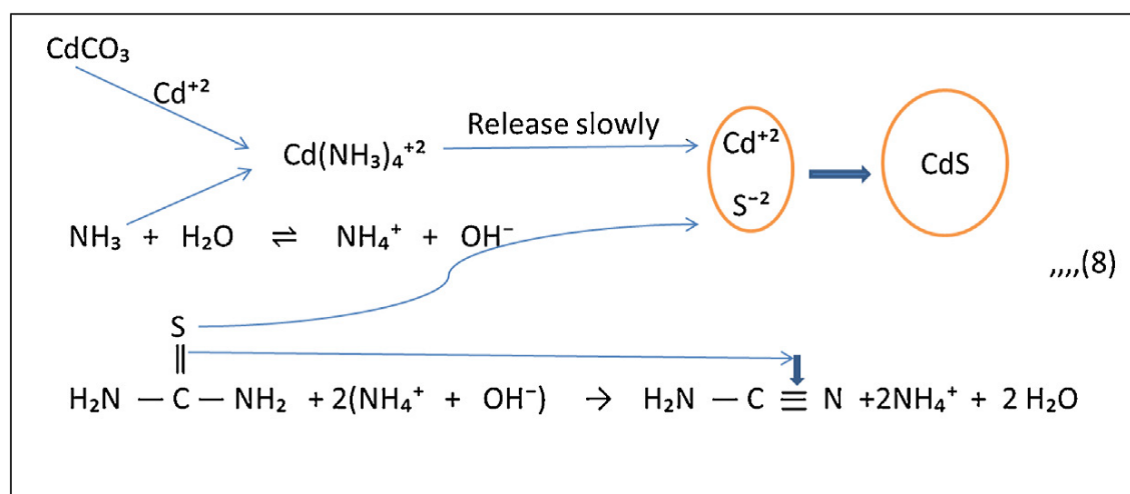


Figure 3.13: Schematic illustration of the formation process of CdS.

time of the deposition depends on the quantity of the starting solution.

### 3.3.2 Results of the XRD measurements

In this study the X-ray diffraction traces of all samples were taken at room temperature. The horizontal axis of the graph is  $(2\theta)$ , twice the Bragg angle and the vertical axis is the intensity count rate.

Fig. 3.15 shows the typical XRD patterns of the prepared CdS thin films grown on the glass substrate at  $55^{\circ}\text{C}$  for different deposition time ranging from 15 to 90 min. The absence of peaks in the patterns of film deposited at 15 min indicates that film deposited in early stage is amorphous. With increasing deposition time to 30 min, a small peak located at the angle  $26.7^{\circ}$  emerges in the XRD spectrum, the latter is assigned the (111) plane of the *CdS* cubic phase or (002) plane of the hexagonal phase. With further increasing deposition time, in addition to the previous peak we notice also the emergence of two minor peaks at  $44.3$  and  $51.9^{\circ}$ , that confirmed the cubic nature of the films, corresponding to reflection from the (220) and (311) planes in the *CdS* cubic structure [JCPDS card No: 80 - 0019]. The main obtained results suggested that increasing deposition time yields to a cubic phase structure with a preferred orientation in the (111) plane. The

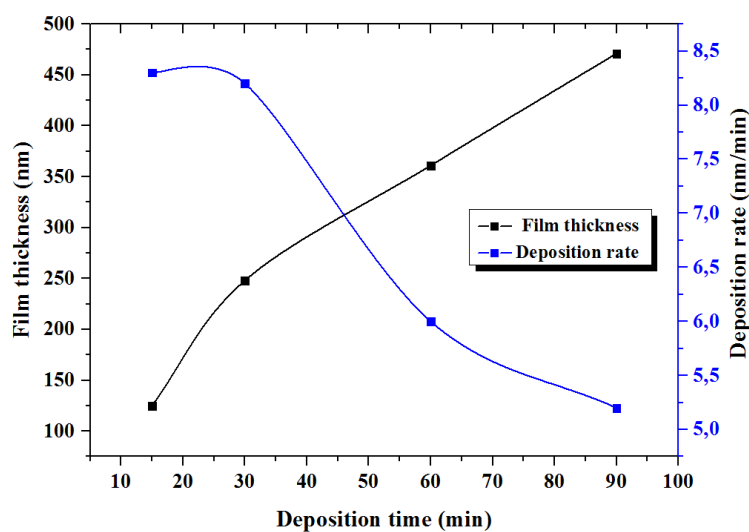


Figure 3.14: Variation of film thicknesses and growth rate as a function of deposition times.

same results were obtained by many authors [36, 37, 38]. By comparing the peak positions in the XRD patterns of the samples some information about substrate mismatch and/or lattice defects can be derived. From detailed investigation of position of peak corresponds to (111) plane, a shift in peak positions of the samples ( $CdS_2$ ,  $CdS_3$ ,  $CdS_4$ ) was determined towards higher  $2\theta$  values with decreasing deposition time. This shift indicates the presence of an increasing lattice strains in the film structures. On other side, as can be seen in Fig. 3.15, when the time deposition equal to 30 min, the films present a peak which corresponds to the plane (111), this peak indicates that the ion-by-ion deposition process tends to promote the preferred orientation for growth. beyond 60 min of deposition time, the homogeneous deposition occurs and the cluster-by- cluster mechanism becomes more and more dominant. The peaks associated with the planes (311) and (220) emerge, corresponding to the aggregations of the  $CdS$  particles [39], indicating that the crystallization of the films gradually intensifies with the long deposition times, the growth during the last stage occurs by the formation of clusters on the surface or by the adhesion of the clusters from the solution.

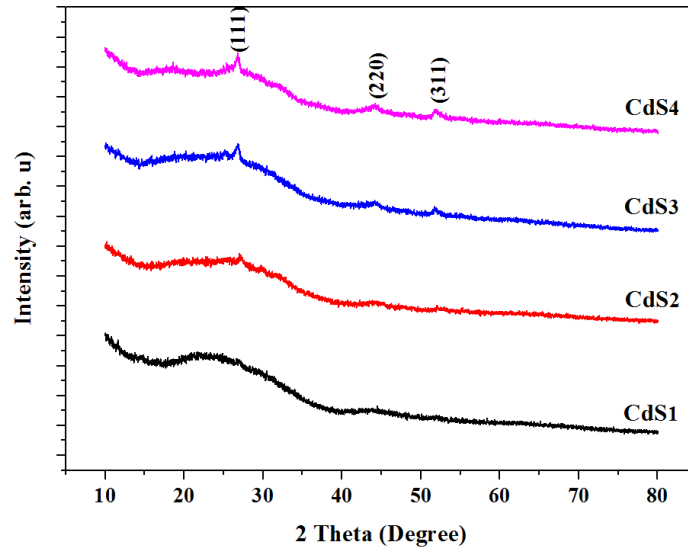


Figure 3.15: XRD spectrum of CdS thin films under different deposition times.

### 3.3.2.1 Interplanar Spacing and Lattice Constants

The interplanar spacing  $d_{hkl}$  can be calculated from the X-ray diffraction profiles using the well known Bragg diffraction law (see eq. 2.8), while the lattice constants can be determined using the relation for cubic systems (eq. 2.11). Their obtained values are reported in Table. 3.II. From these values we can notice that with increasing the deposition time the lattice constants and interplanar spacing found to be increased, maybe due to the increase in thickness of the film which in turn reduces the strain in the film [7, 8]. These values are in good agreement with those reported for *CdS* cubic structure in [JCPDS card No: 80 - 0019].

### 3.3.2.2 Crystallite Size

The crystallite sizes can be found using the Scherrer formula (eq. 2.9). The crystallite size is enhanced with deposition times, the estimated values are illustrated in Table. 3.II. In Fig. 3.16, we report the variation of crystallite sizes and growth rate as a function of deposition times.

As can be seen in Fig. 3.16, the grain size changes in the converse sens to

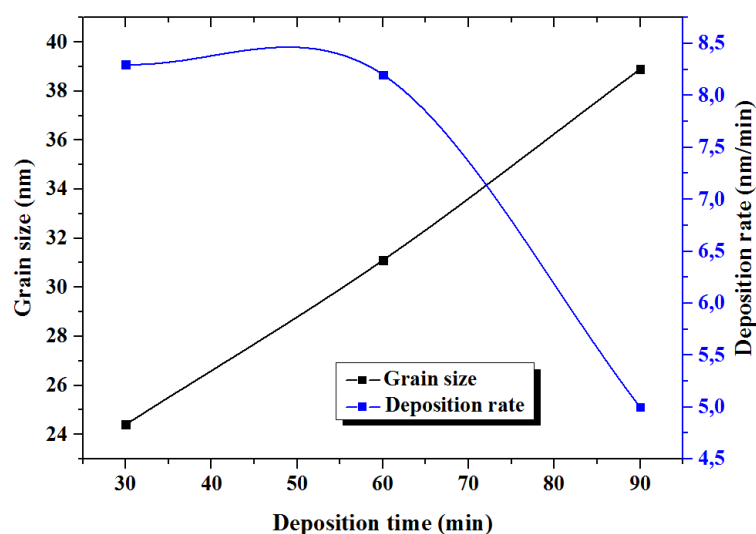


Figure 3.16: Variation of crystallite size and growth rate as a function of deposition times.

the growth rate. This suggests that deposition time affects grain size through its influence on growth kinetics. When the growth rate is high, the concentration of the nucleation centers is high, so the increasing of the nuclei size is limited and blocked by the nuclei surrounding it, which explains the limited grow of the nuclei. Prolonged time decreases the growth rate, which allows the grains to increase slowly their size . Since the temperature of the solution is low, prolonged deposition time and slow growth rate allow the grains to reorganize, leading to an improvement in the crystal structure.

### 3.3.2.3 Strain and Dislocation

Microstrain and dislocation density were estimated using the formula given previously (eq. 2.14) and (eq. 2.15) respectively and their values are represented in the Table. 3.II, its clear that both strain and dislocation decrease with deposition times, which may due the film thickness as we have explained earlier.

Material	(hkl)	Intensity		Interplanar spacing (Å)		Lattice constant (Å)		Average grain size (nm)	Dislocation density ( $10^{15}$ lines/ $m^2$ )	Strain ( $10^{-3}$ )
		observed	reported	observed	reported	observed	reported			
<i>CdS</i> <sub>1</sub>	-	-	-	-	-	-	-	-	-	-
<i>CdS</i> <sub>2</sub>	111	100	100	3.314	3.350	5.763	5.818	24.4	0.94	1.06
<i>CdS</i> <sub>3</sub>	111	100	100	3.321	3.350	5.794	5.818	31.1	0.60	0.85
	220	43	47	2.047	2.054					
	311	29	35	1.750	1.752					
<i>CdS</i> <sub>4</sub>	111	100	100	3.324	3.583	5.807	5.818	38.9	0.36	0.65
	220	46	47	2.048	2.054					
	311	42	35	1.753	1.752					

Table 3.II: Various structural parameters calculated for CdS thin films with different deposition times

### 3.3.3 Optical properties of the *CdS* thin films

#### 3.3.3.1 Transmittance

The variation of optical transmittance spectra as a function of wavelength was recorded for the *CdS* thin films deposited with different deposition times in the wavelength range 300 - 900 nm in the Fig. 3.17. As can be seen, the transmittance in the range 600 to 900 nm ; it is in order of 40 to 80%. Its also noticed that for both films deposited at 60 and 90 min exhibit a law transmittance. The reduction in the transparency in films deposited after 60 min of deposition time can be explained by the thickness and the optical losses through the light diffraction at the top film surface. The latter loses its smoothness with increasing deposition time, due to the deposition process transition from the heterogeneous (ion-by-ion) to the homogeneous ones (cluster-by-cluster), as generally recognized and reported previously.

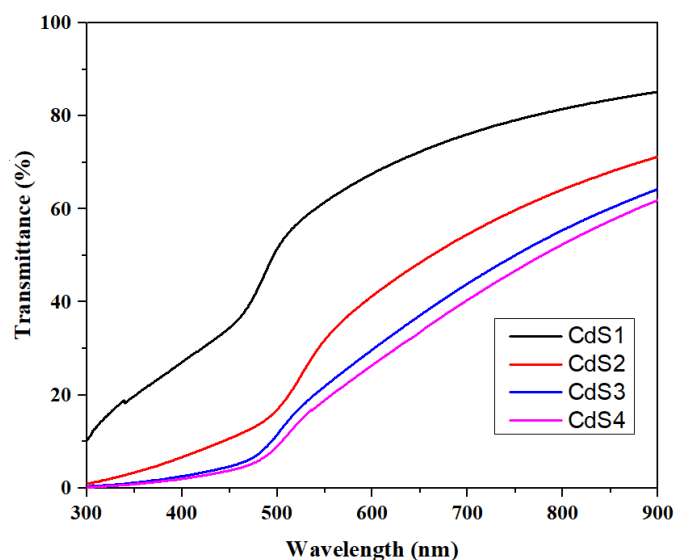


Figure 3.17: Optical transmission spectra of *CdS* thin films deposited with different times.

### 3.3.3.2 Band gap and disorder

From the transmittance spectra we have estimated the optical band gaps  $E_g$  and the disorder  $E_u$  in the  $CdS$  thin films according to the methods described in the previous chapter. It is well known, that the growth of chemically-deposited  $CdS$  thin films occurs as a result of both ion-by-ion condensation of the impinging particles ( $Cd^{2+}$ ,  $S^{2-}$ ) and colloidal particle formation of  $CdS$  adhering to the substrate surface, therefore, the atoms in the thin films are not generally in a typical position, hence the appearance of deviations in the length or angle of the  $Cd-S$  bond, which are considered as defects of structure. These defects serve as recombination centers, formed at the tail of the band at the boundaries of the band gap in the valence and conduction bands, which is capable of receiving one type of carrier and capturing the other, thereby annihilating the pair. The width of the band located near the conduction or valence bands are generally called Urbach energy  $E_u$  [40].

Fig. 3.18 shows the variation of  $(\alpha \cdot E)^2$  as a function of photon energy ( $h\nu$ ) for different deposition times, which have been used for the estimation of optical band gap values. In Fig. 3.19 we have reported the variation of the optical gap together with the band tail width as a function of the deposition times. The optical gap variation with the deposition time is opposite to the disorder variation. This suggests that the optical gap is controlled by the disorder in the film network.

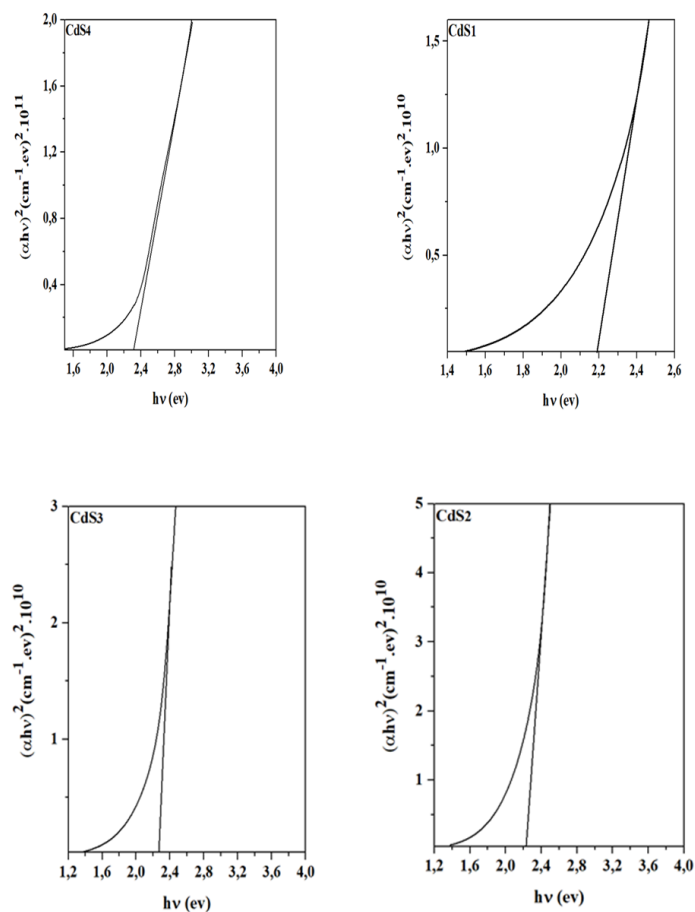


Figure 3.18: Tauc's plot used for determination of optical band gap of CdS thin films.

For CBD deposition technique, it is known that there are two possible growth mechanisms: (i) ion-by-ion process (heterogeneous process) and (ii) cluster-by-cluster process (homogeneous process) the former process leads to a pure hexagonal structure or mixed cubic and hexagonal. However, the later process leads to a pure cubic structure. Thereafter, the presence of the pure hexagonal phase in the deposited *CdS* films suggests that the growth process is achieved through the ion-by-ion mechanism. This is consistent with the low growth rate of films. Several authors have emphasized that the low deposition rate is achieved through ion-by-

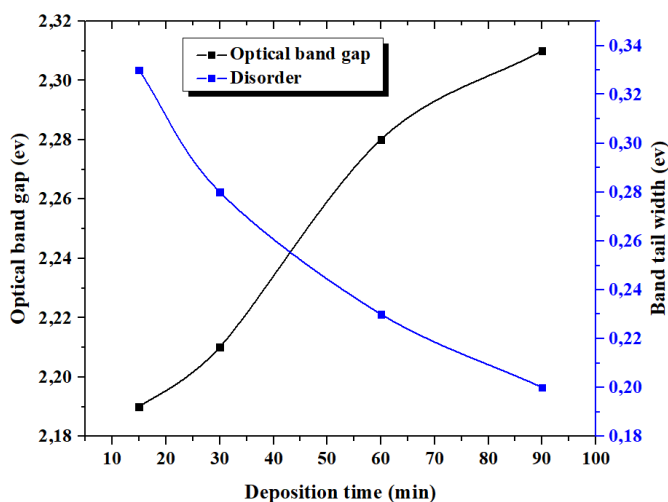


Figure 3.19: Variation of the optical gap and the band tail width as a function of the deposition times.

ion growth process. The obtained *CdS* thin films of the first set of this work are of pure hexagonal structure, since the growth rate was relatively low, we believe that this may indicate that the deposition process was dominated by ion-by-ion deposition and not by cluster-by-cluster deposition conversely to the films of the second set. This suggests that the existence of  $CO_3^{2-}$  ( $CdCO_3$ ) in the solution leads up to minimize the deposition rate, maybe it acts as a second complexing agent with ammonia leading to a slower release of  $Cd^{2+}$  ions. Hexagonal structure is mostly recommended due to its higher stability relative to the cubic structure. High quality *CdS* hexagonal films were obtained. Both films were found to be highly transparent, with  $E_g$  around 2.4 eV.

## References

- [1] D. Fernando, M. Khan, Y. Vasquez, *Materials Science in Semiconductor Processing* 30 (2015) 174 – 180
- [2] R. Call, N. Jaber, K. Seshan, J. Whyte, *Sol. Energy Mater.* 2 (1980) 373
- [3] I. Kaur, D. K. Panday, K. L. Chopra, *J. Electrochem. Soc.* 127 (1980) 943
- [4] A.Y. Jaber, S. N. Alamri, M. S. Aida, *Thin Solid Films* 520 (2012) 3485 - 3489
- [5] K.S. Ramaiah, R.D. Pilkington, A.E. Hill, R.D. Tomlinson, A.K. Bhatnagar, *Mater. Chem. Phys.* 68 (2001) 22-30
- [6] C. Agashe, M.G. Takwale, B.R. Marathe, V.G. Bhide, *J. Mater. Sci.* 24 (1989) 2628 – 2636
- [7] V. A. Shchukin, D. Bimberg, *Rev. Mod. Phys.* 71 (1999) 1125
- [8] M. Pinczlit, G. Spingholz, G. Bauer, *Appl. Phys. Lett.* 73 (1998) 250
- [9] S. Gorer, G. Hodes, *J. Phys. Chem* 98 (1994) 5338.
- [10] K. Ravichandran, P. Philominathan, *Appl. Surf. Sci.* 255 (2009) 5736
- [11] H.E. Maliki, J.C. Bernede, S. Marsillac, J. Pinel, X. Castel, J. Pouzet, *Appl. Surf. Sci.* 205 (2003) 65
- [12] I. Kaur, D. K. Pandya, K. L. Chopra, *J. Electrochem. Soc.* 127 (1980) 943
- [13] H. Khallaf, I. O. Oladeji, L. Chow, *Thin Solid Films* 516 (2008) 5967
- [14] A. I. Oliva, O. Solis-Canto, R. Castro-Rodriguez, P. Quintana, *Thin Solid Films* 391 (2001) 28 – 35
- [15] T. Nakanishi, K. Ito, *Sol. Energy Mater. Sol. Cells* 35 (1994) 171 – 178
- [16] Y. Wang, N. Herron, *J. Phys. Chem.* 95 (1991) 525
- [17] A. S. Obaid, M. A. Mahdi, Z. Hassan, M. Bououdina, *International Journal of Hydrogen Energy* 38(2013) 807–815
- [18] C. D. Lokhande, K. M. Gadave, *J. Phys.* 18 (1994) 83 – 87
- [19] W. Hanke, K. Miiller, *Zeolites* 4 (July 245) (1984)
- [20] M. Chávez Portillo, L. A. Chaltel Lima, U. Peñna Rosas, G. Hernández Téllez, R. Gutiérrez Pérez, O. Portillo Moreno, *Mater. Lett.*

120 (2014) 130 Ű 132

- [21] C. S. Patterson, D. Carson, A. Phenix, H. Khanjian, K. Trentelman, J. Mass, C. Hirschmugl, *e-Preserv. Sci. (e-PS)* 10 (2013) 1 Ű 9
- [22] G. Y. Zhang, D. Peak, *Geochim. Cosmochim. Acta* 71 (2007) 2158Ű2169
- [23] S. V. Lalonde, L. T. Dafoe, S. G. Pemberton, M. K. Gingras, K. O. Konhauser, *Chem. Geol.* 271 (2010) 44 Ű 51
- [24] G. Della Ventura, F. Radica, F. Bellatreccia, C. Freda, M. CestelliGuidi, *Phys. Chem. Minerals* 42 (2015) 735Ű745
- [25] M. Ristic, S. Popovic, S. Music, *Mater. Lett.* 58 (2004) 2494 Ű 2499
- [26] S. A. Sandford, F. Salama, L. J. Allamandola, L. M. Trafton, D.F. Lester, T.F. Ramseyer, *Icarus* 91 (1991) 125 Ű 144
- [27] J. Sárkány, *Top. Catal.* 18 (February) (2002) 3 Ű 4
- [28] K. Nakamoto, *Infrared and Raman Spectra of Inorganic and Coordination Compounds*, Sixth ed, John Wiley Sons, (2009)
- [29] R. K. Singh, R. Srivastava, M. N. Kamlasanan, *J. Nano. Electron. Phys.* 3 (1) (2011) 514 Ű 520
- [30] L. Pejov, V. M. Petrusovski, *J. Mol. Struct.* 482Ű483 (1999) 257 Ű 262
- [31] D. Podsiadla, O. Czupinski, *J. Mol. Struct.* 889 (2008) 251 Ű 258
- [32] J. Regalbuto, *Catalyst Preparation: Science and Engineering*, CRC Press, Taylor Francis, (2007)
- [33] N. Kharasch, *Org. Sulfur Compd.* 1 (1961)
- [34] L. Xia, R. L. McCreery, *J. Electrochem. Soc.* 146 (10) (1999) 3696 Ű 3701
- [35] J. T. J. Prakash, L. R. Nirmala, *Int. J. Comput. Appl.* 6 (7) (2010) 0975-8887
- [36] S. Mahanty, D. Basak, F. Rueda, M. Leon, *J. Electron. Mater.* 28 (5) (1999)
- [37] S. Soundswarm, O. Senthil Kumar, R. Dhanasekaran, *Mater. Lett.* 58 (2004) 2381
- [38] H. Moualkia, S. Hariech, M.S. Aida, *Thin Solid Films* 518 (2009)

1259-1262

[39] Y. Liu, T. Tang, B. Wang, R. Zhai, X. Song, E. Li, H. Wang, H. Yan,  
Journal of Colloid and Interface Science 320 (2008) 540

[40] F. Urbach, Phys. Rev. 92 (1953) 1324

# Chapter 4

## Characterization of *PbS* thin films

This chapter deals with the detailed characterization of PbS thin films grown by the *CBD* process as discussed in the previous chapter. In particular, this chapter presents the effects of deposition time and the concentration of lead nitrate  $\text{Pb}(\text{NO}_3)_2$  on the evolution of crystal structural and optical properties of the *CBDPbS* thin films.

### 4.1 Effect of deposition time

#### 4.1.1 Evolution of crystal structure

##### 4.1.1.1 Results of the XRD measurements

XRD analyses were employed to study the crystal structures of the films. Fig. 4.1 shows the typical XRD patterns of PbS thin films grown on the glass substrate at 55 °C for different deposition times (30, 45, 60 and 90 min), analyzed over the diffraction angle  $2\theta$  between 5 and 100 °.

In the XRD as the deposition time was increased, a clear evolution of multiple peaks was observed. indicating polycrystallinity of the films. For all samples, the XRD pattern were characterized by seven peaks, namely at about 25.96°, 30.07°, 43.05°, 50.97°, 53.41°, 62.54° and 70.96°. These peaks were identified with the planes corresponding to the (111), (200), (220), (311), (222), (400), and (420)

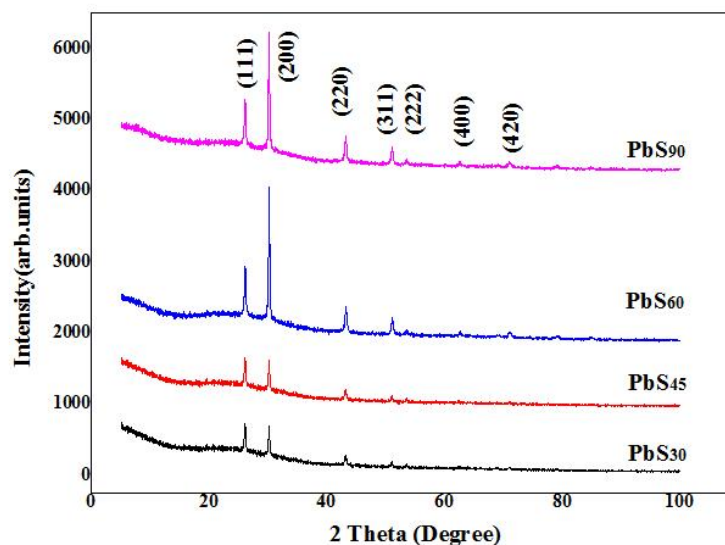


Figure 4.1: XRD spectra of PbS thin films deposited with different deposition times.

planes of the *PbS* face centered cubic structure respectively. They are confirmed by comparing the peak positions ( $2\theta$ ) of the XRD patterns of the films with the standard X-ray diffraction data file [JCDPS card: 05 - 0592]. It can be noticed from the XRD pattern that a pair of peaks is followed by a single peak, which is again followed by a pair. This is a typical characteristic observation of a face centered cubic structure [1]. It is also noticed, that as the deposition time increased the peaks become narrower, indicative of improved crystallinity. In literature many researchers have attributed this to the merger of smaller crystallites and growth of the crystallites with simultaneous increase in the film thickness. As we can notice that all the samples are preferentially oriented along the (200) direction which is perpendicular to the substrate and which intensity depends on the deposition time value. Quantitative analysis based on Gauss fit to the (200) peak, the highest intensity peak, revealed that the intensity gradually increased reaching its maximum for a growth time equal to 60 min, while the FWHM of the peak decreased as the deposition time was increased. However, for time equal to 90 min, the intensity of (200) decreases and the FWHM increases.

This effect for films deposited from 30 to 60 min can be related to the increase of both, thickness and grain size of the *PbS* films with. Similar results were obtained by [2, 3]. However, for time deposition equal to 90 min, the intensity of (200) decreases, that might have been due to the depletion of the *Pb* and *S* ions in the solution. Fig. 4.2 shows the thickness variation of *PbS* thin films as a function of deposition time. The growth phase ( $t < 60$  min) at which the thickness is obtained in a linear dependence. It increases steadily with dipping time up to 60 min to reach the max value and then the terminal phase in which the growth slows down. We can conclude the uniformity, the good adhesion and the best crystallinity of *PbS* thin films on glass substrate is obtained for an immersion time equal to 60 min from the bath described above. A similar tendency in the increase in the thickness of the chemical bath deposited *PbS* thin films with increasing immersion time throughout the deposition regime has been observed by other authors [4, 5]. The phenomenon of increase and decrease of thickness films can be explained by considering two competing processes taking place in the deposition bath: one process includes the heterogeneous and homogenous precipitation of *PbS*, which leads to the film growth; the other one involves the dissolution of the preformed *PbS* film, which result in the decrease of film thickness. In the initial time of deposition, the source materials are sufficient; the process of heterogeneous and homogenous precipitation play a more important role than the dissolution process, leading to the increase in film thickness. When the deposition time is prolonged (above 60 min in our case), the source materials become less. Therefore, the dissolution process predominates over the heterogeneous and homogeneous precipitation, resulting in the decrease of film thickness. It was also observed that the peak positions remained slightly constant, although the deposition time increased from 30 to 90 min. The absence of any other prominent diffraction peaks indicates that no other crystalline phases, such as oxides or carbonates of *Pb*, exist with detectable concentration within the layers. Therefore, the obtained films are of pure *PbS*. The two main properties extracted from peak width analysis are the crystallite size and lattice

strain, while the interplanar spacing and lattice constants can be estimated from the peak position ( $2\theta$ ).

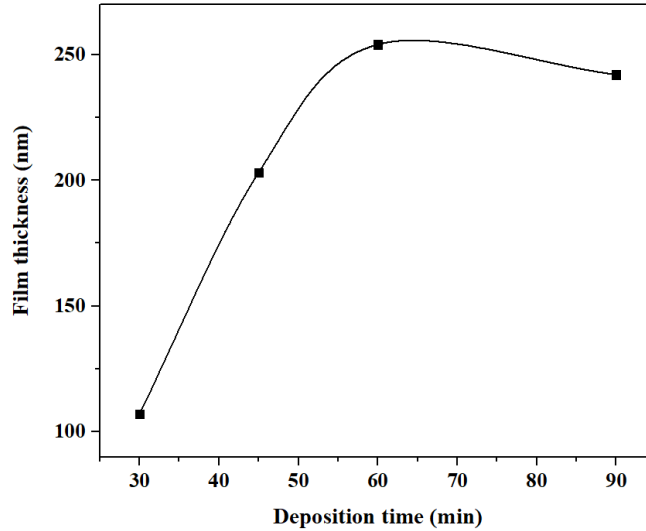


Figure 4.2: Variation of film thicknesses as a function of deposition times.

#### 4.1.1.2 Crystallite Size

The crystallite sizes of the films as a function of deposition time are determined by measuring full width at half maximum of each peak using the Debye-Scherrer formula (eq. 2.9), these values are shown in Table. 4.1.1.3. We notice that the crystallite size enhances with increasing deposition time to be 27.8 nm for deposition time 60 min and then decreases to be 26.5 nm for 90 min as duration of deposition, these obtained values are similar to reported values [2], similar behavior with that observed for the thickness. The observed increase in the crystallite size with deposition time is due to the complete deposition process occurring. The latter passes through the nucleation, coalescence stage and the subsequent vertical growth, in other word When the deposition process begins, many nucleation centers and small crystallites on the substrate are produced during the deposition process. For a short deposition time, the small crystallites on the substrate are

not able to grow into large crystallites, therefore the thinner films have smaller crystallites than the thicker films. With increasing immersion time, film thickness increases hence, the crystallinity of the films is improved and the crystallite sizes become larger.

#### 4.1.1.3 Interplanar Spacing and Lattice Constant

The values of interplanar spacing  $d_{hkl}$  can be calculated from the X-ray diffraction profiles using the Bragg condition (eq. 2.8) and lattice constant  $a$  were determined using the relation for cubic systems (eq. 2.11). Table. 4.1.1.3 displays the values of interplanar spacing and lattice constant for  $PbS_{30}$ ,  $PbS_{45}$ ,  $PbS_{60}$  and  $PbS_{90}$  thin films. From the Table. 4.1.1.3, we can note that the observed values of the different peaks of  $PbS$  thin films are slightly less compared to the reported values of the [JCDPS card: 05 0592] data for cubic  $PbS$  structure. This finding clearly indicates that crystallization and stress result in compression of the lattice constant [6]. The lattice constant and interplanar spacing found to be increased as deposition time was increased which maybe due to the increase of the film thickness. Generally the change in lattice constant and interplanar spacing for the thin film deposited up on the substrate suggests that the grains of the thin film are under stress and it may be due to the change in the nature and concentration of the native imperfections. This may cause either elongation (tensile) or compression of the lattice parameters, in our case compression, a compressive stress would make the  $d$  spacings and  $a$  smaller than the standard values.

Table. 4.1.1.3. Also displays the values of relative diffraction peak intensities for  $PbS_{30}$ ,  $PbS_{45}$ ,  $PbS_{60}$  and  $PbS_{90}$  thin films. Its clear for all films that the intensities increase with time deposition up to 60 min, beyond this time decrease. This effect can be related to the increase of thickness and particle size of the  $PbS$  films with deposition time. Its clear that the main features of the diffraction patterns are similar and only the peak intensity varied, Obaid et al [6] explained this observation by the presence of preferential orientation of crystallites as well as

the formation of texture within the prepared films.

Material	(hkl)	Intensity		Interplanar spacing (Å)		lattice constant (Å)		Grain size (nm)	Average grain size (nm)
		observed	reported	observed	reported	observed	reported		
<i>PbS</i> <sub>30</sub>	111	90	84	3.4067	3.4273	5.9156	5.9362	26.6	21.9
	200	100	100	2.9606	2.9681			27.0	
	220	30	57	2.0952	2.0988			23.4	
	311	14	35	1.7858	1.7898			10.6	
<i>PbS</i> <sub>45</sub>	111	96	84	3.4113	3.4273	5.9171	5.9362	25.8	24.8
	200	100	100	2.9584	2.9681			27.6	
	220	35	57	2.0912	2.0988			22.8	
	311	16	35	1.7874	1.7898			22.9	
<i>PbS</i> <sub>60</sub>	111	35	84	3.4261	3.4273	5.9354	5.9362	31.6	27.8
	200	100	100	2.9649	2.9681			36.8	
	220	18	57	2.0921	2.0988			20.5	
	311	11	35	1.7929	1.7898			22.4	
<i>PbS</i> <sub>90</sub>	111	40	84	3.4167	3.4273	5.9241	5.9362	27.7	26.5
	200	100	100	2.9621	2.9681			32.3	
	220	23	57	2.0969	2.0988			23.6	
	311	16	35	1.7873	1.7898			22.7	

Table 4.I: Various structural parameters calculated for PbS thin films with different disposition times.

#### 4.1.1.4 Strain, Dislocation and texture coefficient

The micro strain ( $\epsilon$ ), average stress ( $S$ ), the dislocation density ( $\delta$ ) and the texture coefficient ( $TC$ ) of thin films deposited at different deposition times were calculated and are represented in Table. 4.1.1.4. The later parameters ( $\epsilon$ ), ( $S$ ), ( $\delta$ ) and ( $TC$ ) of the samples are calculated by using the relations: (eq. 2.14, eq. 2.13, eq. 2.15 and eq. 2.16) respectively.

The micro strain ( $\epsilon$ ) and the dislocation density ( $\delta$ ) are found to exhibit a slow decreasing trend with increase of deposition times which in turns increases the thickness of the films. In Fig. 4.3, we can notice that the thickness increases until its max at 60 min then decreases, while the dislocation density decreases until its min at 60 min then increases.

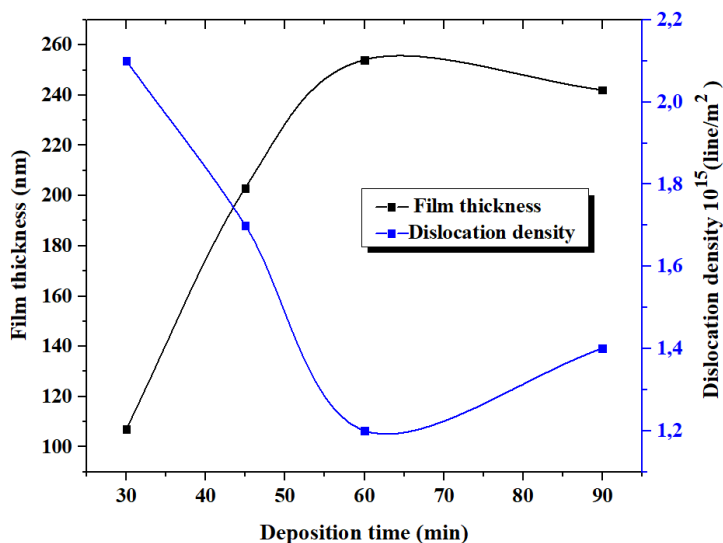


Figure 4.3: Variation of film thicknesses and dislocation density as a function of deposition times.

The average internal stress for the lead sulphide thin films deposited at different deposition times is found to be compressional in nature. The negative sign indicates that the films may be in a state of compressive stress. The total stress in the film commonly consists of two components. One is the intrinsic stress may be arise due to impurities, defects and lattice distortions in the crystal, and the other is the extrinsic stress arise due to the lattice mismatch and thermal expansion coefficient [7, 8]. It is observed that with increase deposition time the average internal stress increases, that maybe do to the increase of the film thickness with dipping time.

The texture coefficient  $TC$  represents the texture of a particular plane, whose deviation from unity implies the direction of preferred growth. The value of  $TC(hkl) = 1$  represents randomly oriented crystallites, while the higher values indicate the abundance of grains oriented in a given  $hkl$  direction [8]. From the Table. 4.1.1.4. The highest  $TC$  was obtained for (200) plane for all deposition times 30, 45, 60, and 90 min.

Samples	Dislocation density ( $10^{15}$ lines/ $m^2$ )	Strain ( $10^{-3}$ )	Average stress $\sigma$ (GPa)	TC(hkl)%
<i>PbS</i> <sub>30</sub>	2.1	1.9	-0.44	9.62
				10.68
				3.20
				1.49
<i>PbS</i> <sub>45</sub>	1.7	1.5	-0.40	9.71
				10.12
				3.54
				1.62
<i>PbS</i> <sub>60</sub>	1.2	1.2	-0.16	5.34
				15.24
				2.74
				1.68
<i>PbS</i> <sub>90</sub>	1.4	1.3	-0.25	5.59
				13.97
				3.21
				2.23

Table 4.II: Various structural parameters calculated for PbS thin films with different disposition times.

## 4.1.2 Optical properties of the PbS thin films

### 4.1.2.1 Transmittance

Typical transmittance spectra for *PbS* thin films obtained for different deposition times are presented in Fig. 4.4, for the thinner film (i.e, deposition time of 30 min), the maximum transmittance in the wavelength range of 300 to 1200 nm remained less than 30 %. As observed from the Fig. 4.4, the 30 min film showed very high transparency compared to the other films in the entire wavelength range studied here owing to its small thickness. With increase in deposition time, the transmittance decreased gradually due to the increased of the thickness of the films. These results can be explained through the film morphology, as the film thickness increases the grain size increases too, as we mentioned previously, the surface roughness increases with increasing grain size which led to decrease in transmission. The lower transmittance, which is the ideal for use as p-type material in a solar cell.

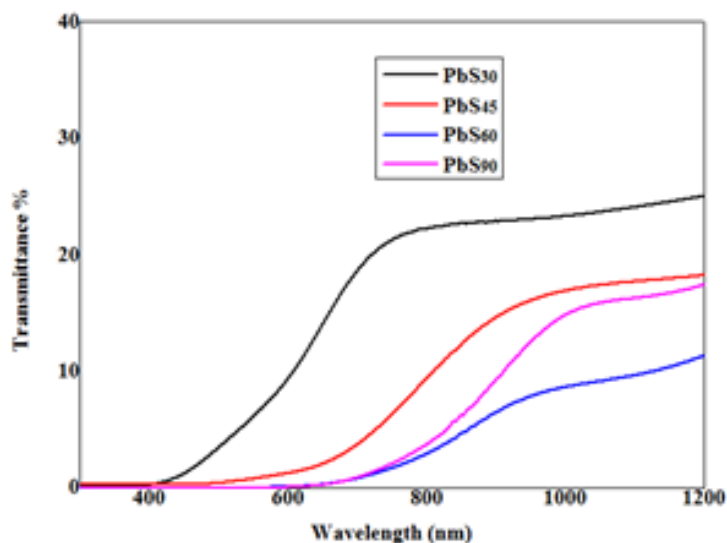


Figure 4.4: Wavelength dependence of transmittance of *PbS* thin films deposited for different durations.

Fig. 4.4 shows that all the films have no transmittance in the ultraviolet UV region below 400 nm which is due to the strong absorbance in this region. Thereafter, the transmission increases with increasing wavelength towards the NIR regions. It's also observed a shifting of the transmittance towards the long wavelength with the time deposition.

#### 4.1.2.2 Absorbance

Fig.4.5 shows the optical absorption spectra recorded for the *PbS* thin films for different deposition times. It is observed that the shapes of the curves were similar although differences in absorbency were observed. The absorption increases with increasing deposition time, thereby the absorbance of the films increased with the thickness which shows that thicker films have more atoms present hence more states are available for the photon energy to be absorbed [9]. It is clear that the films have high absorption at short wavelength range of 375 - 550 nm (above 70 % absorbance for both  $PbS_{60}$  and  $PbS_{90}$ , around 50 % for  $PbS_{45}$ ), except for  $PbS_{30}$  the range is around 375 - 425 with absorption less than 50 %. Then, the

absorption decreases at different rates dependence on the films structure to reach constant values at long wavelengths ( 850 nm), where the films become transparent at this wavelengths.

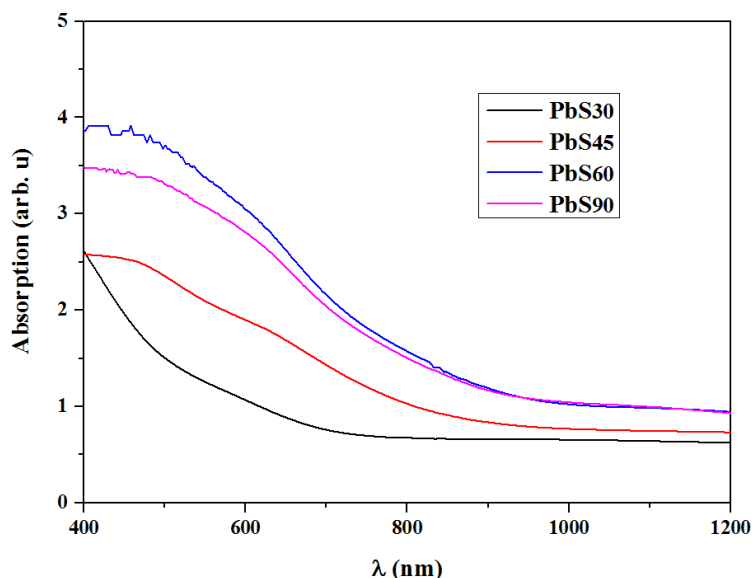


Figure 4.5: Absorbance versus wavelength of *PbS* thin films deposited for different durations.

#### 4.1.2.3 Reflectance

Fig.4.6 shows the reflectance spectra of films deposited at 55 °C for different deposition times. It is observed that the reflectance decreases with increasing deposition times. Also, it is observed that the reflectance of all the films increases with increasing wavelength in the range of 400-850. Thereafter, it seems to be slightly constant at 60 to 65 % depending on the deposition time.

#### 4.1.2.4 Energy band gap

As mentioned in chapter 2, the band gap of the films was determined from the plots of  $(\alpha hv)^2$  vs  $(hv)$ . The linear portion of the curves was extrapolated to the zero value of y-axis to determine the band gap.

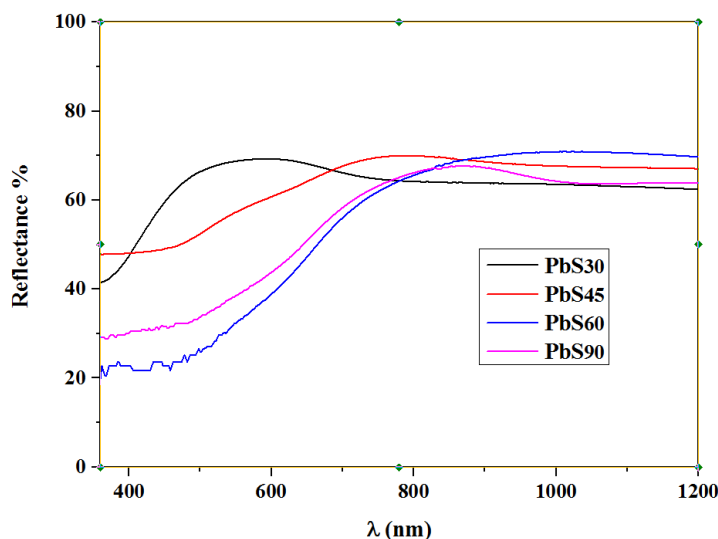


Figure 4.6: Reflectance versus wavelength of *PbS* thin films deposited for different durations.

Fig. 4.7 shows the variation of  $(\alpha hv)^2$  vs the photon energy ( $hv$ ) for the films deposited at 55 °C for different deposition times (30, 45, 60 and 90 min). A linear least-square fitting was carried out in the linear portion of the curves to determine the band gap.

The estimated values of the band gap for different deposition times are illustrated in the Table. 4.1.2.5. These values are much higher than the 0.4 eV reported for the bulk PbS [10], this shift phenomenon was reported in the literature by several authors [11, 12]. This phenomenon has been attributed to the quantum size effect [11, 13]. The quantum size effect causes a perturbation in the electronic structure, the conduction and valence band are broken down to discrete states resulting in the widening of the forbidden band gap compared to the bulk [14, 15]. As the diameter of the semiconductor crystallite approaches to the exciton Bohr diameter, its electronic properties start to change. Thus, one observes an increase in the band gap of the semiconductor with a decrease in the particle size [11, 12]. It is found that  $E_g$  decreased from 1.80 to 1.60 eV as the deposition time was increased may be due to the increase in the crystallite size following the crystallite

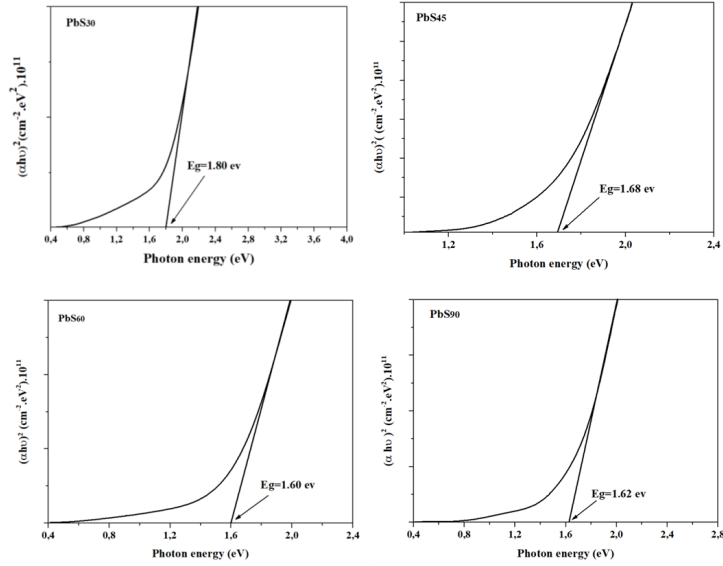


Figure 4.7: Plot of  $(\alpha hv)^2$  vs the photon energy ( $hv$ ) of the *PbS* thin films deposited at 55 °C for different time durations.

size dependant properties of the energy band gap [16]. In literature, similar band gaps for films having small crystallite sizes were reported by many authors [6, 17]. However, in the present case, the crystallite size is in the range of 21.9 - 26.5 nm as estimated from the analysis of XRD patterns which is not much higher than the Bohr radius of *PbS* which is around 20 nm [18] .

#### 4.1.2.5 Urbach energy

The band tail width (commonly called Urbach energy) is related to the disorder in the film network. The disorder is due to the presence of weakly bonded atoms, it corresponds to the deviation of bond distance and angle from their standard value in the crystalline structure. These band tail states are responsible of the sub-gap absorption in the low energy range, the spectral dependence of the absorption edge follows the well known Urbach formula [19]. The tail width  $Eu$  in the energy gap were obtained by plotting  $\ln(\alpha)$  as a function of  $(hv)$ , and the value of  $Eu$  extracted from the reciprocal slope of the linear part. The estimated values of the Urbach energy for different deposition times are illustrated in the Table. 4.1.2.5.

Deposition time (min)	Band gap ( $E_g$ )(ev)	Tail width ( $E_u$ ) (ev)
30	1.80	0.943
45	1.68	0.769
60	1.60	0.526
90	1.62	0.568

Table 4.III: Estimated values of the Urbach and band gap energies for different deposition times.

The variations of the film disorder and optical band gap as function of deposition time are represented in Fig. 4.8. As seen the disorder decreases with increasing the deposition time up to 60 min, beyond this time it increases that is maybe due to the film thickness which increases with the duration of deposition up to 60 min then reduces, the particle size changes around a certain limiting value, where the band gap energy decreases with increasing cristallite size[20]. Therefore, both band gap energy and Urbach energy decrease with deposition times up to 60 min then increase as shown in Fig. 4.8.

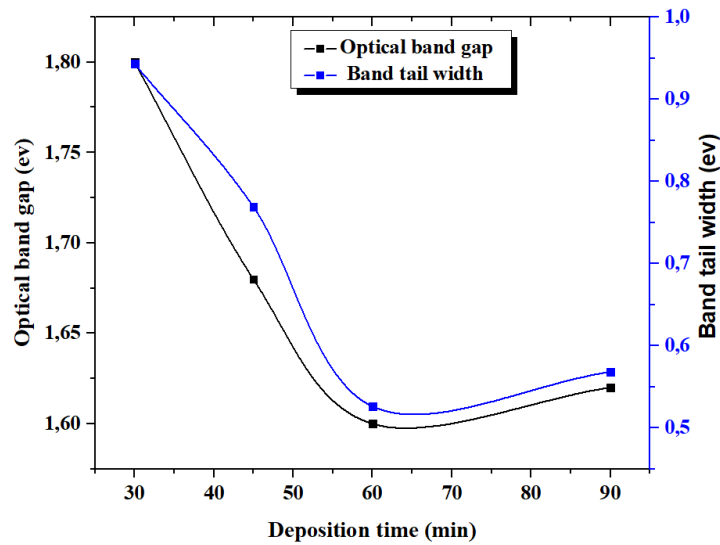


Figure 4.8: Variation of the films disorder and optical band gaps as function of deposition times.

There is a significant change in the interplanar spacing, lattice constant, crystal-

lite size, transmittance and so on ... for different deposition times. The crystallite size increases with increasing deposition time. The crystallite size of the *PbS* film deposited for 60 min was found to be 27.8 nm, which is similar to reported values [1, 2] and 203 nm as thickness with optical band gap of 1.60 eV which are suitable for solar cell. We can conclude the uniformity, the good adhesion and the best crystallinity of *PbS* on glass substrate is obtained for an immersion time equal to 60 min from the bath described above, therefore, we have selected 60 min deposition time for further studies.

## 4.2 Effect of lead nitrate concentration

### 4.2.1 Evolution of crystal structure

In this study we set deposition time at its optimal value equal to 60 min and various molar concentrations (0.01, 0.05, 0.075 and 0.1) mol/l of lead nitrate  $Pb(NO_3)_2$  in the final solution were used, we reduced the concentration of lead ions while keeping the rest of parameters the same. The films are abbreviated as *PbS*<sub>1</sub>, *PbS*<sub>2</sub>, *PbS*<sub>3</sub>, and *PbS*<sub>4</sub> respectively.

Fig. 4.9 shows the typical XRD patterns of *PbS* thin films grown on the glass substrate at 55 °C for different concentration of lead nitrate  $Pb(NO_3)_2$  with deposition time equal to 60 min, analyzed over the diffraction angle  $2\theta$  between 20° and 80°.

Fig. 4.9 shows the XRD pattern of the *PbS* thin films deposited for various molar concentrations. The crystallography of the films is good and characterized by five principal peaks at  $2\theta$  values of approximately 26.09, 30.19, 43.06, 50.94 and 53.41°, corresponding to (1 1 1), (2 0 0), (2 2 0), (3 1 1), and (2 2 2) planes of the face centered cubic (*fcc*) structure of *PbS* respectively. They are confirmed by comparing the peak positions  $2\theta$  of the XRD patterns of the films with the standard X-ray diffraction data file [JCDPS card: 05 0592]. The narrow peaks confirmed that the material has good crystallinity. It was observed that the films grow preferentially

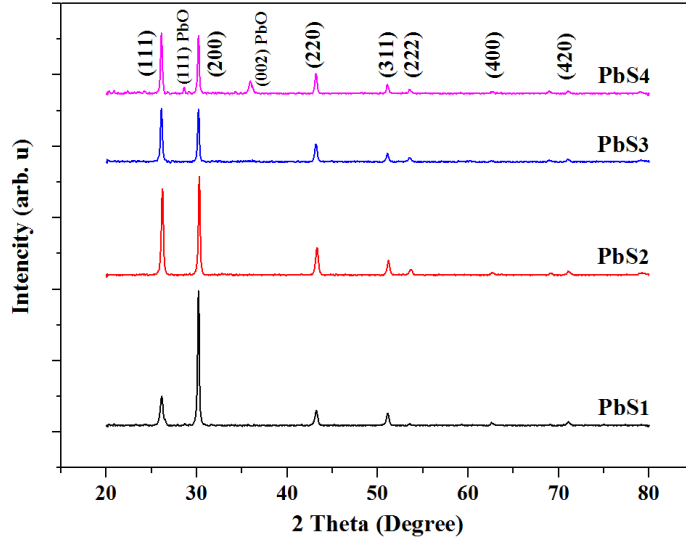


Figure 4.9: XRD pattern of the *PbS* thin films deposited for various molar concentrations.

along (111) or (200) directions depending on the molar concentration, the same result is reported by many researchers [13, 21]. It was also observed a preferred orientation growth along the (2 0 0) direction for *PbS*<sub>1</sub> and *PbS*<sub>2</sub> samples, while for *PbS*<sub>3</sub> and *PbS*<sub>4</sub> the preferred orientation growth is (111) plane indicating the three dimensional growth of the as deposited film. It was noticed that the intensity of the (1 1 1) peaks increases with increasing the lead nitrate concentration from 0.01 to 0.1 mol/l, the same observation is reported by Preetha et al.[17]. As result, the intensity of the growth of crystallographic orientation and microstructure of the films depend on  $Pb^{2+}$  ion concentration in the solution of the deposition process. Table. 4.2.1 shows that peak ratio of (111)/(200) is (0,2) at less concentration, when we increased the concentration of lead nitrate, the peak ratio of (111)/(200) also increased up to (1,08) value. The values of the intensity ratios  $(I_{111})/(I_{200})$  and  $(I_{220})/(I_{200})$  for different lead nitrate concentrations are indicated in Table. 4.2.1.

Table. 4.2.1 Variation of *PbS* peak orientation degree as a function of the lead nitrate concentration. From the table 4.2.1 we can notice that the peak ratio

Sample	$(I_{111})/(I_{200})$	$(I_{220})/(I_{200})$
$PbS_1$	0.20	0.13
$PbS_2$	0.86	0.28
$PbS_3$	1.02	0.34
$PbS_4$	1.08	0.35

Table 4.IV: Variation of  $PbS$  peak orientation degree as a function of the lead nitrate concentration.

of  $(I_{111})/(I_{200})$  is reduced to 20/100, when we lowered the concentration of lead that is an indicative that decreased  $Pb^{2+}$  ion concentration favors growth along (200) plane. This can be explained by the fact that when  $Pb^{2+}$  ion concentration decreases, the reaction rate slows down enough to allow progressive deposition on the substrate ( ion-by-ion process )and chances of rapid precipitation of  $PbS$  salt decrease and hence nucleation growth increases. While increasing the lead nitrate concentration increases the free  $Pb^{2+}$  concentration in the bath solution. One effect of this is that the reaction rate is increased, cluster by cluster is believed to occur, leading to difficulties in obtaining high quality  $PbS$  thin films and formation of lead oxide phases became more probable and the favors growth along (111) plane. One of the most important aspect revealed from these patterns is the growth of lead oxide at  $2\theta$  equal to  $28,74^\circ$  and  $35,90^\circ$  for  $PbS_4$  corresponding to (111) and (002) planes of lead oxide phase  $PbO$  according to [JCPDS No: 35 - 1482] unlike other samples. This observation means that an oxidation occurred during the preparation, it may be due to the imperfections in the ratio of cations to anions either due to the presence of extra cations in the interstitial sites when the lead nitrate concentration increases, the same behavior was seen by many authors [22, 23].

#### 4.2.1.1 Film Thickness and deposition rate

There is by no means a single way to measure the thickness of a given thin film. The different methods have different strengths and weaknesses. Studying the

light reflected or transmitted by a thin film can reveal information about the film thickness. Thin film interference is a natural phenomenon in which light waves reflected by the upper and lower boundaries of a thin film interfere with one another, either enhancing or reducing the reflected light. The light reflected from the upper and lower surfaces will interfere. The degree of constructive or destructive interference between the two light waves depends on the difference in their phase. This difference in turn depends on the thickness of the film layer. When the thickness of the film is an odd multiple of one quarter-wavelength of the light on it, the reflected waves from both surfaces interfere to cancel each other. Since the wave cannot be reflected, it is completely transmitted instead. When the thickness is a multiple of a half-wavelength of the light, the two reflected waves reinforce each other, increasing the reflection and reducing the transmission. The films thickness were estimated from the reflectance spectra. In Fig. 4.10 we report the variation of film thicknesses and growth rate as a function of lead nitrate concentration. From the later figure, it is observed that lead ion concentration has marked effect on film thickness. The film thickness initially increases with an increase in the lead nitrate concentration until 0.05 M, beyond this concentration the film thickness it decreases, the same behavior for the deposition rate. The observed results can be explained on the basis of ion-by-ion condensation. At a particular temperature  $PbS$  will be deposited if the ionic product of  $Pb^{2+}$  and  $S^{2-}$  exceeds the solubility product. The  $Pb^{2+}$  ions are released from lead nitrate-TEA complex due to hydrolysis; while sulfide ions  $S^{2-}$  are provided by dissociation of thiourea in an alkaline medium combine at the nucleation centers on the substrate to produce  $PbS$ . The quantity of ions utilized for film formation depends on the rate of formation of  $PbS$  on the substrate surface, which in turn, depends on the rate of release of  $Pb^{2+}$  and  $S^{2-}$  ions. As we reduce the concentration of  $Pb^{2+}$  ions in chemical bath, the release of  $Pb^{2+}$  from its complex becomes slow and the whole deposition process slows down, as a result chances of rapid precipitation of  $PbS$  decrease and that of nucleation growth at the substrates increase. Due to increased nucleation growth,

the growth along (200) plane dominated and as a result thickness of *PbS* film also increased. We can note that for a  $[Pb(NO_3)_2]$  equals to 0.05 M, the quantity of  $Pb^{2+}$  is high enough, so it favours the growth of lead sulphide thin films with a maximum thickness. As far as lead nitrate concentration exceeds 0.05 M, that increases the free  $Pb^{2+}$  concentration in the bath solution. One effect of this is that cluster by cluster process is believed to occur, and the precipitation becomes very fast leading to difficulties in obtaining high quality *PbS* thin films and formation of lead oxide phases became more probable, so the solution becomes depleted of ions which reduce *PbS* deposited on the substrate, resulting in a lower rate of deposition, the growth along (111) plane dominated and the terminal thickness of *PbS* layer decreases. The result seems to affirm that the nucleation rate is mainly controlled by the concentration of  $Pb^{2+}$  ions in solution, which results in the development of *PbS*.

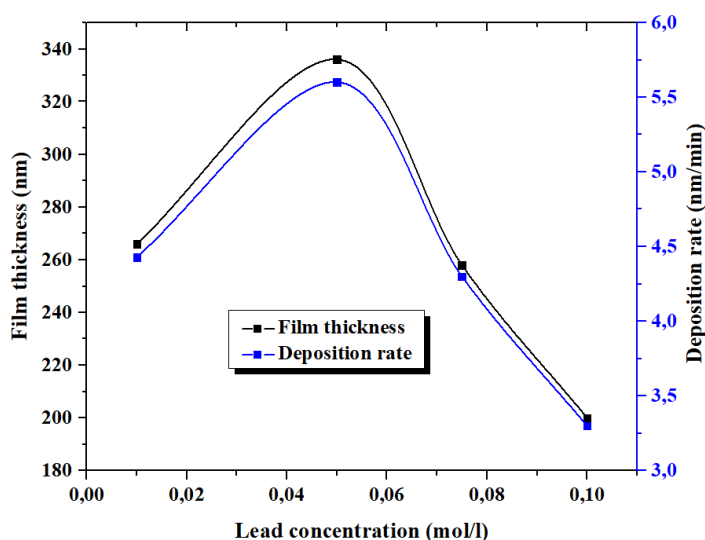


Figure 4.10: Variation of film thicknesses and growth rate as a function of lead nitrate concentrations.

#### 4.2.1.2 Interplanar Spacing, Lattice Constants and Crystallite Size

The average lattice constant ( $a$ ) is calculated from the measured lattice constant ( $a$ ) obtained by using the observed values of  $2\theta$  for the four principal peaks of the  $PbS$  thin films, the average values is found to be increased from 5.914 to 5.925 nm with increasing molar concentration, which clearly indicates that the crystallization and stress result in lattice compression [14]. These values are summarized in Table. 4.V The same behaviour for the interplanar spacing is observed. The values of the crystallite sizes of the films as a function of lead nitrate concentration are determined by measuring full width at half maximum (FWHM) of the diffraction peak corresponding to a particular crystal plane using the Debye-Scherrer formula [24], these values are shown in Table. 4.V. We notice that the calculated crystallite size value enhances with increasing molar concentration, from 28,0 up to 32,6 nm for the molar concentration ranging from 0.01 to 0.1 mol/l. This is in good agreement with the results reported in the literature [25, 26].

#### 4.2.1.3 Strain, Dislocation and texture coefficient

The average internal stress for the lead sulphide thin films deposited with different lead nitrate concentration is found to be compressional in nature. The negative sign indicates that the films may be in a state of compressive stress. It is observed that with increase of lead nitrate concentration the average internal stress decreases. The micro strain ( $\epsilon$ ) and the dislocation density ( $\delta$ ) are found to exhibit a slow decreasing trend with increase of lead nitrate concentration.

The texture coefficient ( $TC$ ) represents the texture of a particular plane, where the deviation from unity implies the direction of a preferred growth [27].

The variation of ( $TC$ ) for  $PbS$  thin films diffraction peaks are reported in Table. 4.VI. The highest ( $TC$ ) value was obtained for (200) plane for  $PbS_1$  and  $PbS_2$ , while for  $PbS_3$  and  $PbS_4$  the highest value was obtained for (111) plane. In other word for less concentrations (200) plane and (111) plane for high concentrations, that is exactly what we have seen previously.

Material	(hkl)	Intensity		Interplanar spacing (Å)		lattice constant (Å)		Grain size (nm)	Average grain size (nm)
		observed	reported	observed	reported	observed	reported		
<i>PbS</i> <sub>1</sub>	111	20	84	3.4078	3.4273	5.917	5.936	32.9	30.9
	200	100	100	2.9621	2.9681			35.7	
	220	13	57	2.0943	2.0988			27.1	
	311	9	35	1.7844	1.7898			28.2	
<i>PbS</i> <sub>2</sub>	111	86	84	3.4142	3.4273	5.924	5.936	35.1	32.6
	200	100	100	2.9630	2.9681			37.7	
	220	28	57	2.0952	2.0988			29.3	
	311	15	35	1.7890	1.7898			28.2	
<i>PbS</i> <sub>3</sub>	111	100	84	3.4142	3.4273	5.913	5.936	33.5	29.5
	200	96	100	2.9592	2.9681			30.3	
	220	32	57	2.0948	2.0988			27.2	
	311	17	35	1.7844	1.7898			27.0	
<i>PbS</i> <sub>4</sub>	111	100	84	3.4013	3.4273	5.910	5.936	33.1	28.0
	200	93	100	2.9591	2.9681			31.1	
	220	33	57	2.0938	2.0988			22.0	
	311	15	35	1.7844	1.7898			26.2	

Table 4.V: Various structural parameters calculated for PbS thin films with different lead nitrate concentrations.

## 4.2.2 Optical properties of the *PbS* thin films

### 4.2.2.1 Transmittance-Reflectance

The reflectance spectra of *PbS* thin films deposited at different molar concentration were displayed in Fig. 4.11. It is observed that the shapes of the curves were similar although differences in reflectivity were observed. From the reflectance spectra of the films we can notice that the reflectivity increased with the thickness. In all cases, a clear interference pattern is seen which confirm that the *PbS* films have uniform thickness and good surface homogeneity [28], therefore, it has been used to estimate the thickness of the films. Thin films interference is a natural phenomenon in which as light strikes the surface of a film, it is either transmitted or reflected at the upper surface. Light that is transmitted reaches the bottom surface and may once again be transmitted or reflected. The light reflected from the upper

Samples	Dislocation density ( $10^{15}$ lines/ $m^2$ )	Strain ( $10^{-3}$ )	Average stress $\sigma$ (GPa)	TC(hkl)%
<i>PbS</i> <sub>1</sub>	1.14	1.11	-0.41	3.5
				17.61
				2.29
				1.58
<i>PbS</i> <sub>2</sub>	0.94	1.04	-0.24	9.39
				10.91
				3.06
				1.64
<i>PbS</i> <sub>3</sub>	1.18	1.15	-0.47	10.20
				9.80
				3.26
				1.73
<i>PbS</i> <sub>4</sub>	1.26	1.28	-0.52	10.37
				9.65
				3.42
				1.56

Table 4.VI: Various structural parameters calculated for PbS thin films with different lead nitrate concentrations.

and lower surfaces will interfere. The degree of constructive or destructive interference between the two light waves depends on the difference in their phase. This difference in turn depends on the thickness of the film layer. Therefore, this phenomenon can be used to estimate the films thickness which we have done by using the Swanepoel model[29] . The transmission spectra of *PbS* thin films deposited with different molar concentrations, recorded at 55 °C in the wavelength range of 300 - 1800 nm is reported in Fig. 4.11. It showed a decrease in transmission with increasing molar concentration, due to the increase in the thickness in the range 300 to 1000 nm. The effect of change of molar concentration can be observed in the long wavelength portion of the spectra, where interference effects took place. Also, it is noticed that all the films have low transmittance in the ultraviolet UV region below 400 nm, which is due to the strong absorbance in this region. Thereafter, the transmission increases with increasing wavelength towards the NIR regions. It could be observed in Fig. 4.11 that for each curve, the maximum of reflectance corresponds to the minimum of transmission and vice versa.

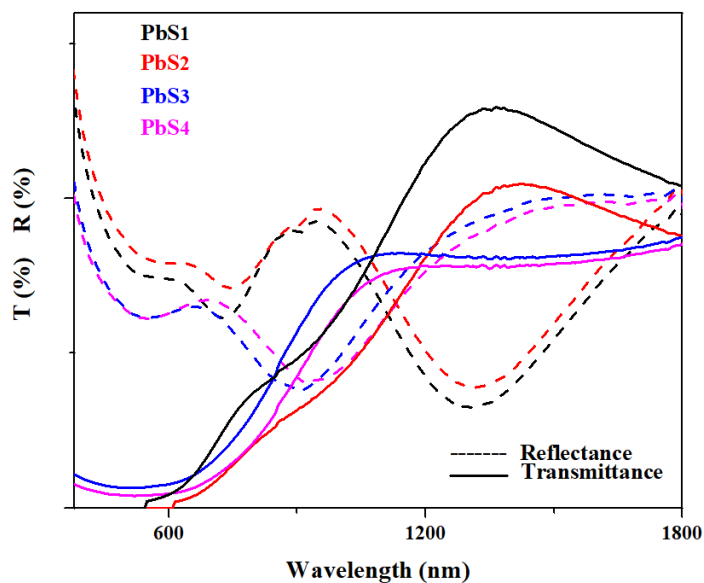


Figure 4.11: Transmittance and Reflectance versus wavelength of *PbS* thin films deposited for different molar concentrations.

#### 4.2.2.2 Energy band gap and Urbach energy

The transmittance data were analyzed to determine the optical band gap of the samples using the classical relation (see eq. 2.19 for near edge optical transmission of semiconductors). The band gap energy is obtained by extrapolating the linear portion of  $(\alpha h\nu)^2$  vs the photon energy ( $h\nu$ ) to the energy axis at  $(\alpha h\nu)^2 = 0$ . Fig. 4.12 shows a typical plot of  $(\alpha h\nu)^2$  vs  $h\nu$ , which allow estimating experimentally the value of the band gap. The value of the energy gap is greatly influenced by the change of the molar concentration. It is found that the value of  $E_g$  increases from 1.58 to 1.64 eV with increasing molar concentration of lead nitrate, then decreases for furthermore increasing the lead nitrate concentration, due to the crystallite size dependant properties of the energy band gap[16]. This dependence can be explained by the increase of molar concentration increases the grain size which in turn decreases the energy band gap. The variation in  $E_g$  with molar concentration is summarized in Table. 4.2.2.2, which are higher than that for bulk, i.e.0.41 eV, this shift is due to quantum size effect [13]. Similar results were reported in the

literature [12, 30].

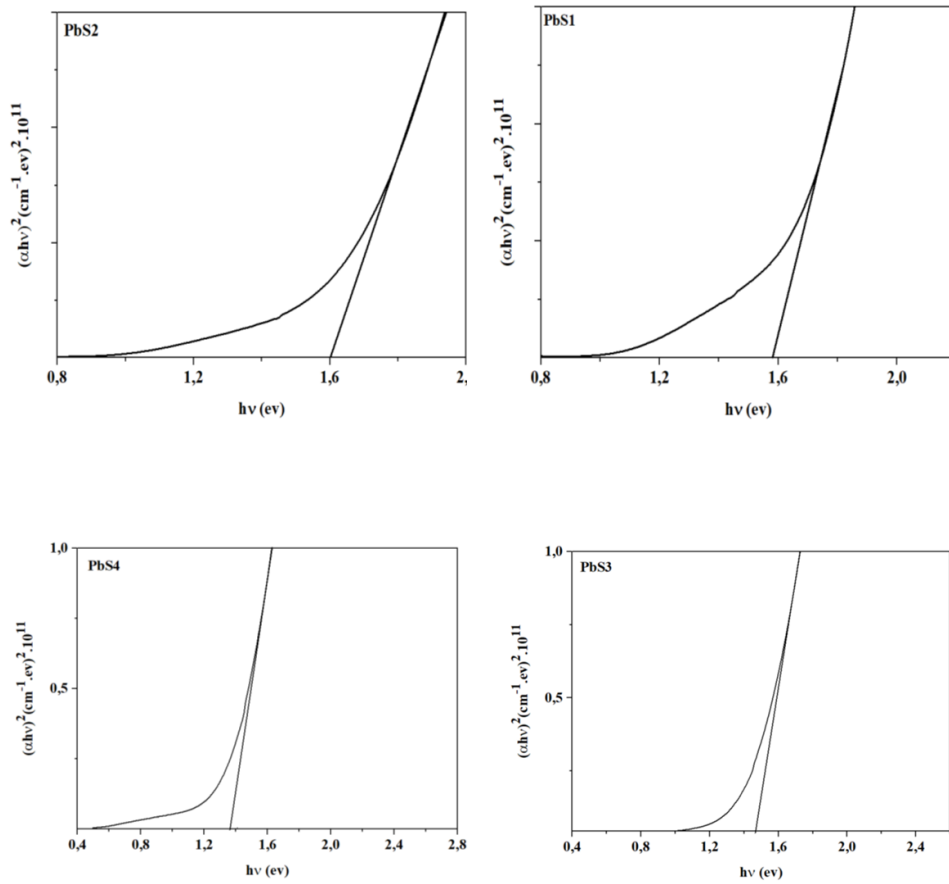


Figure 4.12: Tauc's plot used for determination optical band gap of PbS thin films deposited for different molar concentrations.

The transmittance data of the different films obtained with different molar concentrations were used again to determine the band tail width by the method described in the previous chapter. The value of the Urbach energy is influenced by the change of the molar concentration. It is noticed that the value of band tail width decreases from 0.680 to 0.610 eV with increasing molar concentration of lead nitrate, then increases for further increasing the lead nitrate concentration,

due to the strain and defects dependant properties of the Urbach energy [19]. On the other hand the increase and decrease in the optical band gap corroborate well with the disorder reduction and increment in films' network as shown in Fig. 4.13. This indicates clearly that the optical gap in the obtained films is governed by the disorder. The values of band tail width are illustrated in Table. 4.2.2.2.

Samples	Band gap ( $E_g$ )(ev)	Tail width ( $E_u$ ) (ev)
$PbS_1$	1.58	0.68
$PbS_2$	1.64	0.61
$PbS_3$	1.50	0.83
$PbS_4$	1.37	0.88

Table 4.VII: Estimated values of the Urbach and band gap energies for different lead nitrate concentrations.

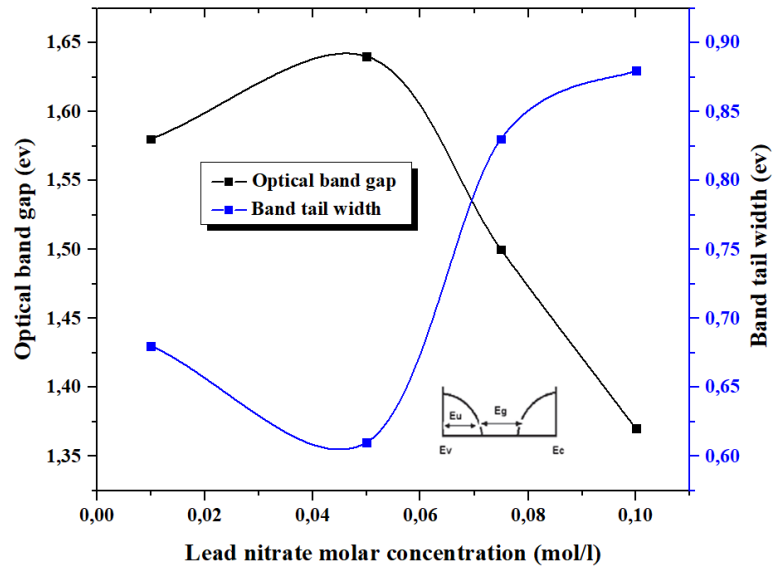


Figure 4.13: Variation of the films disorder and optical band gaps as function of lead nitrate molar concentration.

### 4.2.3 FT-IR measurements

PbS have no adsorption peaks in IR region of spectrum, thus, the determination of FT-IR spectra was made in order to establish if the obtained *PbS* thin films are pure. Fig. 4.14 shows FTIR spectra of all *PbS* thin films measured at room temperature. One can see from the thin films spectra that there are some adsorption bands, the broad band at  $3450\text{ cm}^{-1}$  is assigned to  $O - H$  bending vibration of the water molecules, this proves the moisture absorbing capacity of the samples, which might have been resulted due to the exposure of the synthesized samples to open atmosphere [31]. The peak at  $1946\text{ cm}^{-1}$  corresponds to  $C = O$  stretching vibrations related to carbonyl group. The spectra show a peak around  $2360\text{ cm}^{-1}$  is assigned to the antisymmetric stretching mode of  $CO_2$  [32]. The band around  $2922\text{ cm}^{-1}$  which is due to antisymmetric vibration of  $C - H$  bonds arising from the alkyl chains of the TEA. Also, the symmetrical stretching mode  $CH$  is expected around  $2845\text{ cm}^{-1}$  in which all the three  $CH$  bonds extend and contract in phase, while peaks at  $908\text{ cm}^{-1}$  is assigned to  $CH$  (out-of-plane vinyl  $C - H$  bending) [33, 34]. The strong and intense peaks around  $1409\text{ cm}^{-1}$  is could be due to  $OH$  bending vibration in adsorbed water [34]. One of the most important aspect revealed from these spectra is the bands at around  $688$  and  $609\text{ cm}^{-1}$  were observed for  $PbS_4$ , which are attributed to vibrations of  $PbO$  [34, 35] unlike other samples. The FTIR spectra confirm the presence of  $PbO$  vibrations in the synthesized  $PbS_4$  sample is supported to the XRD analysis.

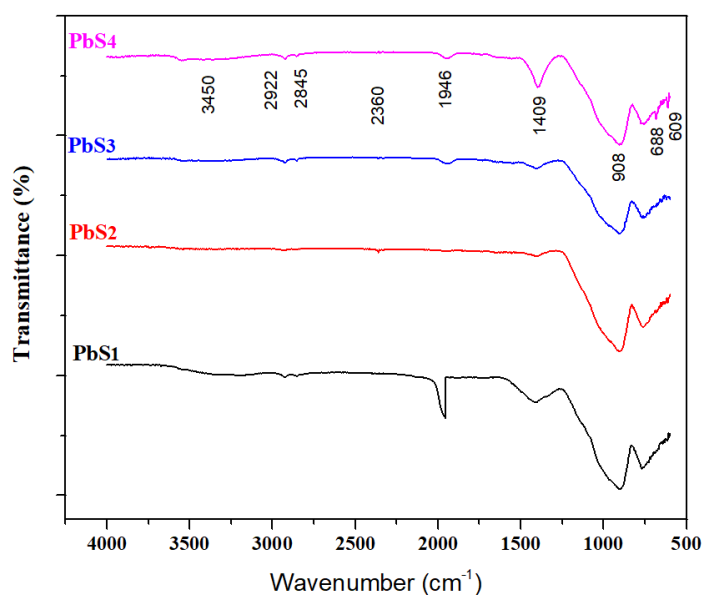


Figure 4.14: FTIR spectra of all *PbS* thin films obtained of different lead nitrate concentrations.

## References

- [1] P. P. Hankare, S. D. Delekar, V. M. Bhuse, K. M. Garadkar, S. D. Sabane, L. V. Gavali, *Materials Chemistry and Physics*, 82 (2003) 505 - 508.
- [2] S. Seghaier, N. Kamoun, R. Brini, A. B. Amara, *Mat. Chem. and Phys.* 97 (2006) 71-80
- [3] J. J. Valenzuela-Jauregui, R. Ramirez-Bon, A. Mendoza-Galvan, M. Sotelo-Lerma, *Thin. Solid. Films.* 441 (2003) 104-110
- [4] J.A. Garca-Valenzuela, M. R. Baez-Gaxiola, M. Sotelo-Lerma, *Thin Solid Films* 534 (2013) 126-131
- [5] P.K. Nair, M.T.S. Nair, *J. Phys. D: Appl. Phys.* 23 (2) (1990) 150.
- [6] A. S. Obaid, M. A. Mahdi, Y. Yusof, M. Bououdina, Z. Hassan, *Mat. Sci. Sc. Proc*, 16 (2013) 971-979
- [7] C. Agashe, M.G. Takwale, B.R. Marathe, V.G. Bhide, *J. Mater. Sci.* 24 (1989) 2628-2636.
- [8] K. L. Chopra, *Thin film phenomena* , New York; Mc Grow Hill, (1969)

- [9] F. I. Ezema, A. B. C. Ekwealor, R. U. Osuji, *Superficies Vacio.* 21 (1) (2003) 6.
- [10] H. Kenazawa, S. Adashi, *Journal of Applied Physics* 83 (1998) 5997
- [11] Y. Wang, N. Herron, *J. Phys. Chem.* 95 (1991) 525
- [12] M.A. Rafa, N. Rousdy, *Philosophical Magazine Letters* 90 (2010) 113-120
- [13] A. S. Obaid, M. A. Mahdi, Z. Hassan, M. Bououdina, *International Journal of Hydrogen Energy* 38(2013) 807-815
- [14] V. Probst, W. Stetter, W. Riedl, H. Vogt, M. Wendl, H. Calwer, S. Zweigart, K. D. Ufert, B. Freienstein, H. Cerva, F. Karg, *Thin Solid Films* 387 (2001) 262
- [15] A. Ashida, Y. Hachiuma, N. Yamamoto, T. Ito and Y. Cho, *J. Mater. Sci. Lett.* 13 (1994) 1181
- [16] F.I. Ezema, A.B.C. Ekwealor, R.U. Osuji, *Journal of Optoelectronics and Advanced Materials* 9 (2007) 1898-1903
- [17] K. C. Preetha, K.V. Murali, A. J. Ragina, K. Deepa, T. L. Remadevi, *Curr. App. Phys.* 12 (2012) 53-59
- [18] A. P. Gaiduk, P. I. Gaiduk, A. N. Larsen, *Thin Solid Films* 516 (2008) 3791-3795
- [19] F. Urbach, *Phys. Rev.* 92 (1953) 1324
- [20] K.S. Suslick, R.E. Cline, and D.A. Hammerton, *Symp. Proc.* 21 (1985) 1116-1121
- [21] A. S. Obaid, M. A. Mahdi, Y. Yusof, M. Bououdina, Z. Hassan, *Mat. Sci. Sc. Proc.* 16 (2013) 971-979
- [22] M. M. Abbas, M. Shehab, N. A. Hassan, A. K. Al-Samuraee, *Thin Solid Films* 519 (2011) 4917-4922
- [23] A. M. Mousa, S. M. Al-Jawad, S. M. K. Al-shammari, *Eng. Tech. Journal*, Vol 31, Part (B), No. 5, (2013)
- [24] B. D. Cullity, S. R. Stock, *Elements of X ray diffraction*, Third edition,

New Jersey, Prentice Hall, (2001)

[25] Y. Zhao, X. H. Liao, J. M. Hong, J. J. Zhu, *Materials. Chemistry. Physics* 87 (2004) 149-153

[26] D. Kumara, G. Agarwal, B. Tripathi, D. Vyas, V. Kulshrestha, *J. of Alloys and Compounds* 484 (2009) 463 - 466

[27] M. J. Weber, *Handbook of Optical Material*, California, CRC Press, (2003)

[28] S. H. Jeong, S. Kho, D. Jung, S. B. Lee, J. H. Boo, *Surface and Coatings Technology* 174-175 (2003) 187-192

[29] R. Swanepoel, *J. Phys. E: Sci. Instrum.* 6 (1983) 1214.

[30] M. M. Abbas, A. Ab-M. Shehabb, A-K. Al-Samuraee, N-A. Hassan, *Energy Procedia* 6 (2011) 241-250

[31] E. Esakkiraj, K. Mohanraj, G. Sivakumarb, J. Henry, *Optik* 126 (2015) 2133-2137

[32] T.M. Khan, M.F. Mehmood, A. Mahmood, A. Shah, Q. Raza, A. Iqbal, U. Aziz, *Thin Solid Films* 519, 5971 (2011)

[33] S. K. K. PASHA, K. DESHMUKH, M. B. AHAMED, K. CHIDAMBARAM, M. K. MOHANAPRIYA, N. A. RAJ, *Polymer Technology*, Vol. 00, No. 0, 1 15 (2015) 21616 21616

[34] K. T. Arulmozhi, N. Mythili, A. I. P. *ADVANCES* 3, 122 122 (2013)

[35] A. K. Hassan, L. BÅŕjesson, L. M. Torell, *J. of Non-Crystalline Solids*, vol. 172-174, no. 1, pp. 154-160 (1994)

# Conclusions and Outlook

## Conclusions

- In the present work, *CdS* and *PbS* thin films were successfully grown on glass substrates using the chemical bath deposition (*CBD*) process under different preparation conditions. *CBD* technique is a thin film depositing method from an aqueous solution. Due to its feasibility, it has become an attractive method based on many reasons, including ease of manufacturing, low cost, suitability for large scale deposition areas and the ability to deposit thin films on different substrates and ease of controlling thin film properties by controlling the deposition parameters.

- The main advantage of this method is, during the growth of a film on a substrate, it is possible to ensure that the reaction occurring in the deposition bath takes place sufficiently slowly. The film deposited by this technique has possible applications in solar. Thus, *CBD* technique has been a user friendly technique. Therefore, we are very much interested to prepare the *CdS* and *PbS* thin films using chemical bath deposition technique. Since the control of process parameters is relatively easier.

- *CdS* and *PbS* thin films were successfully prepared on glass substrates using *CBD* technique under different preparation conditions. The effect of deposition time of both materials was investigated by varying the time from 30 to 90 min. On the other hand, different concentrations of lead nitrate were used to investigate its effect on *PbS* thin films, while for *CdS*, sulphuric acid was added to investigate the effect of  $(CO_3)^{2-}$ . The properties of resulting thin films were char-

acterised by various techniques such as X- ray diffraction (XRD) and UV-visible spectroscopy. FTIR technique was used to identify the chemical reactions leading to *CdS* formation.

- Composition analysis of different solutions leading to the formation of *CdS* products using *FTIR* analysis indicates that, for calcined precipitate and different steps solution,  $Cd^{2+}$  released from cadmium carbonate by the activation of sulphuric acid then complexes with  $NH_3$  to form cadmium tetramin  $[Cd(NH_3)_4]^{2+}$ , while the  $S^{2-}$  released from thiourea by  $(NH_4^+ + OH^-)$  action on it. Chain of chemical and mechanism reaction leading to *CdS* thin film formation were proposed.

- Cadmium sulfide thin films were successfully deposited on glass substrate using ammonium hydroxide as a complexing agent, thiourea as source of  $S^{2-}$  and cadmium carbonate as source of  $Cd^{2+}$  at a bath temperature of  $55^\circ C$ . The XRD analysis of as-deposited *CdS* thin films revealed that a uniform hexagonal phase of *CdS* nanocrystalline thin films with preferred orientation along the (002) plane were deposited for time high than 30 min. For film deposited at low time 30 min, only a broad hump in the range of  $20-36^\circ$  was observed indicating that the film is poor crystallizing or is not thick enough for XRD analysis and the broad hump is due to the glass substrate on which the film is deposited. It was observed that the peak intensity increases with increasing deposition time; this is a consequence of thickness increasing which leads to better crystallinity of *CdS* thin films. The average crystallite sizes were found to increase from 14,3 to 30.4 nm with increasing deposition times. The optical study revealed that both deposited thin films exhibit a high transmittance in the visible range, varying from 70 - 92% , it decreased with increasing deposition times, while the direct band gap decreased from 2,58 to 2,42 ev with increasing the durations. For the second set of *CdS* thin films where the  $(CO_3)^{2-}$  ions are completely eliminated by the sulphuric acid. The XRD analysis of later *CdS* thin films revealed that are uniform cubic structure with preferred orientation along the (111) plane. The crystallite sizes were found to increase from 24.4 to 38.9 nm with increasing deposition times. The optical study revealed that

both deposited thin films exhibit a high transmittance in the visible range, varying from 40 - 80% , it decreased with increasing deposition times, while the direct band gap increased from 2,19 to 2,35 eV with increasing the deposition times.

PbS films have been prepared on glass substrates by Chemical bath deposition. By investigating the influence of deposition parameters on the kinematics of the deposited films, we studied the influence of two factors: deposition time and the concentration of lead nitrate.

The growth rate can be controlled “fast” and “slow” by controlling the amount of  $Pb^{2+}$  in the reaction mixture. Despite the energy gap of the studied samples revealed a strong dependence of the gaps values of the films on the deposition parameters, it is possible to produce thin films of  $PbS$ , with energy band gaps in the range 1.80 - 1.60 eV, and with proper manipulation of reaction parameters could be near to the optimum for photovoltaic energy conversion (1.5 eV).

## Outlook

There are several directions that can be further pursued in the future:

- Study of other metal-thiourea complex precursors can be useful to synthesize metal sulphide nanomaterials of good properties.
- It is also very interesting to study the effect of chemical doping on PbS and CdS films to improve their performance in thin film solar cell.
- Deposit the ternary ( $Pb_{1-y}Cd_yS$ ) thin films and investigate their optical, structural, morphological and electrical properties.
- Using other types of substrates

# Abstract

Chemical bath deposition, which is a very attractive method, used to produce thin films for polycrystalline solar cells such as *CdS* and *PbS*. This work was based on this method. Our objective is to provide a comprehensive study on the effect of the deposition parameters on the structural and optical properties of CdS and PbS thin films and to monitor all reactions steps leading to *CdS* thin films formation. For the *CdS* thin films the bath solution is a mixture of cadmium carbonate  $CdCO_3$  and thiourea as source of cadmium and sulphur respectively, ammonia was used as complexing agent. In this study, two sets of samples were prepared, in each set only one parameter is varied while the rest of parameters were fixed. In the first set, a few drops of sulphuric acid were added while in the second more of sulphuric acid were added. In order to investigate the deposition time. For both sets, films were deposited for different durations ranging from 30 to 90 min at bath temperature 55°C. X-ray diffraction, UV-visible spectrophotometry and Fourier transform infrared techniques were used to investigate *CdS* thin films and the different steps of reactions leading to *CdS* product. For the first set, the growth of films occurs by the mechanism ion-by-ion with low deposition rate. Hexagonal *CdS* thin films were obtained with (002) preferred orientation and having average crystallite size in the range of 14.3 to 30.4 nm. All the films exhibit a high transmittance in the visible range; it is in order of 70 to 92% , the values of the optical gap are between 2.42 and 2.58 eV, this according to deposition time. Studies of different solutions and steps leading to the formation of *CdS* products were carried. The formation mechanism of *CdS* thin films was proposed based on FTIR results. For the second set. The obtained *CdS* films in this case have cubic structure with a preferential

orientation along the axis (111) and crystallite size between 24.4 and 38.9 nm. The transmittance of the films was found to be in order of 40 to 80%, the values of the optical band gap increases with deposition times from 2.19 to 2.35 eV.

In this work, PbS thin films were prepared for different deposition times ranging from 30 to 90 min and different lead nitrate molar concentrations (0.01, 0.05, 0.075 and 0.1) mol/l at a bath temperature of 55°C, using thiourea as source of  $S^{2-}$  ions and TEA as complexing agent. For different deposition times the films grow preferentially along (200) direction. With increase in deposition time, and at fixed molar concentration the transmittance remained less than 30% and the values of the optical band gap decreases from 1.8 to 1.6 eV, while the crystallite size increases from 21.9 to 27.8 nm. For various molar concentrations of lead nitrate and with time deposition equal to 60 min, it was observed that the films grow preferentially along (111) or (200) directions depending on the molar concentration. The energy band gap decreases from 1.58 to 1.37 eV and the crystallite sizes increases from 28.0 to 32.6 nm with increasing the concentration of lead nitrate.

**Keywords:** Thin films, Chemical synthesis, FTIR, Optical properties, Structural properties, Chemical bath deposition.

# **Elaboration et caractérisation des films minces à base de chalcogénure par la technique bain chimique**

## **Résumé**

Ce travail de recherche porte sur l'élaboration et la caractérisation des couches minces de CdS et PbS par une technique simple et bon marché en l'occurrence la méthode de dépôt par bain chimique CBD (Chemical Bath Deposition). Notre objectif est de donner une étude compréhensive sur l'effet des paramètres de dépôt (concentration de précurseur et temps de dépôt) sur les propriétés structurales et optiques des films minces CdS et PbS et d'observer toutes les étapes de réactions menant à la formation de films minces de CdS en utilisant FTIR technique. Dans cette étude, deux séries de films CdS ont été préparées, dans chaque série, un seul paramètre est modifié tandis que les autres ont été fixés. Pour la première série, quelques gouttes d'acide sulfurique ont été ajoutées tandis que pour la deuxième, on a ajouté de l'acide sulfurique jusqu'à la transparence de la solution.

Les films de la première série du CdS à base du sulfate de cadmium ont une structure hexagonale avec une orientation préférentielle suivant l'axe (002), la croissance des films se produit par le mécanisme ion par ion. La taille des grains varie entre 14.3 et 30.4 nm. La transparence dans nos films varie entre 70 et 92 % et les valeurs du gap optique sont entre 2.42 et 2,58 eV, ceci en fonction du temps de dépôt. Le mécanisme de formation des couches minces de CdS a été proposé en basant sur les résultats de FTIR. Pour la deuxième série, les films CdS obtenus ont une structure cubique avec une orientation préférentielle suivant l'axe (111), la taille des grains varie entre 24,4 et 38,9 nm. La transmittance dans ces films varie entre 40 et 80% et les valeurs du gap optique sont entre 2,19 et 2,35 eV, ceci en fonction du temps de dépôt.

Dans ce travail, les films du PbS préparés à une température fixe à 55°C mais avec différents temps de dépôt ont une structure cubique avec une orientation préférentielle suivant l'axe (002), la transmittance reste inférieure à 30% et les valeurs du gap optique diminuent de 1,8 à 1,6 eV, tandis que la taille des grains augmente de 21,9 à 27,8 nm. Pour un temps de dépôt optimal égal à 60 min et avec des différentes concentrations molaires de nitrate de plomb, on observe que ces films ont une orientation selon (111) ou (200) directions ceci en fonction de la concentration molaire de nitrate du plomb. Les valeurs du gap optique diminuent de 1,58 à 1,37 eV et la taille des grains augmente de 28,0 à 32,6 nm en augmentant la concentration de nitrate du plomb.

# تحضير ودراسة خواص الشرائح الرقيقة لكبريتيد الكاديوم وكبريتيد الرصاص (PbS, CdS)

## ملخص

موضوع هذه الرسالة يتناول تحضير ودراسة خواص الشرائح الرقيقة لكبريتيد الكاديوم وكبريتيد الرصاص والتي تم تحضيرها بطريقة الترسيب بالحمام الكيميائي (CBD) عند الدرجة 55 درجة مئوية. هدفنا من هذا البحث هو تقديم دراسة موضحة لتأثير وسائط الترسيب على الخواص الفيزيائية للشرائح (PbS, CdS) وكذا اقتراح نموذج لآليات التفاعلات الكيميائية التي تؤدي إلى تشكل الأغشية الرقيقة وذلك باستعمال الأشعة تحت الحمراء.

في الجزء الأول من هذه الدراسة حضرت الأغشية الرقيقة للمركب CdS بطريقة الترسيب بالحمام الكيميائي وذلك باستعمال الثيوريا كمصدر للكبريت و كربونات الكاديوم كمصدر للكاديوم (والذي حسب علمنا لم يستعمل سابقا) ومحلول هيدروكسيد الامونيوم للحصول على وسط قاعدي وكعامل معقد. قمنا بدراسة تأثير زمن الترسيب بوجود شوارد الكربونات في المحلول (إضافة قطرات قليلة من حمض الكبريت) وبعدها (إضافة كمية كافية من حمض الكبريت حتى الاختفاء التام لشوارد الكربونات) على الخصائص البنيوية والضوئية لشرائح الـ CdS وكذا اقتراح نموذج لآليات التفاعلات الكيميائية التي تؤدي إلى تشكل الأغشية الرقيقة للمركب CdS وذلك باستعمال الأشعة تحت الحمراء. من دراسة طيف الحيود للأشعة السينية للأغشية الرقيقة للمركب CdS نستنتج أن أغشية المركب هي متعددة التبلور ذات تركيب سداسي من نوع Wurtzite في حالة وجود شوارد الكربونات ومكعب من نوع Zinkblend في غيابها، والاتجاه المفضل لنمو الغشاء الرقيق هو (002) للتركيب السداسي و (111) للتركيب المكعب. كما أن نمو الشرائح في الحالة الأولى يتم بألية أيون-ف-أيون بينما في الحالة الثانية يتم بعنقود-ف-عنقود. الشرائح الأولى تتميز بشفافية عالية تتراوح بين 70 و 92 %، أما قيم النطاق الطاقى الممنوع فهي تتغير بين 2.42 و 2.58 eV بينما الشرائح الثانية شفافية في المجال من 40 إلى 80 % وقيم نطاقها الطاقى يتراوح بين 2.19 و 2.35 eV حسب تغير زمن الترسيب.

كما تم تحضير مجموعتين من شرائح رقيقة من كبريتيد الرصاص، بالنسبة للمجموعة الأولى قمنا بتغيير عامل الزمن فقط أما المجموعة الثانية فقمنا بتغيير تركيز نترات الرصاص الذي استعمل كمصدر لشاردة الرصاص  $Pb^{2+}$  وتم استعمال الثيوريا كمصدر للكبريت وثلاثي إيثان أمين (TEA) كعامل معقد بزمن ترسيب قدره 60 دقيقة. تم فحص التركيب البلوري لشرائح كبريتيد الرصاص بحيود الأشعة السينية، حيث وجد أن تركيب الشرائح متعدد التبلور بالطور المكعب والاتجاه البلوري المسيطر هو (200) بالنسبة للمجموعة الأولى، بالنسبة للمجموعة الثانية وجد أن الاتجاه البلوري المسيطر يتعلق بتركيز نترات الرصاص فهو (200) بالنسبة للتركيز المنخفضة و (111) بالنسبة للتركيز المرتفعة. بالنسبة للمجموعة الأولى الشفافية بقيت أقل من 30 % وقيم النطاق الطاقى الممنوع تغير من 1.8 إلى 1.6 eV أما بالنسبة للمجموعة الثانية فان قيم النطاق الطاقى الممنوع تتناقص من 1.58 إلى 1.37 eV بزيادة تركيز نترات الرصاص.

**الكلمات المفتاحية:** الشرائح الرقيقة، كبريتيد الكاديوم، كبريتيد الرصاص، الخصائص البنيوية، الخواص الضوئية.